School of Civil Engineering of Barcelona
UPC BARCELONATECH

MASTER'S DEGREE THESIS

Mechanical characterisation of masonry walls and vaults in a modernist building in Barcelona

Thesis written by:

Ioannis Tsioutsios

Tutored by:

Luca Pelà

Master's degree in:
Structural & Construction Engineering

Barcelona, 17, April, 2020

Department of Civil Engineering

The thesis work is dedicated to my parents Nikolaos and Paraskevi, to my sister Evelina and

to all my friends that supported me continuously during the campaign

.

Acknowledgements

Firstly, I would like to express my gratefulness to my thesis supervisor, Professor Luca Pelà for his crucial guidance, continuous encouragement and the useful feedback during this research project. Without his leading support throughout this campaign, the thesis would have not been completed. I am really gratified and I could not ask for a friendlier or more valuable supervisor.

I would also like to thank deeply the PhD candidate Albert Cabané for his help, advices, and continuous assistance throughout this experimental campaign. His interest and his support were very crucial and led to the completion of the thesis. Thanks to him I learned how to deal with the concepts of the masonry assessment and how to execute precisely the experimental tests.

Furthermore, I would like to express my gratitude to Savvas Saloustros for his assistance and guidance in the numerical part of thesis as he guided me thoroughly in order to understand deeply the concept of the numerical analysis and implement it successfully.

I would also like to extend my thanks to the technicians and the staff of the laboratory de Tecnologia d'Estructures i Materials de Construccio ''Luis Aguilo'' (LATEM) of the UPC, Tomas García, Jordi Cabrerizo, Robert Mc-Aloon and Carlos Hurtado who have helped me to obtain the samples that I needed for the experimental campaign in the laboratory and to carry out the in-situ experimental techniques.

I thank all the professors of the UPC for sharing their knowledge during the courses, knowledge that helped me prepare myself for the extensive campaign of the thesis project.

My sincere thanks to all my fellow classmates and friends, who made this MSc degree indelible and enjoyable.

Furthermore, I would like to express my profound gratefulness to my family for their constant support and motivation during these months of the campaign.

Finally, I would like to conclude my thankfulness to the Achillopoulos Sofoklis Foundation for the scholarship that provided for my postgraduate studies which made possible the completion of the master's degree.

Abstract

The research project of the ‘’Mechanical characterisation of masonry walls and vaults in a modernist building in Barcelona’’ is aimed to validate the criteria for the evaluation and the assessment of the mechanical characterization of masonry elements of the building of Escola Industrial.

The first purpose is to understand deeply the behaviour of masonry under compression and the methods to characterize its mechanical parameters that forementioned throughout a comprehensive bibliographical research. Innovative experimental destructive tests are calibrated and carried out in the Laboratory of Structural Technology of the Technical University of Catalonia (UPC – BarcelonaTech) and minor destructive techniques are implemented in situ in order to investigate the compressive behaviour of the masonry.

For the minor destructive techniques, Windsor Pin Penetrometer test, Screw Helix Pull-out test and Torque Penetrometric test are carried out in situ to preliminarly evaluate the parameters and the compressive strength of the masonry. For the destructive techniques, compressive tests are implemented in brick, tile, stone and mortar specimens and the evaluation of Young’s modulus and Poisson’s ratio is carried out on brick specimens.

The double punch test is investigated on the mortar joints along with the numerical analysis and the verification of the test with an objective to evaluate which parameters influence the assessment of the test and provide a novel contribution to the field as it has never been analysed before.

Extraction of core cylinders is a beneficial method since it slightly damages the structure and it is executed both for brick and stone masonry. The extracted cylinders were subjected to compression tests in the laboratory according to the guidelines of UIC 778-3R formed by International Union Railways in order to provide insight on the behaviour and properties of the masonry.

A general objective of this study is to encourage future research on these moderate destructive techniques of testing existing masonry, to facilitate the function on the minor destructive techniques on real existing structures in situ, enhance the development of current standards and provide a novel contribution to the field by implementing a completely new numerical study.

Index

Index of Figures

Index of Tables

Chapter 1 Introduction

1.1 Motivation for the present research

Masonry is an extremely used material in the construction field. It has been the material of choice for shelter for thousands of years for a number of reasons including availability, thermal mass, fire resistance, durability and sustainability.

The analysis of the masonry structures has been based on empirical rules and design criteria as it is a traditional material. Assessments or restorations in masonry buildings according to these rules require deep knowledge of the characteristics of the materials and the structure cause of the material's inherent complexity. Investigations of such characteristics on real structures are usually allowed only one condition. No damage or little in an a way that doesn't affect the architectural value of the building is done to the historic material.

This is happening because a historical structure throughout its lifetime may be subjected to actions or environmental effects which can lead to stability or durability issues. For that, historical structures must be analysed and evaluated as to determine the condition of their materials through on site non-destructive testing techniques or controlled destructive laboratory tests.

Before that, at the stage of the preliminary analysis of the masonry, it is important to define the characteristics of the constituent materials: for the units (stones or bricks) and for the type of mortar (cement, lime, etc.). It is also important to know how the elements are connected (dry joints, mortar joints, etc.) and how they are geometrically linked to each other. Different types of tests can be used to assess the composition of the wall.

The assessment of masonry elements requires the definition of some mechanical parameters, of which the most important is the compressive strength, but also the elastic parameters (E and ν) are necessary for more detailed models. Nevertheless, even if the masonry structure is simple, the evaluation of the mechanical properties is really complex, due to highly nonlinear response of the material, the lack of the standards and the dependency on the modality of the test. For this reason, the parameters needed are often obtained from insufficiently accurate analogies or correlations, which may even lead to incorrect conclusions on the strength capacity and structural safety. The available experimental and theoretical methods pose advantages and uncertainties, which make it difficult to estimate the global error and hence the reliability of the study.

The forementioned destructive tests are not implemented directly on the structure, while through the non-destructive tests only a part of information about the masonry materials can be obtained. Standardized minor destructive tests can provide important knowledge for the mechanical properties of the masonry. These tests may substitute invasive destructive tests by implementing all the necessary information in order to improve the knowledge of the material.

Nowadays, a tremendous effort is being made to better understand the behavior of existing materials by the means of these in-situ minor destructive techniques. A more detailed

knowledge of the cracking or failure phenomena will help to safeguard the cultural heritage and will make it possible to establish more accurate models for the evaluation of buildings.

The research project of the ‘’Mechanical characterisation of masonry walls and vaults in a modernist building in Barcelona’’ is aimed to obtain and validate criteria for the characterization of the mechanical properties of structural masonry elements. It is expected that this research will expand the current methodology which allows the accurate definition of the masonry parameters.

The incompatibilities between the observed actual structural behavior and the predictions resulting from traditional analytical approaches have led to the need for the use of developed and advanced computational techniques in order to compare the experimental analysis with numerical simulation.

For that, the mortar mechanical parameters are the ones necessary for the preparation of numerical models of the double punch test used in the analysis and verification of the mortar. The DPT on the mortar has never been analysed numerically in the literature and for this reason this study is implemented as a novel contribution to the field.

1.2 Objectives

The current work has the objective to evaluate the compressive behaviour of the masonry by the calibration of minor destructive techniques in situ and destructive laboratory tests. The double punch tests on the mortar are going to be verified through numerical modelling as it is a test that have never carried out before numerically.

The aim of this thesis is to provide insight on the behaviour and properties of a masonry element under compression. The technique mainly investigated is the compression test on extracted masonry cylinders, according to the guidelines of UIC 778-3R formed by International Union Railways. This test is also compared with the standard equations using the mechanical values obtained with the characterisation of the components. In addition to that, in order to investigate the properties of the materials, some tests are carried out, using standard and non-standard methods. The standard and non-standard tests performed on masonry are analysed in order to obtain elastic parameters and compressive strengths.

The most investigated of them is the double punch test on the mortar joints and as forementioned is verified and analysed numerically for the first time in order to constitute a novel contribution to the field. The objective is to examine numerically the mortar’s behaviour during the DPT, evaluate the relationship between uniaxial compressive and maximum experimental strength, identify the influence of the various numerical and mechanical properties on the compressive strength and evaluate the effect of the specimen’s geometry.

The general objectives of the thesis project are the following:

- presenting a comprehensive experimental program on a historical modernist building constructed in the XIX century in Barcelona;

- contributing to expand the database on mechanical properties of typical historical masonry components;

- improving the knowledge on minor destructive testing of historical masonry buildings;

The specific objectives of the thesis project are the following:

- assessing the compressive behaviour of the brick and stone masonry by the implementation of these minor destructive techniques in situ and destructive laboratory tests.

- contributing to the development and reevaluation of the standard and non-standard tests that can be performed on masonry and its components;

- providing an insight on the behaviour a masonry element under compression by carrying out compression test on extracted masonry cylinders;

- validating and understanding the DPT technique along with the assessment of the mechanical parameters influence to the test by advanced nonlinear numerical simulations.

1.3 Methodology

The experimental campaign that was carried out consists of minor destructive techniques (MDT) and of destructive techniques (DT) based on the extraction of samples in situ and testing of these specimens in the laboratory of UPC. It also consists of the numerical modelling studies of the double punch test on the mortar in the pre-post processor called GID and a finite element software called COMET both developed at the International centre of Numerical Methods in Engineering (CIMNE, Barcelona, Spain).

In order to achieve the objectives presented in Section 1.2, the research has been organized on the basis of the following steps:

- to gather information on the existing knowledge about the behaviour of masonry under compression and the methods to characterize its mechanical parameters, through a comprehensive bibliographical research in brick, tile, stone, mortar along with the behaviour of brick and stone masonry;

- to determine the parameters and the strength of masonry using different approaches such as the in-situ minor destructive techniques, compressive tests on brick specimens along with the evaluation of the Young's modulus and Poisson ratio, compressive tests on tile specimens, compressive tests on stone specimens, compressive tests on mortar specimens and compressive tests on the extracted masonry brick and stone cylinders;

- to compare the results obtained with analytical and standard formulas in order to validate the reliability of the experimental techniques;

- to examine numerically the mortar's behaviour during the DPT, compare the numerical and the experimental results and evaluate which parameters influence the assessment of the test.

1.4 Outline of the research

The present thesis is divided into six chapters.

The first chapter deals with the objectives and focus of the thesis.

The second chapter deals with the state of the art, where an introduction is given on masonry, brick, tile, stone and mortar, along with the behaviour of masonry in compression and different test approaches and the numerical modelling of the non-standard tests calibrated in the literature.

The third chapter deals with the experimental campaign, along with the research results on bricks, tiles, stone and mortar, three-joint masonry cylinders and two-joint masonry cylinders.

In chapter four, the results obtained in third chapter are analysed. A discussion of results is also proposed as well as a comparison between the results obtained experimentally and those calculated applying the relations suggested by the standards.

The fifth chapter presents the FE modelling of the DPT test on the mortar specimens, the results and the comparison with experimental tests and the evaluation of the parameters influencing the assessment of the test.

The sixth chapter concludes the thesis with the summary and main outcomes of the present research and suggestions for the future work.

Chapter 2: State of the art

2.1 Overview in masonry

Masonry is the oldest material that has application in the construction field. The most crucial characteristic of this material is its simplicity. It is a simple, though adequate technique that has been successfully used ever since older period of times. Laying pieces of stone, bricks or blocks on top of each other, either with or without cohesion of the mortar. Variations of masonry materials, applications and techniques occurred and changed naturally during the course of time. The influence factors were mainly the local culture and wealth, the knowledge of materials and tools, the availability of material and architectural reasons. According to [1] the huge number of possible combinations generated by the geometry, nature and arrangement of units as well as the characteristics of mortars raises doubts about the accuracy of the term "masonry". Just for brick masonry, some usual combinations are shown in Fig. 1. Nevertheless, the mechanical behaviour of the different types of masonry has generally a common feature: a very low tensile strength. This property is so important that it has determined the shape of ancient constructions.

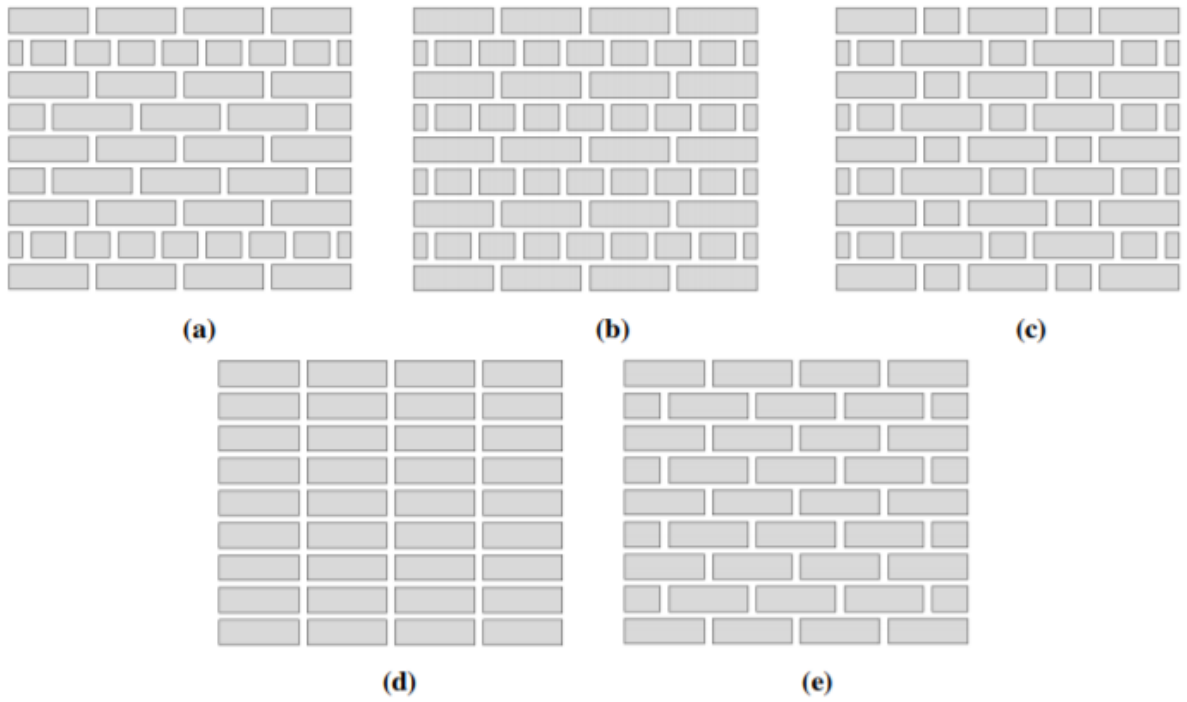

Fig. 1. a) American (or common) bond; b) English (or cross) bond; c) Flemish bond; d) Stack bond; e) Stretcher bond [1]

In the above arrangements, the bricks are named according to their placement in the wall. A stretcher is a brick laid horizontally flat, with its long side exposed on the outer face of the wall. A header is a brick laid flat across the wall's width with its short side exposed. Bricks may be laid in a variety of patterns, or bonds, of alternating headers and stretchers. Masonry can be regarded as a discontinuous material. Bed and head joints are responsible for its discontinuous nature. This feature becomes evident when considering dry joint masonry. The joints induce an anisotropic behaviour in both elastic and plastic domain. As a result, the strength of masonry, highly depends on the geometrical arrangement of units and mortar. There are many

other factors which influence the behaviour of masonry. According to Hendry [2], in general the stress strain behaviour is dependent on:

- units: compressive and tensile strength, type and geometry (solid, perforated, hollow etc.) and absorption capacity;

- mortar: strength, thickness, Poisson's ratio;

- unit-mortar interface: bond between the two, direction of stress and local strain.

The features of the units are possible to be determined during the manufacturing process but the mortar is subjected to variations, since it depends on the constituent materials. A brief introduction on the behaviour of brick and mortar in masonry is given below.

2.2 Brick

The main part of masonry are the brick units which are made by clay, soft slate, shale and calcium silicate. The uses are similar for all the units while they have different properties depending on the raw materials and the way that they are fabricated. Depending on strength, durability, adhesion, thermal properties, fire resistance, aesthetic and acoustic properties occurs the selection of the unit. Bricks are produced in different formats as solid, perforated and hollow (Fig. 2).

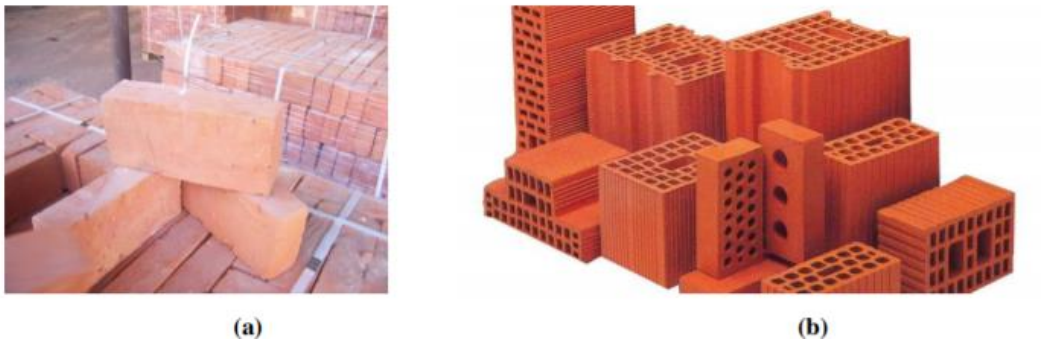

Fig. 2. Types of bricks: a) solid bricks b) hollow bricks

The mechanical characterization of old clay bricks presents a lot of difficulties in collecting samples, the scatter in the properties and the lack of standards for testing [3]. The characterization is important in order to understand the damage, to assess safety, to define the measures and to decide either you can reuse or replace existing materials. Ancient materials have different characteristics compared to the new ones, such as high absorption and porosity and low moduli of elasticity and compressive strength [4]. As for that, a lot of academics have focused on evaluating the aging process, the durability and the physical and chemical deterioration process of clay bricks. Referring to the mechanical parameters, they may vary within the same bath of bricks. It depends on the duration of burning, the temperature, and manufacturing process. All of these parameters contribute to the variation of their properties.

The compressive strength of bricks (f_c) is influenced by the characteristics of the raw material and by the process of production. It is known that the raw clay of old bricks were often from low quality clay and the process of fabricating was primitive and inefficient. This parameter is

characterized by large variability and the range of values found in the literature is quite wide meaning that in situ testing or destructive testing of samples must be carried out when the compressive strength of the brick is required. Other characteristics of existing old bricks can provide information about compressive strength, such as mineral composition, texture, crack pattern and porosity level, by revealing the conditions of drying and firing. Firing was studied and investigated by Elert et al. in [3]. Fig. 3 shows that Viznar clay samples which contain calcite and dolomite have higher compressive strength than Guadix clay samples up to a temperature of 1000 °C which contain no carbonates. At this temperature, the trend is inverted and Guadix samples show higher strength.

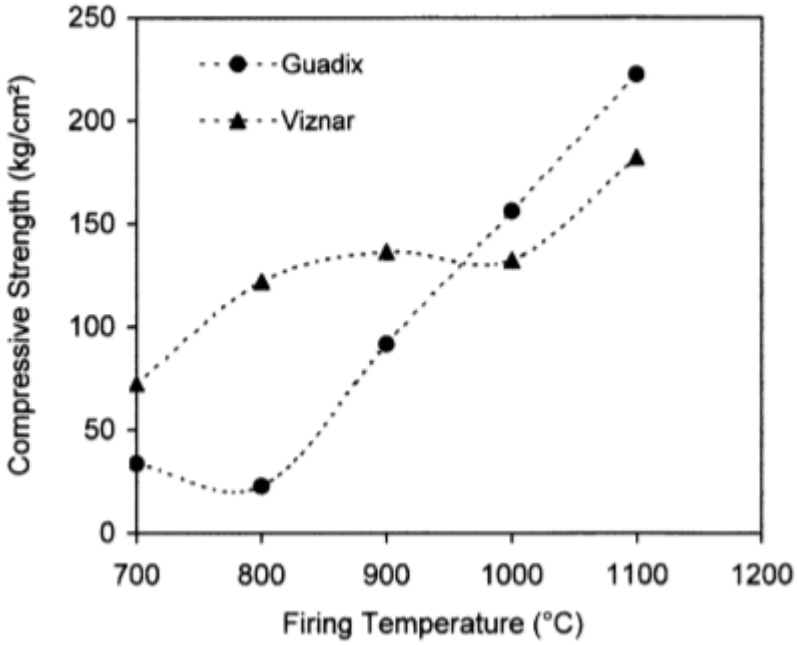

Fig. 3. Compressive strength of evolution upon firing of calcareous (Viznar) and non calcareous (Guadix) clay [3]

The modulus of elasticity (E) is frequently found in the literature and is also characterized by large variability. The values found range from 1 to 18 GPa, which represents a range between 125 and 1,400f_c, where f_c is the compressive strength. The average value of this range that used most in the literature is 350f_c [4]. The Poisson's ratio (ν) influences the relative deformability and appears in certain analytical models of the behaviour of masonry. In the literature, values from 0.15 to 0.20 for the stone and from 0.10 to 0.15 for brick can be found [5].

2.3 Stone

One of the most important parameters used for the classification of the quality of the stone is the strength of the material. It is one of the most reliable methods for classifying rocks and its application for construction purposes. With an acceptable safety margin the strength results can be used directly for the structural requirements. But, rather than the individual properties of the rock-forming minerals, the mechanical strength is influenced more by the heterogeneity of rocks and their fabrics. The strength values apply to the ability of the material to resist stress without failure. The strength of a material depends on the rock fabrics and is affected by its structure, shape and size, the aging of the material and its conditions of storage. Strength is

considered in terms of compressive strength, tensile strength, and shear strength, namely the limit states of compressive stress, tensile stress and shear stress, respectively. For more details see [6].

2.3.1 Compressive strength

Compressive strength demands are made where a planar load to the subsurface surface has to be guaranteed by a material. During an unconfined uniaxial pressure experiment, the test specimen undergoing longitudinal stress would be shortened till failure (Fig. 4). The unconfined comprehensive strength (UCS) of a dry specimen demonstrates the value when the specimen suffers a complete loss of cohesion with a typical stress-strain curve along the fracture surface as shown in Fig. 5.

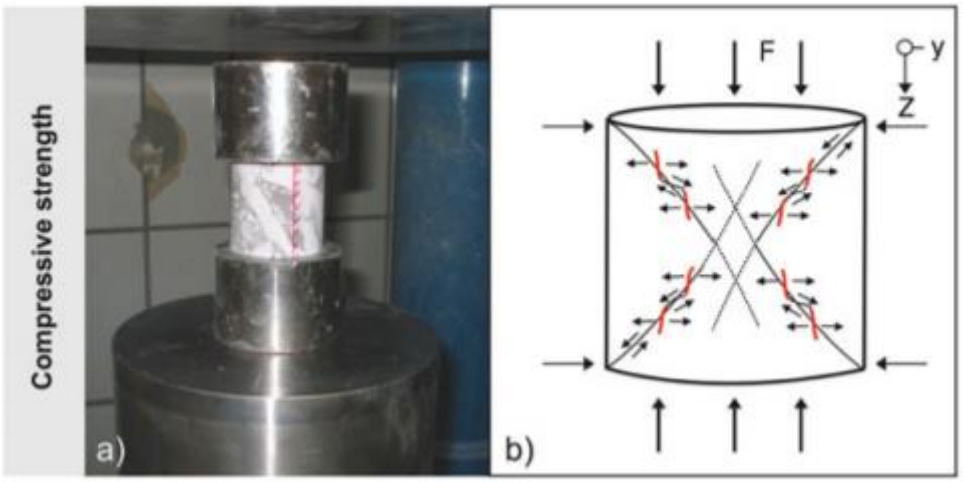

Fig. 4. Experimental setup a) for determining the uniaxial compressive strength. b) Rock failures occur through a combination of tensile and shear cracks, F = loading force [6]

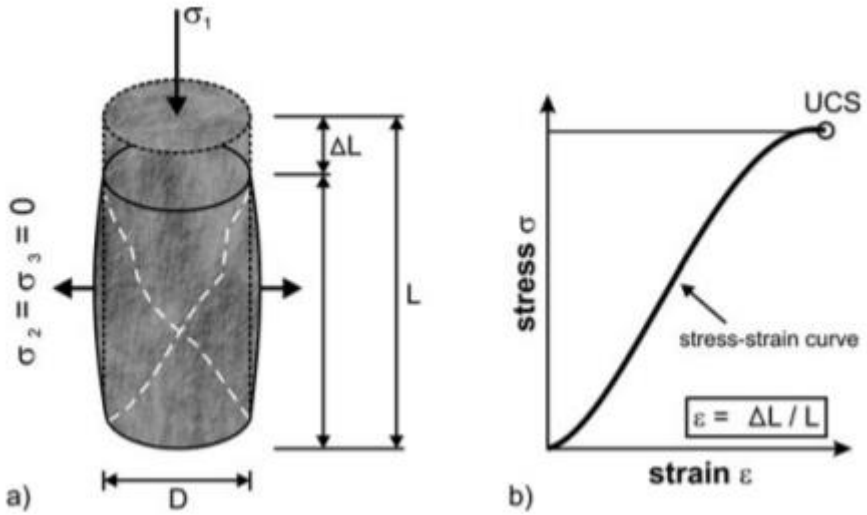

Fig. 5. Unconfined compressive strength (UCS) test: a) a core with failure under unconfined compression, b) a stress-strain curve where the UCS marks the failure of the specimen [6]

During this process, the pre-existing microcracks are sealed, ideally those that are perpendicular to the loading axis. This results in an irreversible shortening of the test specimen, but with fairly small values. At about 30% to 70% of the compressive strength value, the rock

sample shows a nearly linear elastic behaviour. After that there is a rise in the development of microcracks, which eventually contributes to the ultimate material failure. Minimum values for compressive strength are needed for certain applications of natural dimension stones. This criterion demonstrates that the experimental setups and specimens used in the assessment of the compressive strength must be comparable and equivalent. Uniaxial compressive strength is the most important efficiency factor used by engineers for rock quality evaluation. Compressive pressure is measured by cylindrical, cubic or prismatic specimens in a compression testing machine. Usually the compressive load is applied by a servo-hydraulic testing machine with a very stiff testing frame and a class 1 load range up to 300 kN. The most important is the preparation of the sample, the size of the sample and the consistency of the end surfaces, which must be co-planar with precision of 0.1%. The load is applied to the end-faces of the specimen with a strain rate of 10^{-5} s^{-1} until failure. The maximum load is defined as the uniaxial compressive strength.

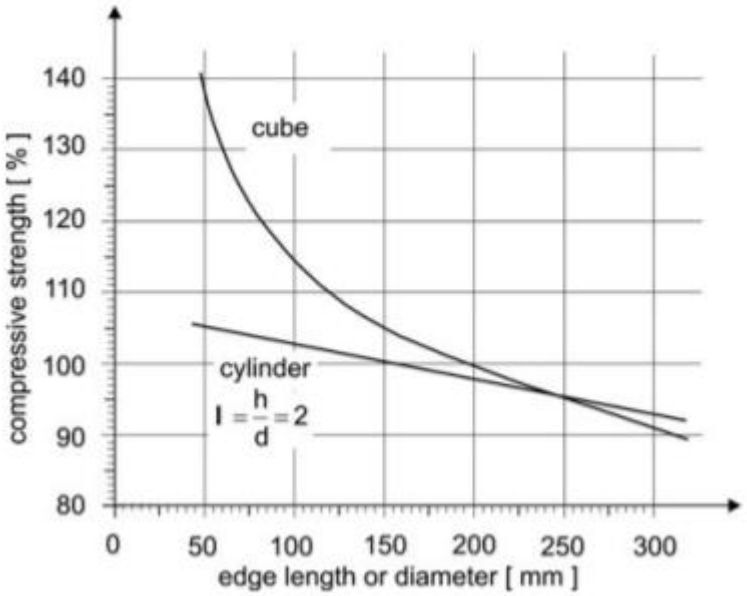

Fig. 6. Effect of the geometric shape of a test specimen (here a cylinder and cube) on its compressive strength

In compliance with DIN EN 1926 (1999), compressive strength can still be calculated by using cubes with an edge length of 50 mm or cylindrical samples with a diameter and height of 50 mm. In particular, the compressive strength calculated with cylindrical samples depends on the length-diameter-ratio as shown in Fig. 6. As for the drying of the samples, on the one hand that the drying is carried out at 70 ° C until a constant mass has been reached; on the other hand, a dry air state which has not yet been specified may be illustrated.

In general, the following discrimination for the classification of the rocks is made: hard rock with more than 110 MPa, medium hard rocks between 70 MPa and 110 MPa and weak rocks between 55 MPa and 70 MPa. Plutonic rocks varies between 60 MPa and 292 MPa, while a much higher value with 427.7 MPa is given for the gabbro “African Blue” from South Africa. Dolerites from Uruguay varies from 400 MPa to 265 MPa while Volcanic rocks range between 50 MPa and 300 MPa. For the group of carbonate rocks, they vary between 4.4 MPa and 265 MPa and sandstones show a variation from 10 MPa to 257 MPa. Finally, metamorphic rocks tend to have a high variation on the compressive strength values. For more details see [6].

Fig. 7 presents the typical value ranges with a regard to the mechanical properties of the stones after a statistical analysis studied in [6].

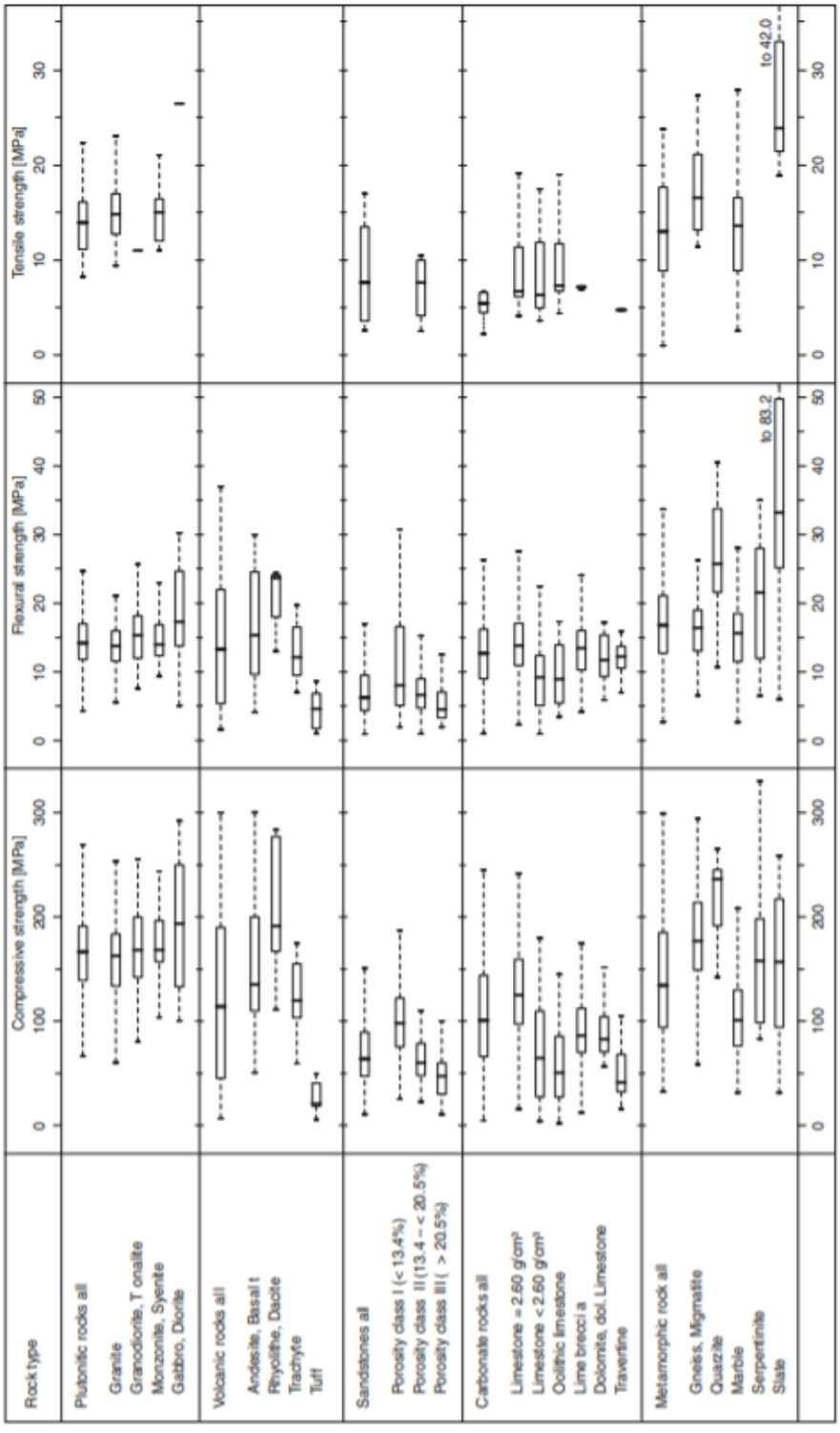

Fig. 7. Typical lithological value ranges with regard to the mechanical strength parameters (e.g. compressive, flexural, and tensile splitting strength) put together on the basis of a statistical analysis of natural stones. The boxplots describe the corresponding median value, the 25% and 75% quartile value as well as the upper and lower extreme value [6]

2.3.2 Young's modulus E

The modulus of elasticity, generally referred to as Young's modulus (E), is based on the interaction between stress and strain. This value is also known as the static module obtained by the tangent, secant or average approach.

The so-called tangent modulus corresponds to the 50 per cent-value of the uniaxial strength, the secant modulus is taken as the gradient of the total uniaxial compressive strength of the stress-strain curve from the origin to the 50 per cent-value, and the average modulus represents the mean slope of the straighter component of the stress-strain curve.

The key variables that affect the static E-modulus are the mechanical properties of the minerals and the dimensions of the grains relative to the compressive strength. The relationship of the modulus of elasticity and the compressive strength for certain magmatic material is indicated in Fig. 8. Nevertheless, these parameters do not inherently correspond to the dynamic E-module. In addition, open microcracks are an important effect parameter. During a uniaxial pressure experiment, a rock specimen undergoes both elastic and, respectively, plastic deformation. The above is not likely to occur during the evaluation of the dynamic E-modulus, as the time intervals for the specimen under loading stress are comparatively short. Because of this, the value of the dynamic E-modulus will always be greater than that of the static E-modulus. The disparity between the two values grows with increasing porosity and fracturing of the rock sample. For more details see [6]

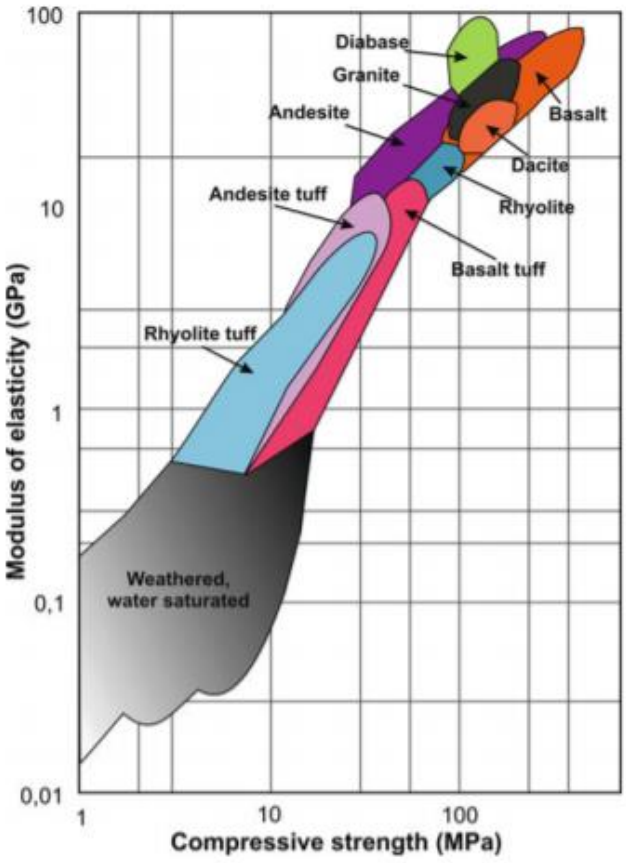

Fig. 8. Relationship between the modulus of elasticity and the compressive strength of selected rock types [6]

2.3.3 Uniaxial compressive behaviour and assessment of the Young's modulus on cylindrical stone specimens

In the study of Lourenco et al [7], cylindrical specimens (Ø50 × 120 mm^2) were used, resulting in a height/diameter ratio (h/d) of 2.4, for which a uniaxial stress state is expected in the centre of specimens.

In order to compute the values of Young's modulus and Poisson's ratio, two stone specimens (SS3.1 and SS4.1) were tested with three double electric resistance strain gauge rosettes attached to each specimen, equally spaced around the perimeter and placed at mid-height. The characterization of specimen's behaviour in terms of its elastic properties, the evolution of Young's modulus (E), Poisson's ratio (ν) and volumetric strain (ε_{vol}) is presented in Fig. 1 for specimen SS3.1, where E_{lvdt} and E_{sg} represent the computed Young's modulus using lvdt and strain gauge data, respectively. In order to represent different quantities in the same diagram, different scales were used which are not represented in Fig. 9.

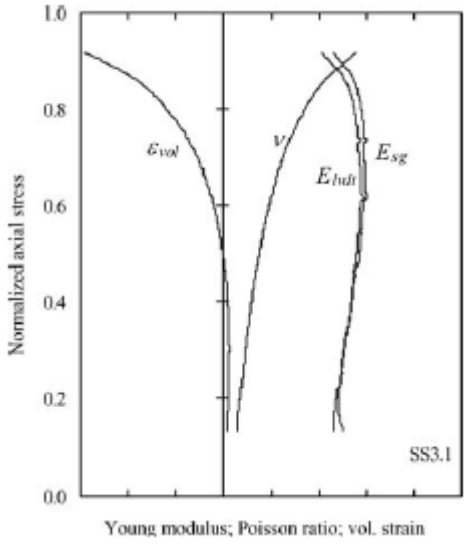

Fig. 9. Typical variation of Young's modulus (E_{lvdt} and E_{sg}), Poisson's ratio (ν) and volumetric strain (ε_{vol}) with stress level for stone specimens (specimen SS3.1 and different units in the abscissa axis) [7]

By increasing the load, the closure of existing microcracks and voids produced an increase in Young's modulus. At higher stress levels, Young's modulus started to decrease due to the initiation of macrocracks, whereas Poisson's ratio increased continually with the load. This behaviour can be explained by microcrack closure, for lower stress levels, and the initiation/propagation of cracks, for higher stress levels. This means that variations in E and ν are clearly related to the fracture of the specimen.

Initially, a slight volume reduction took place, caused by axial compression, being followed by an important volume increase due to crack formation. For half of the peak load, there was no volume variation, which means that crack formation took place for relatively lower stresses. The very large positive volume variation for higher stresses in compression can be explained by splitting fracture. This phenomenon of positive volume variation in compression is known as dilatancy. For a load near half of the ultimate load, Poisson's ratio equals his theoretical

maximum elastic value, equal to 0.5. This means that dilatancy has a major importance in the behaviour of the specimen and that microcracking starts at relatively low stress levels.

Fig. 9 also shows also that E and ν were greatly affected by the nonlinearities in the stone's behaviour, which renders difficult to define the elastic properties from uniaxial test results. The procedure defined by ASTM [7] allows the use of several methods employed in engineering practice, consequence of the difficulties described above. Following the ASTM proposal, Young's modulus can also be defined as the average slope of the linear portion of the stress-strain diagram. For the specimens tested, the straight-line portion is located in the [30%–60%] stress range; the values of E obtained within this range, using linear least square regressions, are presented in Table 1.

Table 1. Young modulus defined in the [30% - 60%] stress range for the specimens SS3.1 and SS4.1 [7]

Specimen	E_{lvdt} [GPa]	E_{sg} [GPa]
SS3.1	13.68	13.86
SS4.1	17.71	19.20

The elastic modulus calculated using strain gauges is greater than the value obtained using the data from lvdts (the axial lvdt measurements could be influenced by the platens movement), but differences are not significant (less than 9%), which seems to indicate that data obtained by means of lvdts may be used to evaluate Young's modulus in specimens tested without strain gauges. Following the test procedure afore-mentioned, four monotonic tests and six cyclic tests were performed in order to characterize the complete stress-strain diagram (based on data acquired via lvdts), as well as the cyclic behaviour of sandstone. Fig. 10 illustrates typical stress-strain diagrams obtained under monotonic and cyclic loading. The diagrams exhibit the well known bedding down effect, characterized by an initial adjustment between the specimen and the machine platens. As expected, pre-peak behaviour was easily followed, but the post-peak branch, where the load decreased in a very unsmooth way, showed to be unstable and could only be characterized with great effort. The first macroscopical cracks were visible only for a load very close to the peak one, starting at the extreme ends and progressing through the entire specimen.

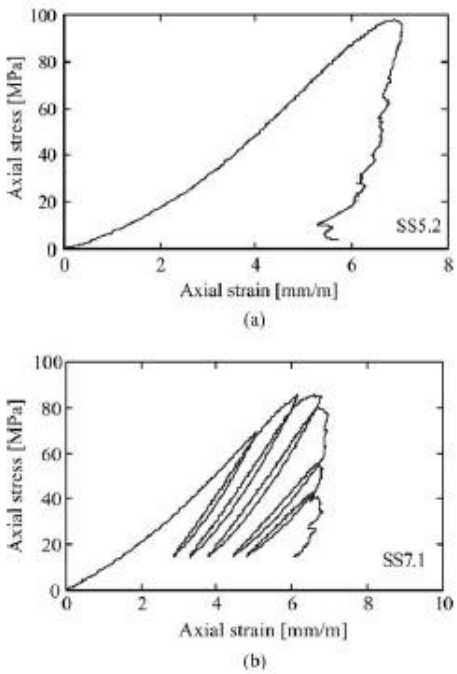

Fig. 10. Typical stress-strain diagrams of stone specimens tested under uniaxial compression: a) monotonic, b) cyclic loading [7]

Table 2. Young's modulus and compressive stremgth of stone specimens tested under uniaxial compressive loading [7]

Specimen	E_{30-60} [GPa]	σ_{peak} [MPa]
SS2.2	9.50	61.1
SS2.3	10.46	68.6
SS3.2	12.64	70.4
SS4.2	15.54	84.5
SS5.1	17.49	93.9
SS5.2	17.89	98.0
SS6.1	19.56	86.6
SS6.2	20.30	87.8
SS7.1	15.62	85.4
SS8.1	16.49	90.2
Average	15.55	82.7
CV (%)	22.26	13.7

The Young's modulus of all stone specimens, evaluated within the [30%–60%] stress range, is showed in Table 2, as well as the compressive strength (CV is the coefficient of variation). The average value shows that the uniaxial compressive strength of the stone is rather high. Furthermore, the maximum Young's modulus value is greater than the double of the minimum value obtained. The differences found between the several tested specimens in terms of compressive strength and Young's modulus indicate that the intrinsic variability of these properties is an important issue that should be considered when dealing with natural stone structures.

Regarding the cyclic behaviour of the stone specimens, unloading-reloading cycles were done both during pre-peak and post-peak. In the pre-peak region, a slight increase of stiffness occurred, which is in agreement with the monotonic results obtained from tests using strain gauges. On the other hand, a monotonic decrease of stiffness in the post-peak region was observed. This decrease is naturally related with the progressive damage growth suffered by the specimen. For more details see [7].

2.4 Mortar

Mortar is a workable paste used to connect masonry blocks and fill the gaps between their surfaces [8]. It becomes hard after its production when it sets and as time passes it gains stiffness and resistance, resulting in a rigid aggregate structure. The mortar in the masonry is carrying out three functions [5]: the filling of the joints, avoiding the passage of water; the regularization of the disposition of bricks and the uniform distribution of the load; cooperate to lead horizontal stresses until the foundations.

Mortars typically are composed of binder, aggregates, water and mixture. Mortar is used for different applications. The properties and characteristics of the mortars mainly depend on the binder. We can mention bitumen, gypsum, clay, lime, cement and etc. as a binder. Admixtures materials (natural or artificial) have been added to mortar for avoiding of shrinkage, crack and for increasing total strength. Different materials like blood, egg, fig juice, pig grease, manure and straw have been used as admixture in different country and periods.

Hydraulic lime was the principal frame for mortar up to the mid 1800's when Portland cement was first developed as a material. Although it was weak and slow in setting and developing strength, when compared to cement mortars, mortars produced with hydraulic lime were adequate for the relatively thick walls and lower stresses that generally characterized the more massive masonry construction of former times.

According to the European standard EN 459-1 hydraulic limes can be classified into three sub families:

- Natural Hydraulic Lime (NHL): this is produced by burning argillaceous or siliceous limestone and then reducing it to a powder by slaking with or without grinding;

- Formulated Lime (FL): it contains air lime and/or natural hydraulic lime with added hydraulic or pozzolanic material;

- Hydraulic Lime (HL): this is a binder consisting of lime and other materials such as cement, blast furnace slag, limestone filler and other suitable materials.

There are three compressive strength grades for these three categories in accordance with EN 459-2. Concerning natural hydraulic lime, it is traditionally classified as shown (Table 3), where the number that follows the acronym NHL, refers to the compressive strength of lime at 28 days.

Table 3. Traditional mortar classification

Type of lime	Name
NHL 2	Feebly Hydraulic Lime
NHL 3.5	Moderately Hydraulic Lime
NHL 5	Eminently Hydraulic Lime

Non-hydraulic lime or aerial lime is the principal binder of most traditional mortars. Air lime is used for the preparation or the production of materials used in building construction. Air

lime when appropriately batched and mixed with water, forms a paste that improves the workability (values of flow and penetration) and water retention of mortars. The carbonation of hydrates in contact with atmospheric carbon dioxide forms calcium carbonate which develops strength and contributes to the durability of mortars containing building lime (hence the name of air lime).

2.4.1 Mechanical characterization of the mortar : Laboratory tests

The tests that needed to be evaluated were the following and studied in [9][10][11]. [9] deals with methods of determining the compressive strength of mortar in the bed joint of masonry for suitability testing purposes and for calculating the compressive strength of masonry. [10] investigates the compressive strength of the mortar samples that have been obtained after the removal of mortar by an existing bulding and has been performed by gradual increase of the compressive force up to the sample failure while the experimental part of [11] describes the testing of specimens made of irregular samples of historic and modern mortars in compression.

- **Mortar compressive test**

The compressive strength is evaluated directly by the compression test of the mortar according to the EN 1015-11:2007 which develops the following technique:

"The cubes are placed in a hydraulic press and apply the load without shock and increase it continuously until failure occurs. The standard suggested diferent loading rates depending of the mortar category.".The compressive strength, f_c [MPa] is calculated like:

$$f_c = \frac{F}{A}$$

Where: F = maximum load [N]; A = load platens area equal to 40 mm^2

- **Double punch test**

The determination of masonry mortar characteristics is a fundamental task for cultural heritage conservation, however, when the analysis occurs to historical masonry which belongs to heritage, only small and irregular mortar specimens are most of the times available for testing. Whereas such specimens can be suitable for performing micro-structural characterization [12]. Some methods also have been proposed in the literature review for estimating the mechanical properties of the mortar by making use of small samples [13]. In particular, one of the most used method is the double punch test [14] following the german standard DIN 18555-9 [9]. In the same investigation the authors found the optimal diameter of the mortar equal to 20 mm.

Investigation on the influence of mortar quality, mortar porosity, mortar curing and confining effect of mortar surrounding the loaded are were reported in the literature. The importance in these tests refers to the mortar joints specimens for punching which are more representative of the realistic behaviour inside the masonry.

As [15] explain in their research, the strength of the mortar join specimens are related with their thickness as shows Fig. 11.

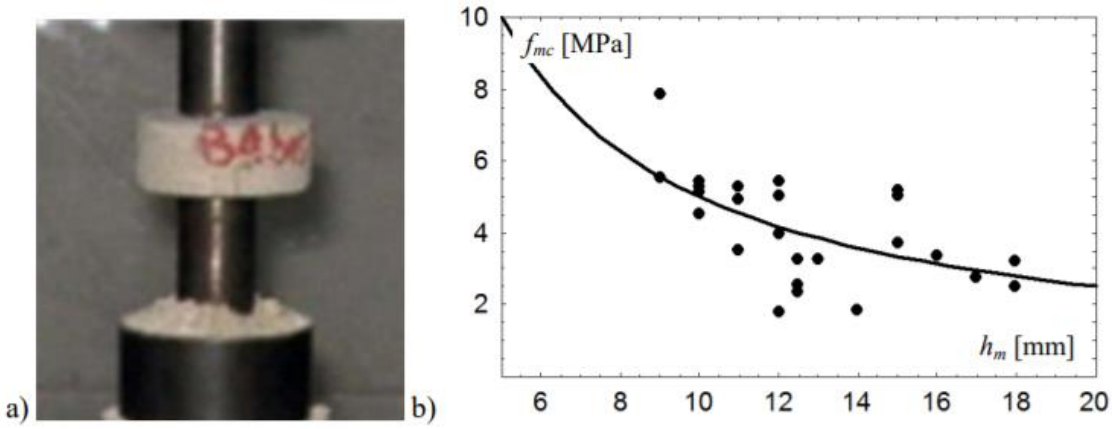

Fig. 11. a) DPT, b) strengths as function of the thickness [15]

2.4.2 In-situ minor destructive testing

- Windsor pin penetrometer system (PPT)

Windsor pin penetrometer test (PPT) is a minor destructive testing technique as to estimate the compressive strength of mortar or concrete. A steel pin is penetrated into the surface of the mortar with the help of the Windsor pin system WP-2000® which shoots that pin. At the top of the WP-2000® there is a reaction nut which is tightened in order to load the spring system with a defined amount of energy. After the shooting at the surface and the penetration of the steel pin, the compressive strength of the mortar can be measured by measuring the overall penetration depth as they are inversely proportional. The instrument is obtained with some table data sheets from which we can estimate the compressive strength depending of the penetration depth. [16]

Fig. 12. Windsor pin penetrometer system

The in-situ procedure of the pin penetration test was done following the steps:

1. insertion of the pin into the removable ring;
2. tightening the reaction nut with the use of a wrench until the trigger is ready to shot and the instrument is loaded;
3. removal of the nut by untightening it;
4. placement of the instrument in a flat mortar surface, absolutely perpendicular to the wall (Fig. 13a);
5. pull the trigger;

6. cleaning of the hole with a rubber bulb-type blower;
7. insertion of the micrometer (Fig. 13b);
8. reading the penetration depth that is visible on the micrometer.

Fig. 13. a) Instrument for the pin penetration, b) micrometer for depth measurement

- Screw (helix) pull-out tests (HPT)

The HPT is a minor destructive technique which is carried out on the joints of the walls. Firstly, a hole of 3 mm is drilled on the mortar joint and a hole of 4 mm is drilled on the brick. A high strength helical tie with a diameter of 6 mm is placed into a driving tool. This driving tool is placed vertically to the wall and hit at the back side with a hammer. The exposed end of the tie enters the pilot hole of the mortar joint or of the brick. This procedure allows the tie to rotate and cut a thread in the mortar during insertion [16]. After the installation, a gripper is screwed onto the end of the helical tie in order to keep the tie fixed and restrained from rotating as to ensure a shear failure in the mortar. Then, the loading device is attached to the gripper and the assembly is rotated to screw down the tie and take up any slack. The load applied to the tie is increased steadily until failure. The peak load reached during each test is recorded as the pull-out force and read by a needle. In order to start the procedure where the helical tie is screwed down the applied force should reach a specific value.

Fig. 14. a) Helical ties ready for extraction, b) Insertion of the helix into the bed joint using the sleeved driving tool, c) Pull-out with the loading device

- Torque Penetrometric Test (TPT)

The apparatus that used for this technique is composed of a designed steel nail and a torque wrench. The nail is obtained from a F212 hexagonal steel piece after a milling procedure (characteristic tensile and yield strengths: 760 MPa and 510 MPa). Due to the high performance of that steel, the risk of torque failure is reduced. It is considered that with this type of geometry the uncertainties of previous studies like Christiansen's X-Drill are reduced. [17] The proposed TPT method presents important technical improvements in order to overcome the limitations of the X-Drill. First, the toothed part of the steel piece is only 15 mm long in order to remove the error related to the measurement of L_w parameter. The remaining part of the steel has a smooth cylindrical shape with 6.5 mm diameter. This solution grants a constant depth of investigation L_w = 15 mm. In fact, once the instrument is completely inserted into the material, only the front part of the nail can be effectively in contact with mortar, whereas the remaining length of the shank cannot (Fig. 15). Second, the TPT apparatus developed in this campaign allows a deeper insertion of the steel, testing an inner volume of material and bypassing the external layer of the mortar joint (Fig. 15). The length of the shaft is 40 mm but it could be modified on the basis of the experimental needs. Finally, the external diameter of the F212 steel piece is reduced to 9 mm (Fig. 15) trying to avoid experimental results spoiled by the undesired contact with the bricks.

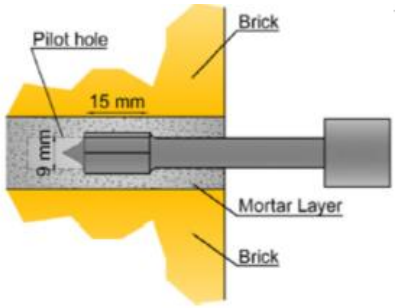

Fig. 15. TPT which was used in the campaign

The in-situ procedure of the torque penetrometric test [18] was done following the steps:

1. realization of a 6 mm diameter pilot hole to drive the instrument into the mortar joint;
2. check that no brick powder is extracted and that the rate of advance is regular and constant;
3. hammering of the nail inside the pilot hole (Fig. 16b);
4. use of a torque wrench to measure the necessary torque to bring the material to failure (Fig. 16c);
5. removal of the toothed nail from the mortar joint;
6. final visual check as to control the material in-between the wings since the possible presence of brick powder might indicate an incorrect measurement, biased by the hit unit.

In this campaign, a dynamometric torque wrench equipped with a digital display was used for torques from 1 to 20 N·m with an accurancy of 0.01 ± 4% N·m (Fig. 16c). The resolution of the digital transducer is higher than the analogic one, although the precision can be very similar since it is based on the quality of the device [18].

Fig. 16. a) Nails ready for the application of the torque, b) Hammering of the nails in situ, c) Use of the digital torque wrench to measure the necessary torque to bring the material to failure

2.5 Brick masonry

2.5.1 Behaviour of the masonry under uniaxial compression

Failure criterion

The uniaxial compressive strength of masonry in the direction normal to the bed joints has been usually considered as the most relevant structural material property. The uniaxial compressive strength in the direction parallel to the bed joints has been less studied, even if it could have an important role on the load bearing capacity, especially in the presence of low longitudinal compressive strength of the units, due to a high perforation. A large amount of studies has been realized in order to understand and describe the behaviour of the masonry under a uniaxial compressive load, among which: [19], [20], [21], [22], [23], [24] and [25]. In particular, the study of Hilsdorf [22] demonstrated that the failure of masonry is due to the different elastic properties of the unit and the mortar. Units are stiffer than mortar, and the difference is even greater in ancient masonry, built with lime mortar. Thus, when masonry is loaded with a uniaxial compression, the mortar in the horizontal joints tends to expand laterally at higher rates than units, which confines it and avoids its lateral extension. This mechanism leads to the formation of a tri-axial compression in the mortar and of vertical compression/horizontal biaxial tension in the unit (Fig. 17). As a consequence, vertical cracks appear in the units and they grow up until the masonry failure.

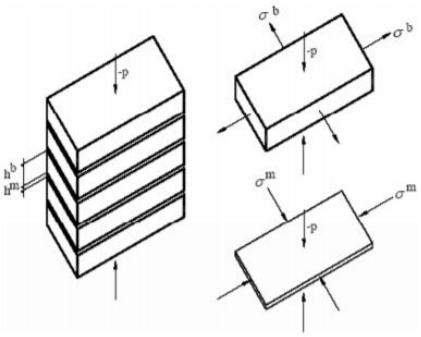

Fig. 17. Masonry prism under uniaxial compression and the stress distributions in units and bed joints

For a compression perpendicular to the bed joints, it could be observed the phenomenon discussed previously: units fail in tension, creating cracks which can coincide with the location of the vertical joints. If the load direction is parallel to bed joints, the splitting of the bed joints in tension occurs. For intermediate states, a combination of both behaviours is observed, with a mixed failure involving cracking of bricks and splitting or sliding in joints [26].

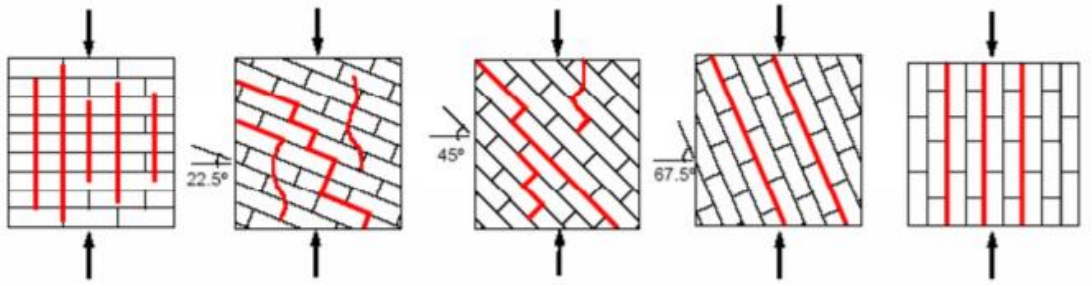

Fig. 18. Modes of failure of clay units masonry under uniaxial compression

The behaviour of the masonry under uniaxial compression was investitaged and carried out through experiments in the UPC laboratory in [24]. The experimental programme included compression tests on two different type of specimens (running bond walls and stack bond prisms), under monotonic and cyclic loading. The types of masonry sample are shown in Fig. 19. For more details on the mechanical characterization of the brick and mortar and the testing procedure see [24].

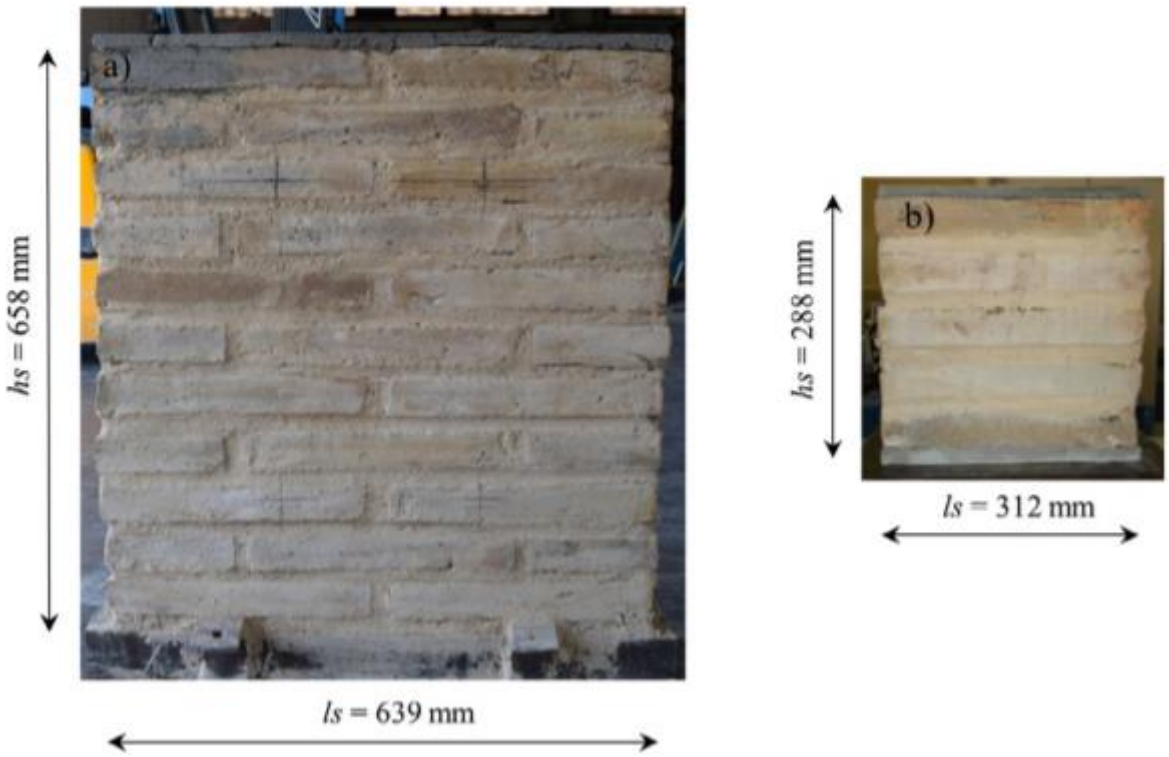

Fig. 19. Masonry samples, average dimensions. a) Running bond walls, b) Stack bond prisms. Common average thickness t_s = 148 mm. [24]

The experimental results are presented for each type of specimen. Compressive strengths were calculated as the ratio between the load and the cross section area. The reading of the LVDTs

were divided by their reference lengths and averaged to obtain axial srains. Stress-strain curves were obtained for all the tests.

For the running bond walls, the Young's modulus was calculated with an average value of 2318 MPa, the compressive strength at an average value of 6.51 MPa and the strain at peak stress of 0.98 %. The results obtained are presented in Table 4, while the stress-strain curves in Fig. 20.

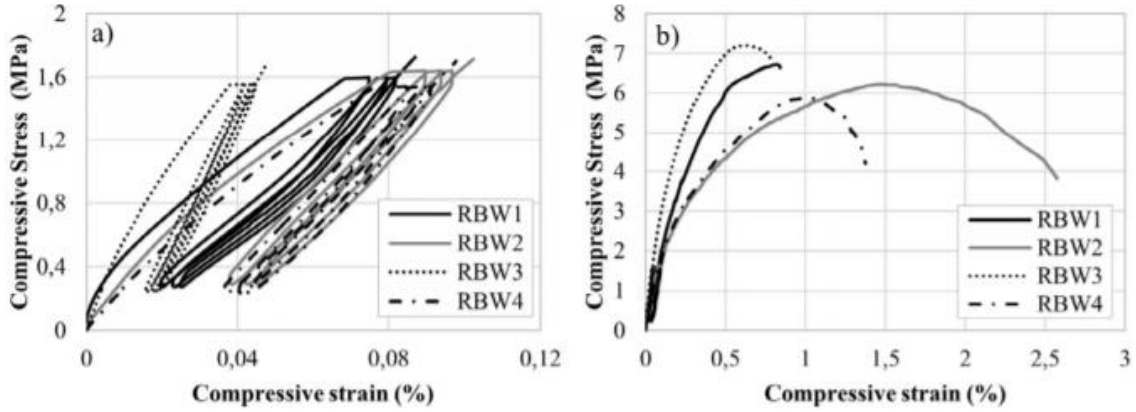

Fig. 20. Stress vs strain experimental curves for running bond walls. a) Detail of three loading/unloading cycles, b) Full curves until failure [24]

Table 4. Compressive strength, stiffness and strain at peak stress of running bond walls [24]

RBW	f_c (MPa)	E_c (MPa)	ε_p (%)
RBW 1	6.72	2205	0.82
RBW 2	6.22	2227	1.48
RBW 3	7.20	4023	0.62
RBW 4	5.88	2521	1.00
Average	6.51	2744	0.98
CV	8.9%	31.5%	37.6%
Average		2318*	
CV		7.6%*	

* The value of E_c for RBW3 is not considered in the average.

For the stack bond prisms, 4 were tested in monotonic loading following the same testing procedure. Young's modulus was calculated with an average value of 2494 MPa, the compressive strength at an average value of 6.49 MPa and the strain at peak stress of 1.2 %. The results obtained are presented in Table 5, while the stress-strain curves in Fig. 21.

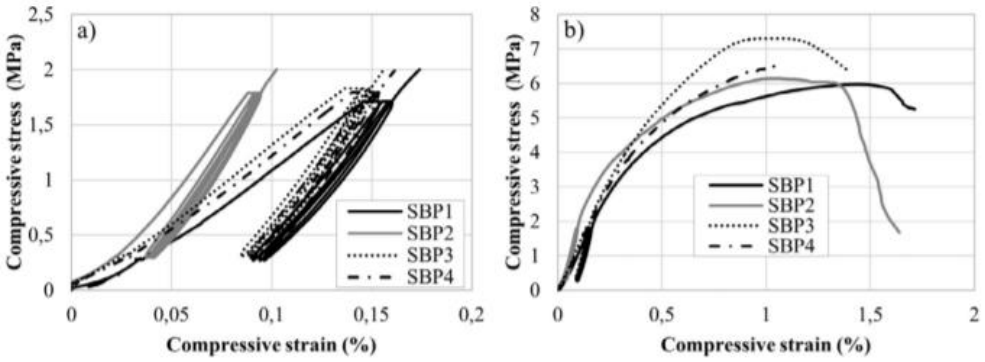

Fig. 21. Stress vs strain curves of the stack bond prisms with monotonic loading. a) Detail of the three loading/unloading cycles and beginning of the second stage, b) Full curves until failure. [24]

Table 5. Compressive results of stack bond prisms [24]

SBP mono	f_c (MPa)	E_c (MPa)	ε_p (%)	SBP cyclic	f_c (MPa)	E_c (MPa)	ε_p (%)
SBP 1	5.98	2249	1.45	SBP 5	6.91	1957	0.90
SBP 2	6.15	2782	1.05	SBP 6	7.34	2549	1.09
SBP 3	7.31	2443	1.10	SBP 7	7.03	2634	1.00
SBP 4	6.52	2502	1.05				
Average	6.49	2494	1.16	Average	7.10	2380	1.00
CV	9.1%	8.8%	16.4%	CV	3.1%	15.5%	9.4%

The failure mode of running bond walls and stack bond prisms under monotonic loading is presented in Fig. 22 and in Fig. 23 respectively. For more details on the crack mechanism see [24]

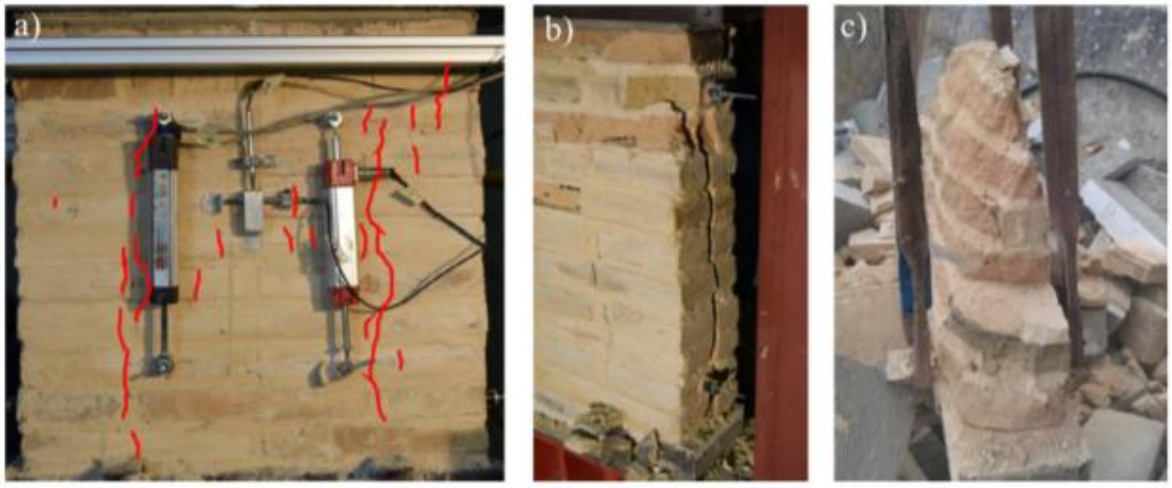

Fig. 22. Failure of running bond walls. a) Crack pattern at peak load, b) State at the end of the test, c) Dismantled specimen [24]

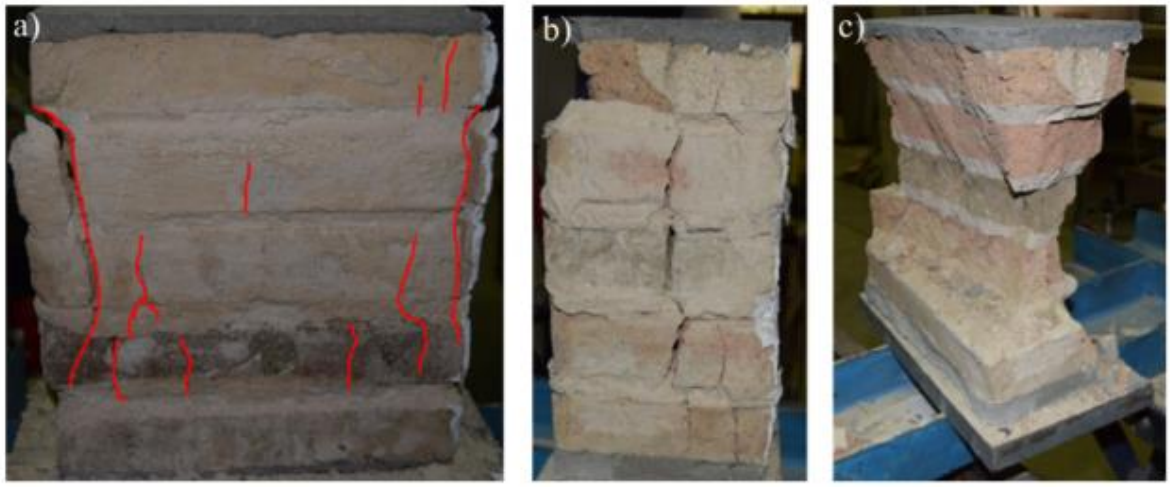

Fig. 23. Stack bond prisms after failure. a) Front view, b) Lateral view, c) Dismantled specimen [24]

Three stack bond prisms were tested cyclically at the second loading stage until displacement control failure. The failure mode observed under cyclic loading was the same as the stack bond prisms under monotonic load. The experimental results are characterized by an average Young's modulus of 2380 MPa, a compressive strength of 6.95 MPa and a strain at peak stress of 1.0 %. The stress-strain curves of the two stack bond prisms are presented in Fig. 24 with a complete set of 8 cycles composed of the three initial ones corresponding to the first stage, two

more cycles on the pre-peak range and three additional cycles after the peak load. For more details see [24].

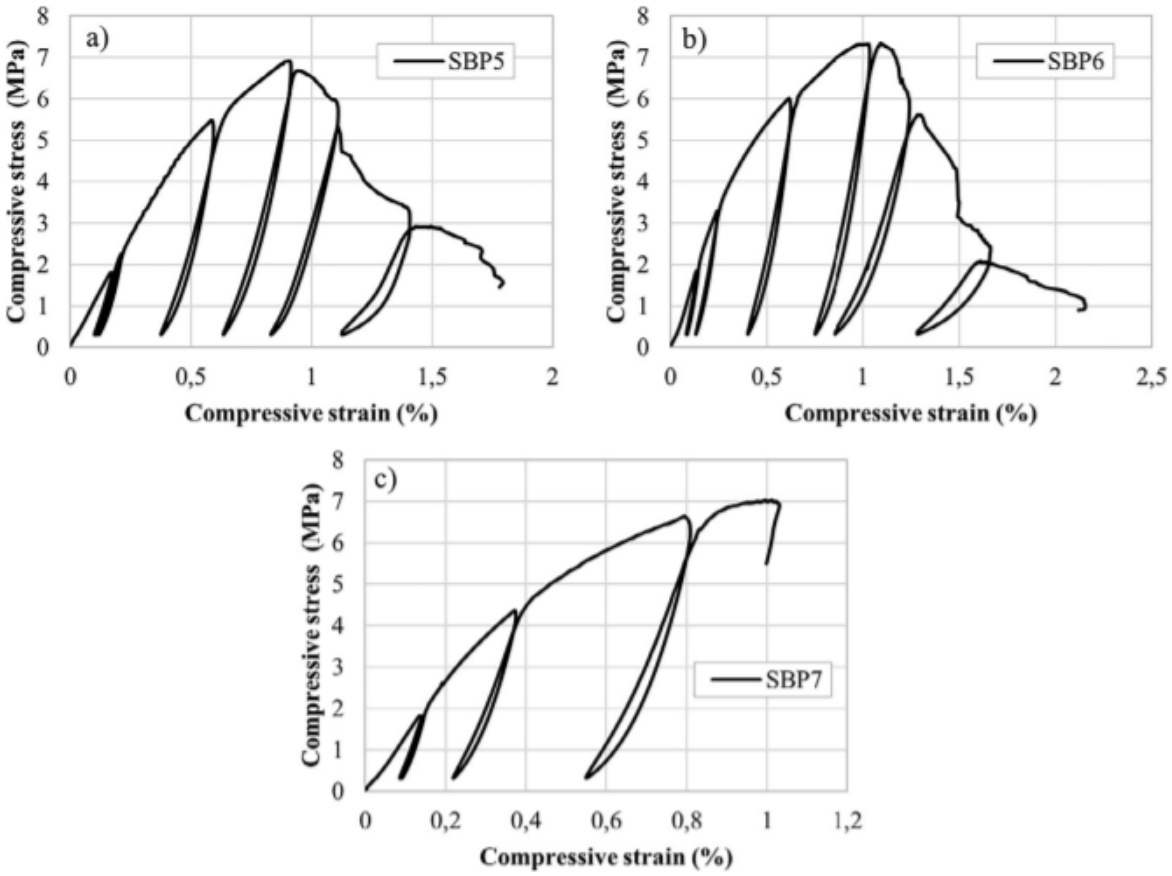

Fig. 24. Stress vs. strain experimental curves of the stack bond prisms with cyclic loading until failure. a) SBP5, b) SBP6 [24]

In Section 4 of [24] the experimental results are compared with analytical and empirical expressions in order to investigate the validity of the existing predictive equations and models for the estimation of the compressive strength and the elastic modulus of masonry and the simulation of its compressive behaviour and the results are presented.

The following conclusions were carried out:

For the specific combination of materials studied, the tests on the two types of standard specimens have provided similar results in terms of compressive strength and deformability. Additional research should be carried out to extend this conclusion to other types of masonry. The results revealed the stiffness degradation of the masonry due to increased strains. Also, the static stress-strain curves can be used as a reasonable approximation of the peak range of the cyclic tests. The modulus of elasticity of the masonry is recommended to be measured after the application of several cycles and finally the evaluation of the masonry's compressive strength have provided similar results for the experimental and the analytical or empirical expressions, while for the evaluation of the Young's modulus, the criteria proposed by the standards have overestimated the experimental values. For more details and analytical discussion, see [24].

2.5.2 Compression test on extracted masonry cylinders

The masonry mechanical properties apart from the brick and the mortar properties depend also on the texture, the presence of voids and the defects. Even the brick properties can be obtained from the construction precisely, the evaluation of the mortar properties is more difficult and the results are scattered. To overcome this issue, a suitable way is proposed with the of laboratory destructive testing on small specimens [14]. Without causing several damage in the construction, the simplest specimen that can be obtained is a cylindrical core either with one or two or three joints. An innovative minor destructive test is the compression test on the extracted cylinders refereed above proposed by UIC 778-3R (International Union Railways 1995).

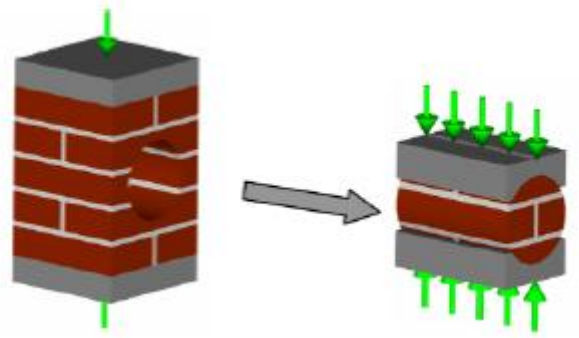

Fig. 25. Extraction of the cylinder, direction of the load

The cylinder diameter is recommended to be 150 mm [27]. The compressive strength of the masonry is given by the following equation:

$$f_c = \frac{F_{coll}}{dl}$$

where all the area of the cylinder is assumed to resist the load.

The test setup is shown in Fig. 26.

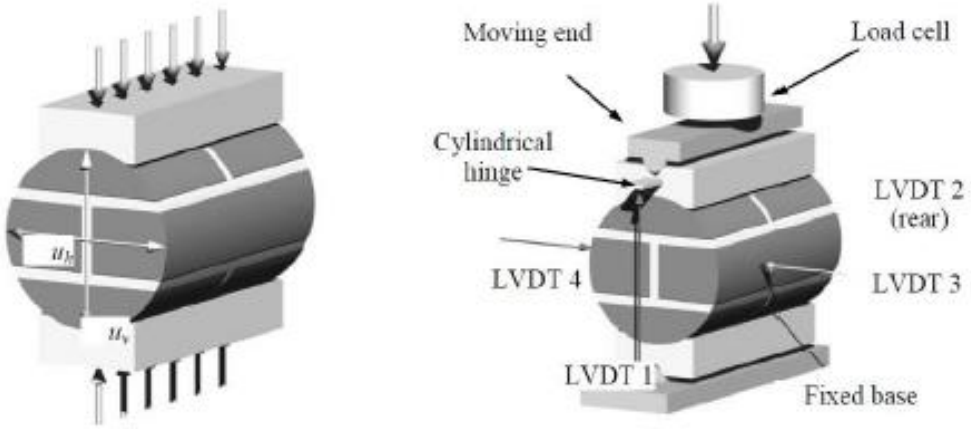

Fig. 26. Test setup [27]

The compressive strength of the extracted cylinders was investitaged through experiments in the UPC laboratory in [28], [29], [30] and [31]. In [28] cylindrical samples of 150 mm diameter

were extracted from masonry with the use of dry core-drilling procedure and after regularization they were tested under compression in the laboratory. The experimental results of the cylinders were compared with the ones obtained from standard compression tests on prismatic samples consisting in stack bond prisms and verified also by numerical simulation of the cylindrical samples under compression. Two-joint cylinders (2JC) with two horizontal joints and three-joint cylinders (3JC) with two horizontal and one vertical mortar joints were extracted and used for compression tests following the procedures presented in [31] and [29]. The test of six 2JC and six 3JC consisted in applying a compressive loading on the regularization caps perpendicularly to the bed joints (Fig. 27). The compression machine was equipped with a 200 kN load cell. Both the vertical and horizontal displacements were recorded through four linear variable differential transformers (LVDTs). The first stage was performed under load control by carrying out three loading/unloading cycles in order to evaluate the elastic response of masonry. The cycles were performed between the 5% and 20% (3 kN - 20 kN) of the originally expected maximum load. The second loading stage was performed under displacement control, at a rate of 0.004 mm/s. For more details on the test setup of the cylindrical cores and the stack bond prisms see [28].

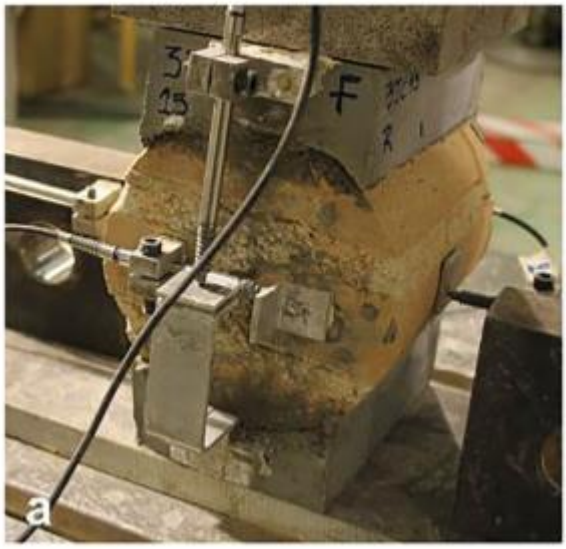

Fig. 27. Experimental setups for compression tests on core samples [28]

As for the results, the compressive stress acting on the cylindrical specimens was evaluated considering two different values. The stress value σ_1 was calculated by considering the total diametric section of the cylinder, while the stress value σ_2 was obtained by using the section of the regularization cap. The first approach is the one suggested by the UIC 778-3 recommendations to calculate the compressive strength of masonry from cylindrical specimens.

Fig. 28 shows the stress-strain curves calculated for the first stage of loading/unloading for both 2JCs and 3JCs, as well as the curves obtained for the last loading stage beyond failure. As mentioned, the loading/unloading cycles were used to evaluate the Young's modulus of the material. They were evaluated making reference to both σ_1 and σ_2 values, leading to the definition of the relevant values E_1 and E_2. As for the evaluation of the compressive strength

values, the value f_{C1} was defined considering the maximum force divided by the diametric cross-section of the cylinder, while the value f_{C2} was obtained considering the maximum force divided by the cross-section of the regularization cap.

Table 6 presents a summary of the experimental results from compression tests on core samples. As for the values of f_{C1} and f_{C2}, the 2JCs provided average values of 4.25 MPa and 6.17 MPa, whereas the 3JCs provided average values of 3.98 MPa and 5.78 MPa, respectively. As for the values of E_1 and E_2, the 2JCs provided average values of 1182 MPa and 1716 MPa, whereas the 3JCs provided average values of 1323 MPa and 1921 MPa, respectively. For more details on the experimental results and the failure mode see [28].

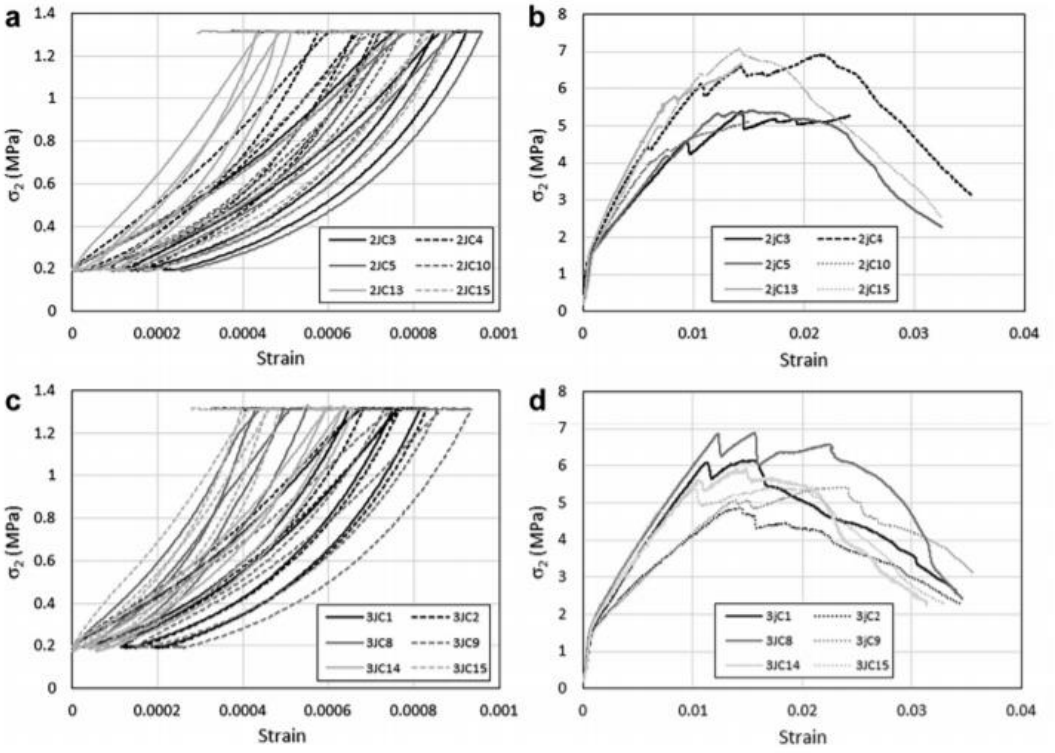

Fig. 28. Stress vs. strain curves of core samples: elastic loading/unloading cycles for two-joint (2JC) (a) and three-joint cylinders (3JC) (c); loading beyond failure for two-joint (b) and three-joint cylinders (d) [28]

Table 6. Experimental results of compression tests on core samples in terms of compressive strength and Young's moduli [28]

Sample 2JC	f_{C1} (MPa)	f_{C2} (MPa)	E_1 (MPa)	E_2 (MPa)	Sample 3JC	f_{C1} (MPa)	f_{C2} (MPa)	E_1 (MPa)	E_2 (MPa)
2JC3	3.72	5.40	1007	1463	3JC1	4.23	6.15	1137	1652
2JC4	4.76	6.91	1272	1848	3JC2	3.36	4.88	1127	1637
2JC5	3.73	5.42	985	1431	3JC8	4.74	6.89	1588	2306
2JC10	3.58	5.20	1109	1610	3JC9	3.73	5.42	1019	1479
2JC13	4.82	7.00	1707	2479	3JC14	4.08	5.92	1254	1822
2JC15	4.88	7.09	1009	1466	3JC15	3.74	5.43	1811	2631
Average	4.25	6.17	1182	1716	Average	3.98	5.78	1323	1921
CV %	13.6	13.6	21.5	21.5	CV %	11.04	11.05	21.4	21.4

Fig. 29 shows the comparison of the experimental results for prismatic and cylindrical samples, in terms of average values of Young's modulus and compressive strength. For more details on the comparison, discussion and verification through numerical models see [28]

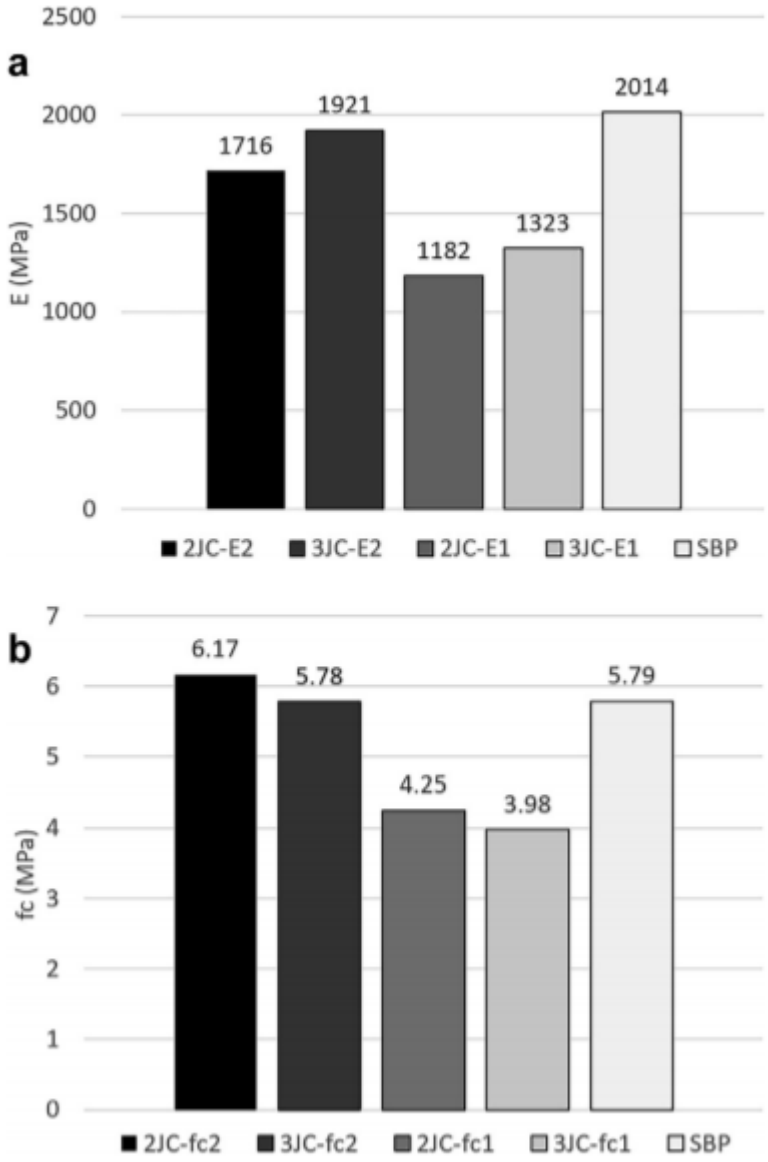

Fig. 29. Comparison between compression tests on cylindrical samples and stack bond prisms: a) Young's modulus, b) compressive strength [28]

In [29] extracted core cylinders made of clay brick and low-strength lime mortar with different diameters are tested in the laboratory of UPC under compression. Two type of specimens were tested: 150 mm diameter cores with two horizontal joints, a vertical mortar joint and four brick pieces (3J) and 150 mm diameter cores with two horizontal joints and three brick pieces (2JC). The 2J and 3J specimens were assigned to the compression test suggested by the UIC 778–3 recommendations after the regularization of the mortar cap (Fig. 30). The results from the proposed non-standard tests are discussed and compared with those derived from conventional tests on the same materials, like tests on mortar prisms or compression tests on stack-bonded prisms. For more details on the test setups and on the stack bond prisms see [29].

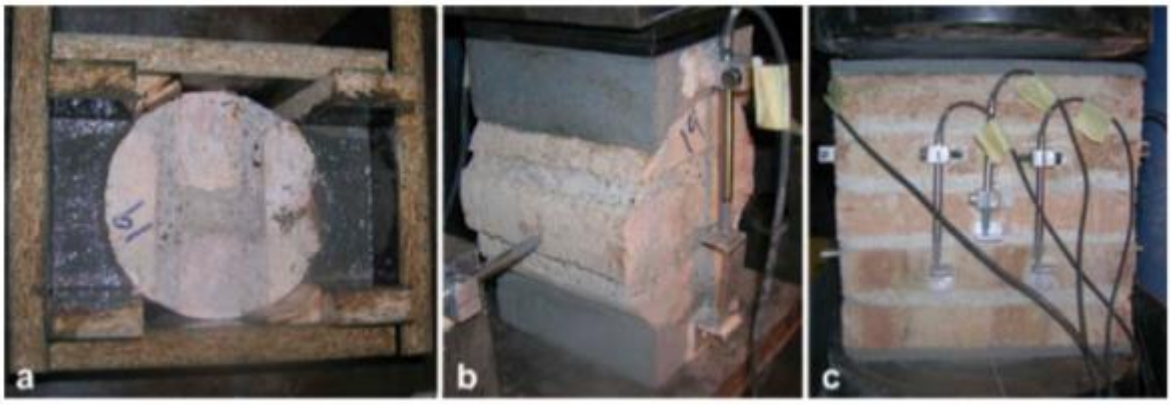

Fig. 30. Regularization of a 150 mm diameter core by cement mortar caps (a). Compression test setups for 3J and 2J cores (b) and stack-bonded prisms (c) [29]

The stack-bonded prisms were tested under initial loading and unloading cycles, showing stiffening behavior due to micro-cracks and voids closure in mortar. Then, the samples were loaded until failure. Table 7 reports the compressive strength (f_c) obtained from the compression tests on stack-bonded prisms and the summary of the main results obtained from compression tests on 3J and 2J cylindrical specimens in terms of ultimate load and strength with the values of f_{C1} and $f_{C2,}$ representing the calculation referring to the whole horizontal section of the cylindrical specimen and to the section of the regularization cap respectively.

Table 7. Experimental results of compression tests on stack-bonded prisms, 3J and 2J cylindrical specimens [29]

Stack Bond Prisms			3J samples				2J samples			
Sample	F_{max} (kN)	f_c (MPa)	Sample	F_{max} (kN)	f_{C1} (MPa)	f_{C2} (MPa)	Sample	F_{max} (kN)	f_{C1} (MPa)	f_{C2} (MPa)
SP1	328.28	8.84	17a	123.95	6.36	7.95	21a	144.41	7.41	9.26
SP2	308.96	8.32	17 b	128.05	6.57	8.21	21 b	172.07	8.82	11.03
SP3	324.83	8.75	19	132.42	6.79	8.49	23a	161.93	8.30	10.38
			20a	141.45	7.25	9.07	23 b	152.81	7.84	9.80
			20 b	140.64	7.21	9.02	24a	165.61	8.49	10.61
							24 b	150.40	7.71	9.64
Average	320.69	8.64	Average	133.30	6.84	8.55	Average	157.87	8.10	10.12
CV (%)	3.2	3.2	CV (%)	5.8	5.8	5.8	CV (%)	6.6	6.6	6.6
Charact. value	288.23	7.76	Charact. value	114.40	5.87	7.34	Charact. value	133.54	6.85	8.56

The compression test on 150 mm diameter cores proposed by the UIC 778–3 R (UIC 1995) has shown to be a suitable technique to evaluate the compressive strength of existing masonry. Some improvements to the test layout have been proposed in this article, like the regularization of the lateral surfaces of the cylindrical specimens by high-strength mortar capping instead of concave steel loading plates, in order to simplify the preparation of specimens and to avoid local stress concentrations during testing. Furthermore, the 2J specimens have provided an average compressive strength 18% higher than the 3J specimens' one, showing that the absence of the vertical mortar joint increases the load bearing capacity of the cylindrical sample. The non-standard compression tests of 3J and 2J cylindrical specimens have provided strength values in good agreement with those derived from standard tests on stack-bonded prisms while the average compression strength of 3J specimens resulted 21% lower than the stack-bonded prisms, whereas the compression strength of 2J specimens was only 6% lower. For more details on the comparison, discussion and the failure mode see [29].

2.5.3 Theoretical determination of the compressive strength of masonry

The comprehensive experimental studies undertaken over recent decades about the characterization of the ultimate strength of masonry under uniaxial compression, have led to the formulation of some empirical relationships which permit to calculate it. Generally, these formulas provide the compression strength of masonry on the basis of the mechanical properties of units and mortar.

One of these empirical relationships can be found in the Eurocode 6 (EN 1996-1-1:2005), that provides the following expression to calculate the characteristic compressive strength of masonry (f_k) in the event of lacking experimental results, and for bed joint thickness comprised between 10 and 15 mm:

$$f_k = k \times {f_b}^{0.7} \times {f_m}^{0.3}$$

Where f_b is the average compressive strength of units [MPa], obtained according to the standard EN 772-1 (2002), f_m is the average compressive strength of mortar [MPa], obtained according to the standard EN 1015-11 (1999) and k is a value that depends on the type of brick used (between 0,35 and 0,55 for clay units).

In the equation contained in the Eurocode it can be observed that in the majority of cases the masonry strength will be lower than that of its individual components and the units strength is more determinant that the mortar strength. According to experimental observations, a masonry structure subjected to a uniaxial compressive state achieved the collapse in the presence of tensional states lower than the bricks compressive strength, due to the weakening effect due to joints. Furthermore, as has also been observed experimentally, the masonry resistance increases with increasing compressive strength of the unit and with reducing the joints thickness, although the latter usually is not reflected in the formulas.

Furthermore, the following recommendations of specific international regulations on existing brick masonry are considered useful in order to compare the values given by them with the experimental results of the brick cylinder compression tests

- The Italian regulation NTC2018 Circolare 21 of 2019, specifically in table C8.5.I, gives maximum values of compressive strength of 4.3 MPa and minimum of 2.6 MPa for masonry of the type “Solid brick masonry and lime mortar” as shown in Table 9.

In case of mortar joints thicker than 13 mm for solid brick masonry it is advisable to reduce the values listed with a reduction coefficient of 0.7 for the compressive strengths and 0.8 for the Young’s modulus.

- The UIC (UIC 1995), specifically in the "Clay brickwork" table in section A3.3.1, gives masonry strength values based on the strength of the components as shown in Table 8.

Table 8. Masonry compressive strength fck in N/mm² as a function of the material and mortar compressive strengths – Clay Brickwork

MATERIAL COMPRESSIVE STRENGTH (N/mm²)	MORTAR COMPRESSIVE STRENGTH (N/mm²)							
	10	7.5	5	2.5	1	0.4	0.2	0
30	6.6	6.0	5.6	5.0	4.4	3.6	3.4	3.0
25	6.0	5.6	5.0	4.4	3.8	3.2	3.0	2.6
20	5.4	5.0	4.4	3.6	3.2	2.8	2.6	2.0
15	4.4	3.8	3.6	3.0	2.6	2.4	2.0	1.6
10	3.6	3.4	3.0	2.4	2.0	1.8	1.6	1.2
5	3.0	2.8	2.4	1.8	1.4	1.2	1.0	0.6

2.6 Stone masonry

In stone masonry walls of great complexity and irregularity, the procedure of the assessment of the compressive strength of the stone wall is complicated. Eurocode 6 (EC6 1996-1-1) and the Basic Document SE-F of the Spanish Technical Building Code do not provide formulas for obtaining the compressive strength of the rubbled stone masonry walls.

However, the following recommendations of specific international regulations on existing stone masonry are considered useful as to compare the values given by them with the experimental results of the stone cylinder compression tests.

- The Italian regulation NTC2018 Circolare 21 of 2019, specifically in table C8.5.I, gives maximum values of compressive strength of 2.0 MPa and minimum of 1.0 MPa for masonry of the type “Disordered Stone Masonry (Gravel, discontinuous and irregular stone)” as shown in Table 9.

- The UIC (UIC 1995), specifically in the "Crushed Stone" table in section A3.3.1, gives masonry strength values based on the strength of the components as shown in Table 10.

Table 9. Reference values of the mechanical parameters of the masonry

Tipologia di muratura	f (N/mm²) min-max	τ_0 (N/mm²) min-max	f_{v0} (N/mm²)	E (N/mm²) min-max	G (N/mm²) min-max	w (kN/m³)
Muratura in pietrame disordinata (ciottoli, pietre erratiche e irregolari)	1,0-2,0	0,018-0,032	- -	690-1050	230-350	19
Muratura a conci sbozzati, con paramenti di spessore disomogeneo (*)	2,0	0,035-0,051	- -	1020-1440	340-480	20
Muratura in pietre a spacco con buona tessitura	2,6-3,8	0,056-0,074	- -	1500-1980	500-660	21
Muratura irregolare di pietra tenera (tufo, calcarenite, ecc.,)	1,4-2,2	0,028-0,042	- -	900-1260	300-420	13 ÷ 16(**)
Muratura a conci regolari di pietra tenera (tufo, calcarenite, ecc.,) (**)	2,0-3,2	0,04-0,08	0,10-0,19	1200-1620	400-500	
Muratura a blocchi lapidei squadrati	5,8-8,2	0,09-0,12	0,18-0,28	2400-3300	800-1100	22
Muratura in mattoni pieni e malta di calce (***)	2,6-4,3	0,05-0,13	0,13-0,27	1200-1800	400-600	18
Muratura in mattoni semipieni con malta cementizia (es.: doppio UNI foratura ≤40%)	5,0-8,0	0,08-0,17	0,20-0,36	3500-5600	875-1400	15

Table 10. Masonry compressive strength fck in N/mm² as a function of the material and mortar compressive strengths - Crushed stone

MATERIAL COMPRESSIVE STRENGTH (N/mm²)	MORTAR COMPRESSIVE STRENGTH (N/mm²)							
	10	7.5	5	2.5	1	0.4	0.2	0
100	5.0	4.4	3.6	2.4	1.6	1.0	0.8	0.7
80	4.4	4.0	3.2	2.0	1.4	0.9	0.7	0.6
60	4.0	3.4	2.8	1.8	1.3	0.8	0.6	0.5
40	3.0	2.6	2.2	1.6	1.1	0.7	0.5	0.4
20	2.2	2.0	1.6	1.2	0.9	0.6	0.4	0.3
10	1.6	1.4	1.2	1.0	0.7	0.5	0.3	0.2
5	1.3	1.1	0.9	0.7	0.5	0.4	0.2	0.1

An experimental campaign in order to characterize the mechanical behaviour of load bearing rubble stone masonry walls is investigated in [32]. Compression tests were carried out in two small specimens of 40×40×40 cm^3 to characterize the compressive strength and the Young's modulus. Two different mortars were used to build the specimens, air lime mortar (to simulate traditional walls in old buildings) and hydraulic lime mortar (to simulate the walls in less older buildings)

As for the specimens execution, the stone used was the most common of Lisbon buildings with an average compressive strength of 50 MPa. During the execution, the stones were chosen to maximize the fitting and to leave the fewest possible voids. The biggest stones were used in the corners and edges and the spaces among them were filled with mortar and small pieces of stone. The obtained mean values for the compressive strength of the mortar were 1.47 MPa for the hydraulic and 0.56 MPa for the air lime mortar. Rubble masonry specimens for compression tests were made using stone units with variable shape and dimensions, which were randomly assembled.

In the compression tests, the two masonry specimens (C1 and C2 – hydraulic and air lime mortar specimens, respectively) were tested in an hydraulic press under the load capacity of 3000 kN with one displacement transducer placed on the panel's sides and were loaded until the rupture. The compressive strength f_c and the Young's modulus E were evaluated as:

$$f_c = \frac{F_{y,max}}{A}, E = \frac{F_{y,max}}{3 \times \varepsilon \times A}$$

where $F_{y,max}$ is the maximum load reached on a specimen, A is the specimen loaded cross-section, and ε is the strain of the specimen when a load of 1/3 of the maximum load was achieved.

Table 11 Presents the results of the compression tests and Fig. 31 presents the force-displacement diagram.

Table 11. Compression test results [32]

Masonry Specimens	Type of mortar	$F_{y,max}$ (kN)	f_c (MPa)	E (GPa)
C1	Hydraulic lime	1282	8.01	1.64
C2	Air lime	1186	7.41	0.56

E is the secant value at 1/3 of the ultimate load.

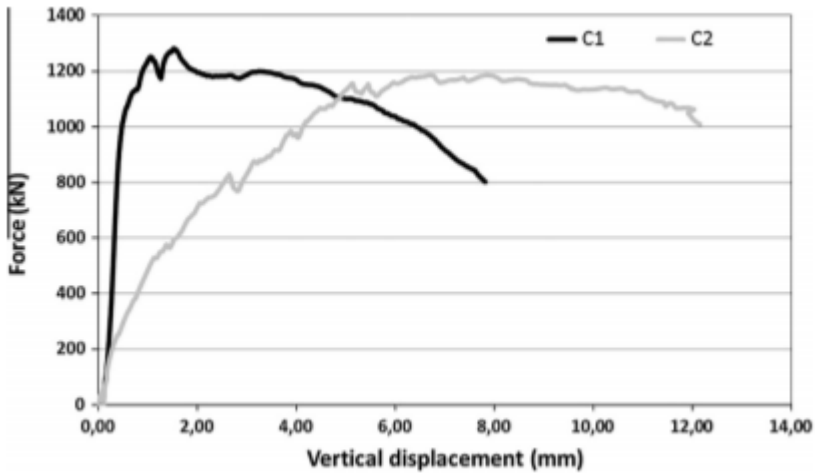

Fig. 31. Compression tests – ''force–displacement'' diagrams [32]

The experimental results revealed an unusual correlation between the strength of the hydraulic and air lime specimens, which can be explained by the observed failure modes. In both cases, the failure involved the crushing of stone to stone, and the mortar type had a minor impact on the ultimate strength of the specimen. Due to the irregularity of the stone units used during the execution of the specimen, the mortar joints had a non-uniform thickness with thin layers of mortar between some of the irregularities of the stones. As a result of the mortar crushing at the advanced stage of loading, some stone edges came into contact with each other, and the strength of the stones controlled the behavior of the specimens under compression. Failure by stone crushing explains the similarities between the strength of the two specimens and also the exceptionally high compression strength obtained for both types of masonry. This effect would possibly be reduced in a larger study, where there would be a greater impact of the quality of the mortar. On the other hand, the lateral expansion at the top and bottom of the specimens was limited by the loading plates in the compression tests recorded in this paper, resulting in a confinement effect that tends to increase the compressive capacity of the specimens. Due to the size of the specimens, the in-plane confinement effect that could occur in long walls has not been simulated. Owing to these variations, the findings of the compression tests must be assumed to be basically representative.

The evaluation of the compressive strength and the Young's modulus for traditional stone masonry showed an f_c = 7.41 MPa, E = 0.56 GPa for air lime mortar specimens and f_c = 8.01 MPa, E = 1.64 GPa for hydraulic lime mortar specimens, results that must be regarded as indicative values due to the limited number of performed tests and to the test boundary condition. Two contradictory effects of the test boundary conditions may have affected the results, i.e.: the dimensions of the specimens do not reproduce the in-plan confinement of real long loadbearing walls; and the confinement imposed by the bearing plates at the top and bottom of the specimens does not exist in real situations. For more details on the other implemented tests and on the discussion of the research see [32].

2.7 Numerical modelling of the non-standard tests on masonry

The double punch test on the mortar joints has been never analysed before in the literature and for this reason is proposed to be performed in this study in Chapter 5 in order to provide a novel contribution to the field.

The compressive test on cylindrical core samples extracted from existing masonry is a test that was carried out in [28] both experimentally and numerically in order to investigate the behaviour of the specimens and evaluate the compressive strength of the material by comparing the results of the two approaches. The experimental ones are presented analytically in [28] and in Section 2.5.2. A numerical insight into the evolution of the resisting and failure mechanisms of two joint cylinders (2JC) and three joint cylinders (3JC) is provided.

The cylindrical samples are simulated by using a continuum finite element approach with distinct modelling of the mortar, the brick and the regularization mortar cap using the finite element analysis software COMET, while GiD is used for the pre- and post-processing, both developed at the International Centre for Numerical Methods in Engineering (CIMNE) in Barcelona, Spain (Fig. 32).

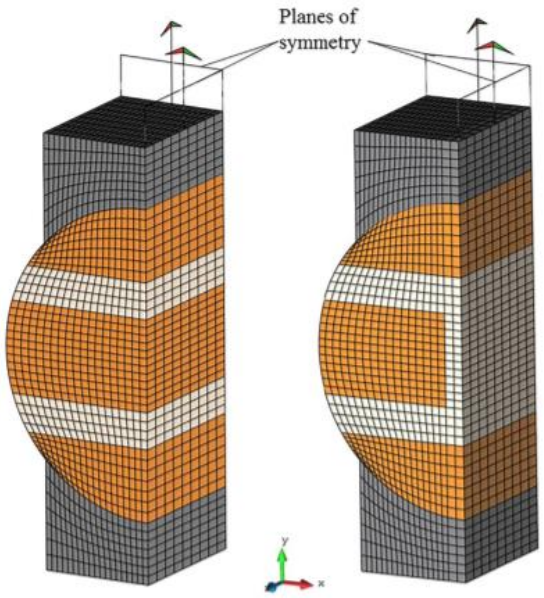

Fig. 32. Finite element meshes used in the numerical simulations for the two joint cylinder (left) and the three joint cylinder (right). The planes of symmetry are those having a normal vector with direction towards the +x and the –z [28]

Table 12 presents the mechanical properties of the brick and mortar used in the numerical model. For more details on the definition and selection of the properties see [28].

Table 12. Mechanical properties of brick and mortar used in the numerical simulations [28]

Property	Brick	Mortar
E (MPa)	7140	100
ν (–)	0.18	0.25
f_t (MPa)	1.64	0.24
f_c (MPa)	21.49	0.91
G_{ft} (J/m^2)	126	80
G_{fc} (J/m^2)	34,400	1440
f_{c0} (MPa)	10.75	0.405
ε_{pc} (–)	0.025	0.045
f_{bc}/f_c	1.15	1.5
ρ (–)	0.75	0.75

Fig. 33 presents the graphs of experimental and numerical force against vertical displacement at the top of the cap for the case of the 2JCs. For each experimental graph, the loading-unloading cycles are omitted and the part of the graph before them is reproduced using the tangent to the curve after the end of the cycles.

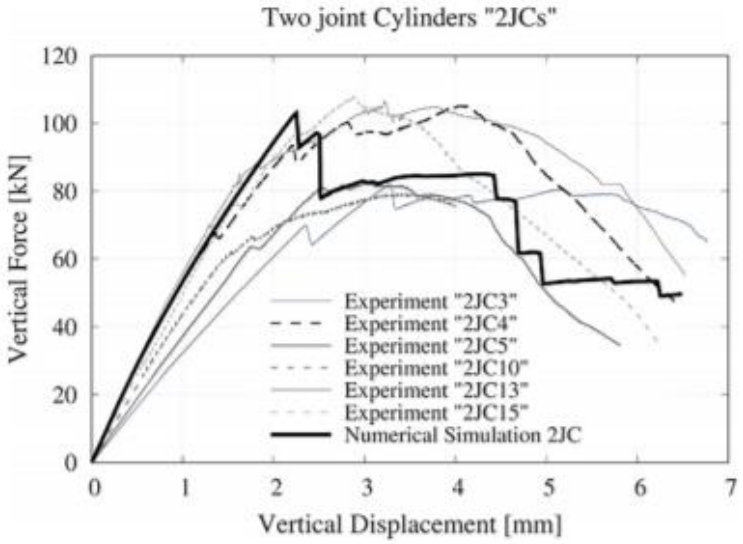

Fig. 33. Two joint cylinder specimens: graphs of experimental and numerical force against displacement at the top of the sample [28]

The numerical simulation predicts a peak strength of 103.0 kN. This value falls within the limits given by the experimental results, which are between 79.1 kN for 2JC13 and 107.9 kN for 2JC15.

Fig. 34 presents the graphs of experimental and numerical force against vertical displacement at the top of the cylinder for the case of the 3JCs. As for the 2JCs, the part before the loading-unloading cycles is reproduced using the tangent to the curve after the end of the cycles. The numerical analysis predicts a capacity of 96.7 kN for the 3JCs, which falls within the limits of the experimental results defined by the capacity of 3JC2 and 3JC8 samples of 74.6 kN and 104.9 kN, respectively. Similar to the experimental results, the numerical simulations predict a reduction of the capacity of the cylindrical cores due to the presence of the vertical joint of -5.9%. This value is very close to the experimentally measured reduction in the capacity of the cylinders of - 6.3%. The numerical simulation represents the ideal case of a perfectly filled head joint attached to the central brick, which is rarely the case of existing masonry. This fact justifies the slightly lower reduction of the capacity due to the existence of the head joint compared to the experimental results. For more details on the failure mechanism, the compressive and tensile damage and the distribution of the stresses on the cylindrical cores see [28].

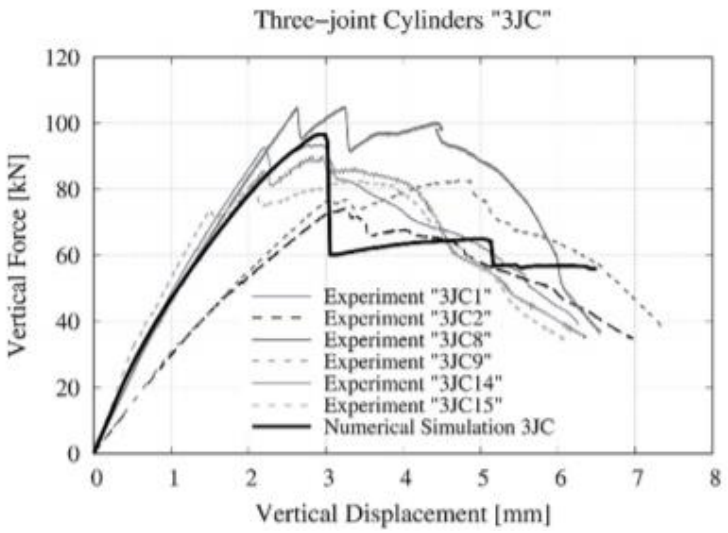

Fig. 34. Three joint cylinder specimens: graphs of experimental and numerical force against displacement at the top of the sample [28]

The paper has presented the numerical simulation of the compression tests of the 2JCs and 3JCs with the aim to interpret their resisting mechanism and identify the procedure for the calculation of the compressive strength. The numerical simulations have predicted correctly the capacity given by the experimental results and the hourglass failure mechanism of both the 2JCs and 3JCs. The vertical stress distributions within the FEM models of the cylinders indicate that the parts outside the regularization parts have a limited contribution to the resistance of the specimen under compressive loading. The numerical study has complemented the experimental outcomes with further insight into the mechanical behaviour of the extracted cylindrical specimens when tested under compression. For more details on conclusions and the discussion see [28].

Chapter 3: Experimental campaign

3.1 Case Study: Escola Industrial

The Escola Industrial, a valuable building of the cultural heritage of Barcelona is protected by the city of Barcelona as a Cultural Asset of Local Interest and consists of a set of modernist buildings located in the neighbourhood of Nova Esquerra of the Eixample in the city of Barcelona. The Municipality of Barcelona is transferring multiple services to the premises of Escola Industrial and as expected the School of Technical Engineering will reopen in the near future. The research project ‘’Mechanical characterisation of masonry walls and vaults in a modernist building in Barcelona’’ is a part of this plan.

The set of buildings that make up the Escola Industrial has its origins in the Can Batlló factory. Created by the brothers Feliu and Joan Batlló, it was a cotton factory whose industrial buildings that stand inside the campus of Escola Industrial were built between 1869 and 1875 according to a project of the prestigious architect Rafael Guastavino. In the campus there are buildings of diverse chronologies and typological variations that correspond to the two great construction phases. The oldest with the forementioned project of Rafael Guastavino and the second which started by Lluis Planes i Calvet and completed by Joan Rubió i Bellvé around 1927. The architecture is characterized by the conception of the interior space according to the premises of clarity, breadth and luminosity that allowed the application of the traditional techniques of tiles especially in vaults and arches. This technique allowed not only to create spaces of gram amplitude but it was also a quick and cheap solution.

Fig. 35. Clock Building of Escola Industrial

The building currently known as the Clock Building and built during the first construction phase stands at the entrance located on Carrer Urgell and Roselló and is configured as a parallelepiped body built of brick and stone, with a tower of square section at each end of the facade as shown in Fig. 35 and a central courtyard of columns inside.

The main façade is configured as a frontispiece of three bodies, the central one with six levels of elevation and seven in the volumes of the angles, which are conceived as towered bodies (Fig. 35). Each level is perfectly defined thanks to the presence of stripes that, like cornices with small corbels , contribute to create an ornamentation, limited only to the games of colors and materials created by the mixed masonry.

The interior of the building is accessible through the door located in the central section of the main facade, which gives access to a large lobby with tile vaults. With a rectangular floor plan, this space is configured as a distributor of the ground floor areas and the accesses to the upper levels. In the shortest sections, stairs that lead to the other floors are located and the access is made through two lowered arches. In the longest section - facing the entrance frontispiece - there are pairs of Ionic columns which support a powerful entablature, allowing the creation of a wide space covered with tile vaults with wooden beams and iron pillars (Fig. 36). As mentioned above, the lobby is also covered with tile vaults, in this case decorated with toral arches, covered with a light-toned plaster in which they are represented through sgraffito plant motifs.

Fig. 36. Interior of the Clock building designed by Rafael Guastavino at 1868

Through the stairs located on both sides of the lobby the first floor is accessed where a large rectangular room is located with two levels of elevation and covered with a lowered vault with skylight. This area known as "noble room" and it was built during the 20th century as a part of the reconstruction carried out by Lluís Planas i Calvet and later by Joan Rubio and Bellvé as forementioned. It consists of high columns which end on the upper floor with capitals of the Doric order , while on the lower floor they are surrounded by a powerful cornice which marks the pavement’s level of the second floor. In the lower level there is a wall extending between the internal columns that at half height is transformed into windows that illuminate the rooms of the first floor. As for the second floor, between the columns there is an iron railing and a

glass enclosure that protects the offices located in this floor. The area of the entablature is configured as a body with arches that are topped with a blind lunette and is used to arrange the decoration of sgraffito, where the date MCMXXVII (1927) can be read (Fig. 37).

Worth to mention is the library of this building which is located on the second floor but with a two storeys height allows to arrange the archive using both floors through a wooden corridor and a staircase in one of the corners.

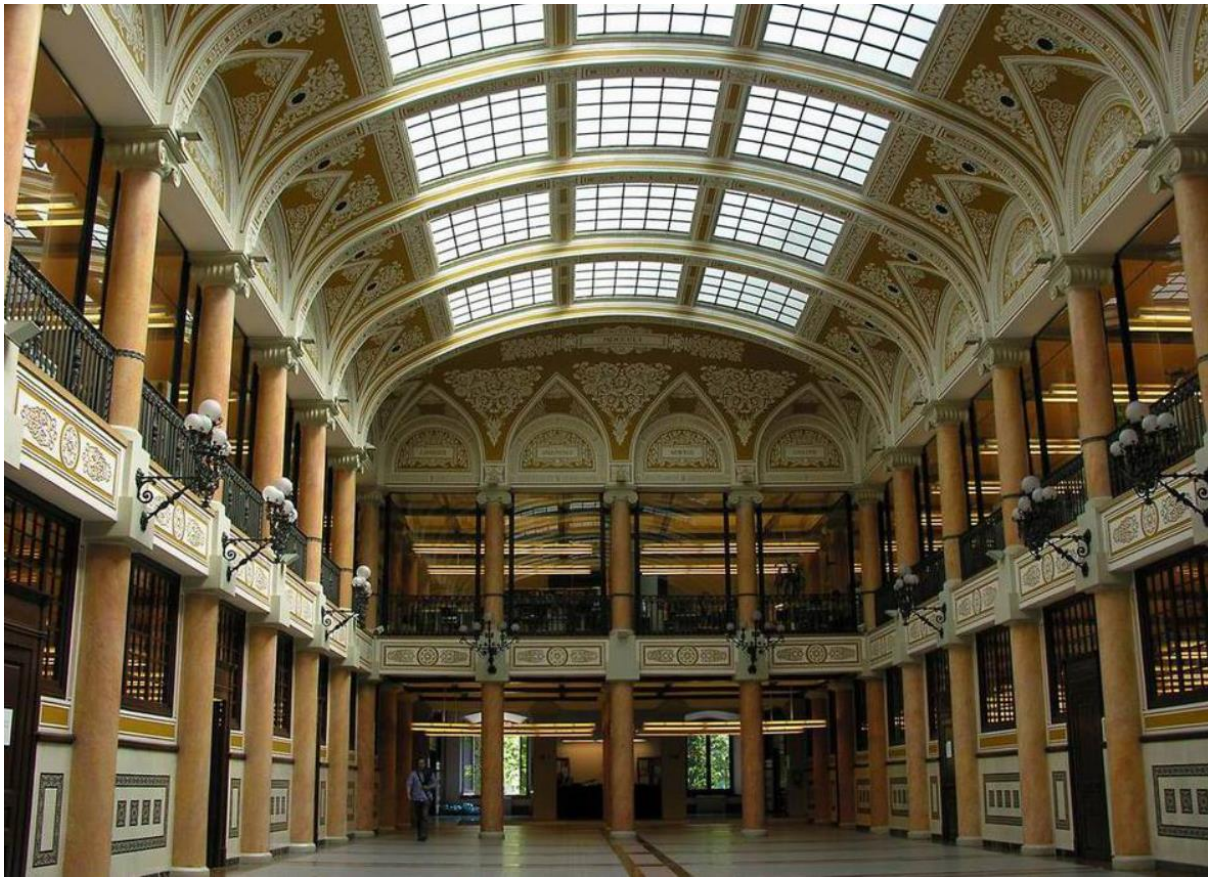

Fig. 37. Noble room of the Escola Industrial

3.2 Description of the experimental campaign

This research project was carried out in the Escola Industrial as forementioned and specifically in the building 12 of the complex (Fig. 38). In this project, the mechanical properties of the masonry were evaluated. The in situ campaign for this purpose and the laboratory experiments were commissioned to Universitat Politecnica de Catalunya. The building 12 of the Escola Industrial is located between Carrer Comte d'Urgell, Carrer Rosselló, Carrer París and Carrer Viladomat as it is shown in Fig. 39.

Fig. 38. Facade of the building 12 of Escola Industrial

Fig. 39. Exact position of the building 12 in Escola Industrial

The zones for inspection and extraction of the masonry components were agreed and given to by the structural engineering company. So the first inspection was carried out together with the technicians on September 16th 2019 in order to determine the areas of extractions on the walls and the area of extraction on the vaults on the underground floor.

The works of the minor destructive techniques (MDT) in situ and the extractions of the components and the cylinders were carried out the following days:

- the works on the components of the brick (bricks and mortar joints) and the cylinders were carried out on November 11th, 12th, 14th and 15th;

- the work of extractions of the components of the facade and of the cylinders were carried out on November 13th and 14th;

- the works of extractions of the components of the vaults (tiles and mortar) were carried out on November 19th;

- on-site characterization work with minor destructive techniques (MDT), executed with the Windsor Pin Penetration Test (PPT) system, the Helix Screw Pull-out Test (HPT) and the Penetrometric Torque Test (TPT) on mortar joints and bricks, were carried out on November 11th, 12th, 13th and 29th;

To characterize the components, five MDT positions were selected on the walls identified as Zone 1, Zone 2int, Zone 3int brick, Zone 3ext stone and Zone 4. To characterize the components of the vault, a position was identified as Zone 5 (Forjat 1 in Fig. 40), where the extraction of the components was carried out from the underground floor. Out of the five positions which used to characterize the walls, the first position (Zone 1) corresponds to the coating of cast iron pillars in the underground floor of the building, the three positions (Zone 2int, 3int brick and 3ext stone) correspond to walls of the facade, while the last location (Zone 4) corresponding to the vertical wall which is similar to the walls of the facade. The zones positions are presented in Fig. 40.

These five positions are built with:

- Zone 1: with joints of mortar of hydraulic lime with thickness between 10 and 20 mm and bricks forming a thickness of 0.15 m of masonry surrounding the column (Fig. 41);

- Zone 2int: with joints of hydraulic lime mortar with thickness between 10 and 15 mm and bricks forming a 0.45 m facade thickness;

- Zone 3int brick: with joints of hydraulic lime mortar with thickness between 10 and 15 mm and bricks organized regularly with a 0.60 m facade thickness. These are placed in two continuous rows on the facade, located under the windows;

- Zone 3ext stone: with joints of hydraulic lime mortar with variable thickness depending on the irregularity of the wall and stones of hexagonal shape (Fig. 42). This position is part of the outer part of the facade wall made up of stone on both sides (interior, exterior) and an interior format by hydraulic lime and irregular bricks, forming a total thickness of 0.60 m wall;

- Zone 4: with joints of hydraulic lime mortar with variable thickness depending on the irregularity of the wall referring to the stone material. This position is part of the rubble masonry made up of stone on both sides and an interior format of hydraulic lime and irregular bricks, forming a total thickness of 0.60 m wall;

- Zone 5: corresponds to the position where the components of the vaults of the underground floor were characterized, positioned at an arch of width of 5.50 m between the columns of the underground (Fig. 43).

In addition, some mortars in other positions were tested in situ using the MDT techniques PPT and HPT. Zone 2ext, Zone 3int stone and Zone 3ext brick were selected as to compare the characterisation with the other positions in order to determine the uniformity of the masonry's characteristics.

The destructive extraction techniques in situ (DT) were carried out with the aim of obtaining representative samples of the investigated materials. The samples were then transferred to the laboratory (LATEM) to proceed with the following experiments:

a. compressive test of brick samples according to EN 772-1 (CEN 2011);
b. young modulus tests of the brick samples according to the standard for stone EN 14580
c. compressive tests of the tiles of the vaults;
d. compressive tests of stone samples according to EN 1926: 2007;
e. double punching tests of samples of mortar joints according to DIN 18555-9: 1999 (Method III);
f. compressive test of mortar cubes according to EN 1015 – 11:1991/A1;
g. compressive tests of the cylindrical samples according to UIC 778-3R (1995).

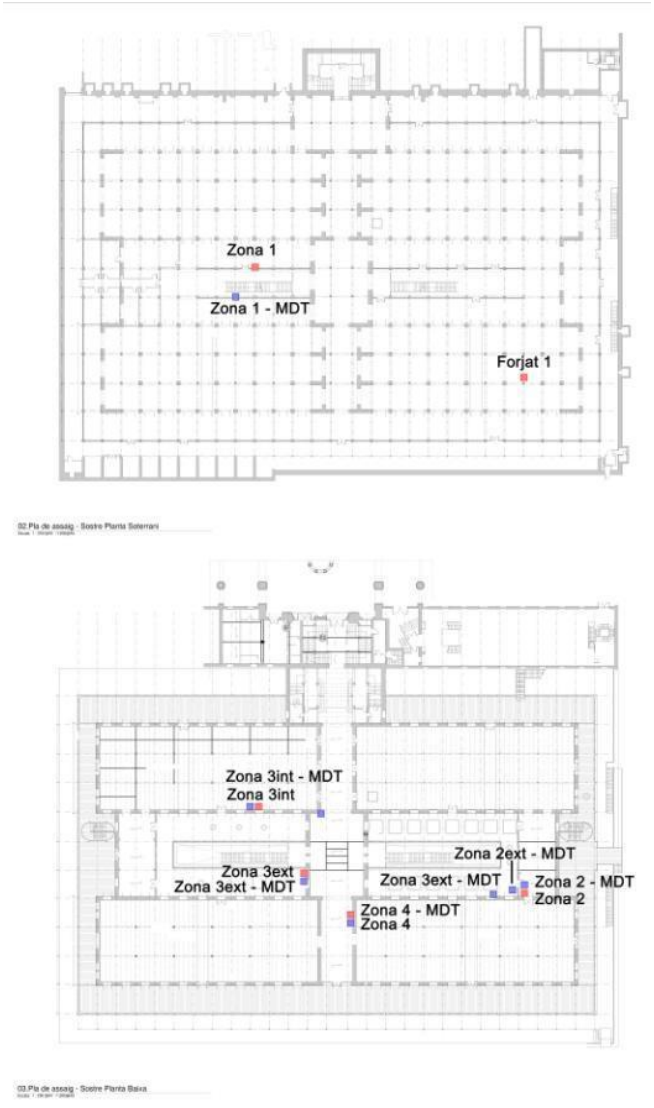

Fig. 40. Positions of the zones for MDT (blue), Positions of the zones for extraction of the samples (red)

Fig. 41. Zone 1 – Evaluation of the brick columns

Fig. 42. Zone 3ext stone – Facade with hexagonal shape stones

Fig. 43. Zone 5 – Characterization of the vault components

Fig. 44. Ground floor of the Escola Industrial

3.3 In-situ minor destructive testing

In the first phase of the experimental campaign, non-destructive in-situ techniques were performed in different construction positions of the building in order to preliminarily evaluate the variability of the surface properties of the component materials of the walls. Windsor Pin Penetration Test (PPT), Helix Screw Pull-out Test (HPT), and Torque Penetration Test (TPT) were implemented in bricks and mortar joints.

- Windsor pin penetrometer test (PPT)

Penetrometric tests (PPT) of bricks were carried out at three positions (Zone 1, 2int, 3int) of the building, while the penetrometric tests of mortar joints with PPT were carried out in nine positions (Zone 1, 2int, 2ext, 3int brick, 3int stone, 3ext brick, 3ext stone, 4 and 5) of the building. The procedure of the PPT is presented analytically in Section 2.4.2.

- Screw (helix) pull-out tests (HPT)

Brick tests with the HPT were performed at the three different construction positions (Zone 1, 2int, 3int), while the mortar joint tests with the HPT were performed at eight different construction positions (Zone 1, 2int, 2ext, 3int brick, 3ext brick, 3int stone, 4 and 5) of the building. The procedure of the HPT is presented analytically in Section 2.4.2.

- Torque Penetrometric Test (TPT)

Mortar joints were tested with TPT at four different positions (Zone 1, 2int, 3int brick and 4) of the building. The procedure of the TPT is presented analytically in Section 2.4.2.

3.4 Testing procedures

3.4.1 Bricks

The bricks were obtained from Zone 1, Zone 2int and Zone 3int brick as whole pieces or smaller with the mortar attached on them and the objective was to prepare them for the compressive tests. Firstly, the remains of the mortar on the brick beds were removed and the surfaces were polished with a diamond polisher saw and water as to guarantee the flatness and the parallelism of the surfaces until reaching a thickness of 40 mm. Then, the specimens were obtained from the bricks with the use of a table saw and water and they were dried in an air oven for 24 hours at a constant temperature of 105 ± 5 ° C.

3.4.1.1 Compressive tests on cubic specimens

Twenty-three brick cubic specimens were tested. The cubes were prepared in the laboratory as to have dimensions of approximately 40×40×40 mm^3 (Fig. 45):

- Zone 1: 6 cubes
- Zone 2int: 6 cubes (Fig. 48)
- Zone 3int brick: 11 cubes (Fig. 47)

Fig. 45. Operations on the bricks: Cutting to create 40×40×40 mm^3 cubes

Tests on cubic specimens are also useful because they allow getting many data on the compressive strength from a small amount of material. In this way a brick could be accurately characterized. The final dimensions of these test specimens are presented in Table 13. Due to the anisotropy of the bricks, the cubic specimens were tested in the same direction by applying the load perpendicularly to the bed surfaces.

The compressive tests on the cubes were performed in the Ibertest hydraulic press with the load cell of 200 kN capacity. The tests were performed under a force control, at an application speed of 0.15 MPa/s. A metal bar was placed on the upper part of the cube to regularize completely the surface while iron plates were placed under it. (Fig. 46).

Fig. 46. Compression test on brick cubes: a) cube ready to test b) Typical hourglass failure

Fig. 47. Brick cubes of Zone 3: a) ready for compression test, b) Typical hourglass failure

Fig. 48. Brick cubes of Zone 2: a) ready for compression test, b) Typical hourglass failure

Table 13. Dimensions of the brick cubic specimens for compressive test

Position of extraction	ID	Thickness [mm]	Dimensions [mm]	
Zone 1	1	40.00	40.00	38.10
	2	41.00	39.15	40.20
	3	38.50	38.00	39.55
	4	39.00	39.00	39.00
	8	40.00	39.20	40.00
	9	40.00	39.20	40.00

Position of extraction	ID	Thickness [mm]	Dimensions [mm]	
Zone 2	1	40.70	38.75	39.95
	2	40.10	40.00	39.50
	3	40.10	40.60	38.50
	4	36.70	40.40	40.00
	5	39.50	39.45	39.40
	6	40.00	39.20	38.60

Position of extraction	ID	Thickness [mm]	Dimensions [mm]	
Zone 3	1.1	40.00	41.30	39.25
	2.1	40.00	42.05	40.20
	2.2	40.30	38.70	41.70
	3.1	40.60	39.90	40.20
	3.2	40.00	40.00	39.00
	3.3	40.40	39.55	39.45
	5.1	40.20	39.75	40.00
	5.2	40.00	40.10	39.10
	6.1	39.80	38.45	38.15
	6.2	40.30	37.40	39.20
	6.3	40.20	40.40	38.90

3.4.1.2 Compressive tests on 100×100×40 mm^3 brick specimens

Twenty-five brick square specimens were tested. The specimens were prepared in the laboratory as to have dimensions of approximately 100×100×40 mm^3. This specimen shape is proposed by the current codes (EN 772-1) and it allows to obtain the uniaxial compressive strength along the bed direction of the brick. Some specimens were created from whole bricks which could be divided into two different specimens while others were created from bricks which didn't have the adequate size in order to be divided in two specimens. The final dimensions of these test specimens are presented in Table 14.

- Zone 1: 12 specimens (Fig. 49)
- Zone 2int: 10 specimens
- Zone 3int brick: 3 specimens

The standard EN 772-1 recommends a minimum number of 6 specimens but in Zone 3int brick the extraction of an adequate number of bricks as to obtain 6 specimens was impossible.

The compressive tests on the specimens were performed in the Ibertest hydraulic press with the load cell of 3000 kN capacity. The tests were performed under a force control, at an application speed of 0.30 MPa/s. An iron plate was placed both on the bottom and on the upper part of the specimen to regularize completely the surfaces (Fig. 50)

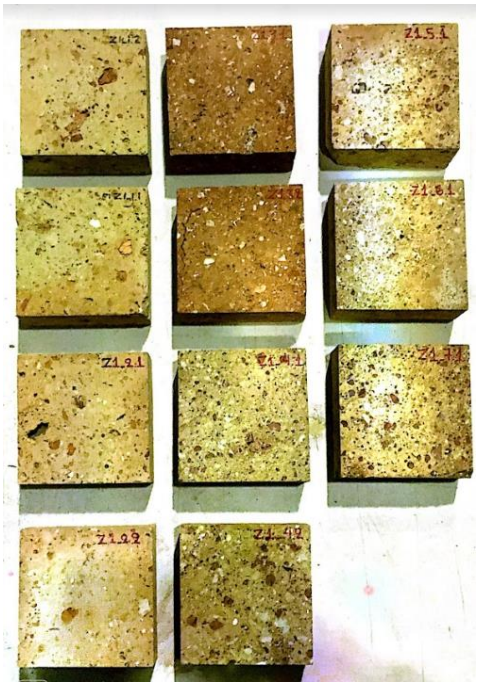

Fig. 49. Rectangular brick specimens ready for compressive test

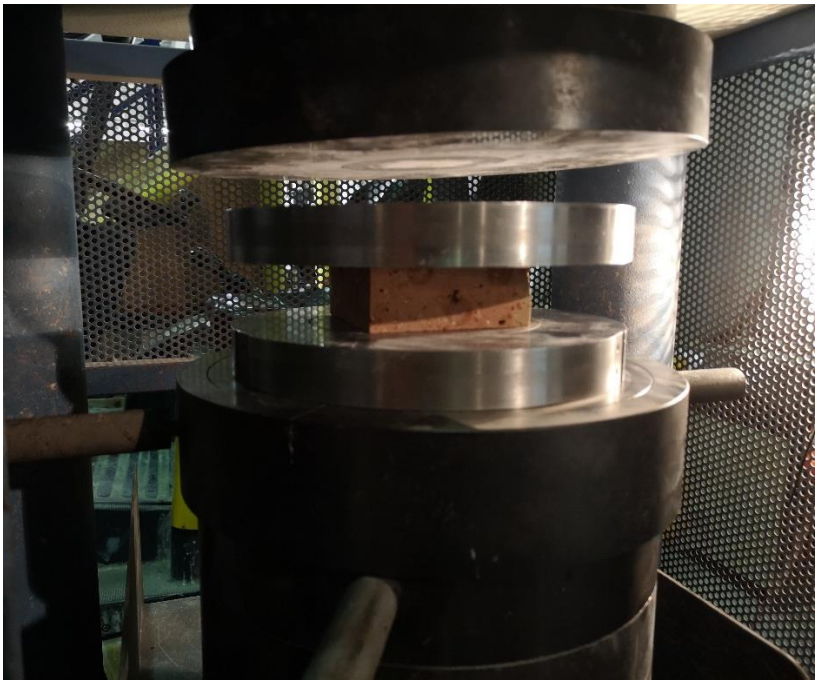

Fig. 50. Brick 100×100×40 mm^3 ready to be tested in Ibertest

Fig. 51. Brick 100×100×40 mm^3 a) Ready for compressive test b) Typical hourglass failure

Table 14. Dimensions of the brick rectangular specimens of 100×100×40 mm^3

Position of extraction	ID	Thickness [mm]	Dimensions [mm]	
Zone 1	1.A	40.00	102.65	100.00
	1.B	40.00	99.55	100.00
	2.A	40.00	101.30	98.95
	2.B	40.00	100.80	99.55
	3.A	39.00	99.70	100.20
	3.B	39.20	100.50	98.80
	4.A	40.00	100.00	100.25
	4.B	40.00	98.70	99.85
	5	40.00	99.00	98.80
	6	39.30	100.20	100.35
	7	39.30	100.00	100.35

Position of extraction	ID	Thickness [mm]	Dimensions [mm]	
Zone 2int	1.A	39.80	100.20	100.35
	1.B	40.30	99.40	99.40
	2.A	40.00	100.95	98.85
	2.B	40.00	100.40	100.70
	3.A	40.10	99.40	100.15
	3.B	40.20	99.85	100.55
	4.A	36.10	99.00	99.80
	4.B	36.00	98.90	101.00
	5	40.00	99.05	100.75
	6	39.80	98.65	100.45

Position of extraction	ID	Thickness [mm]	Dimensions [mm]	
Zone 3int	4	39.70	99.55	100.65
	5	40.60	100.00	99.40
	6	39.70	98.85	99.70

3.4.1.3 Compressive tests on 50×50×40 mm³ brick specimens

At the Zone 3int position, a minimum of 6 test specimens of 100×100×40 mm³ measurements could not be obtained due to the limited disposition of the extraction material. The implementation of a second type of test that also considered in the standard EN 772-1 was chosen, with specimens of dimensions of 50×50×40 mm³, as shown in Fig. 52. The final dimensions of these test specimens are presented in the Table 15.

Fig. 52. Brick specimens of 50×50×40 mm³

Table 15. Dimensions of the brick specimens of 50×50×40 mm³

Position of extraction	ID	Thickness [mm]	Dimensions [mm]	
Zone 3int	7	38.50	51.20	47.45
	8	38.20	49.65	50.90
	9.A	40.60	51.10	48.25
	9.B	40.10	49.40	49.50
	10.A	40.00	49.60	48.75
	10.B	40.00	49.05	48.93
	10.C	40.00	49.00	49.25

The tests of the specimens with measurements of 50×50×40 mm³ were carried out at the Ibertest hydraulic press with a load cell of 200 kN capacity as shown in Fig. 53. The press complies with the requirements of the standards, including, among others, a hinge responsible for the uniform distribution of the load and the avoidance of unnecessary eccentricities. The tests were performed under a force control, at an application speed of 0.15 MPa/s.

Fig. 53. Compressive test in brick specimens of 50×50×40 mm³

3.4.1.4 Young's modulus and Poisson's ratio

The Young's modulus is an important value to define the response of the material in the elastic range. As there is no European Standard reference for the Young modulus of the bricks, we decided to attempt to obtain it based on the procedure described in the standards for concrete and stone Young's modulus. Brick prisms were obtained with dimensions of 40×40×80 mm^3 in order to maintain the height to width ratio at around 1:2. It is important that the top and the bottom of the prism are absolutely parallel to achieve a uniform distribution of the compressive force in the whole prism. In the test for the evaluation of the Young's modulus cycles of compression of loading and unloading were applied, remaining in the elastic range, keeping the minimum load value equal to 10%f_b and a maximum load value equal to the 30% f_b.

As for the test setup, the MGSPlus machine and an apparatus with extensometers DD1 in which the prisms were confined were used in the laboratory. The characteristics of the extensometer are presented in Fig. 55 and in Fig. 56. The test was carried out in the hydraulic press with a load cell of 200 kN capacity. Also, rigid metal plates were placed at the in-contact surfaces of the prisms while a hinge was placed above them in order to have a uniform distribution of the load without having unnecessary eccentricities (Fig. 54). The geometric dimension of the specimens is given in Table 16.

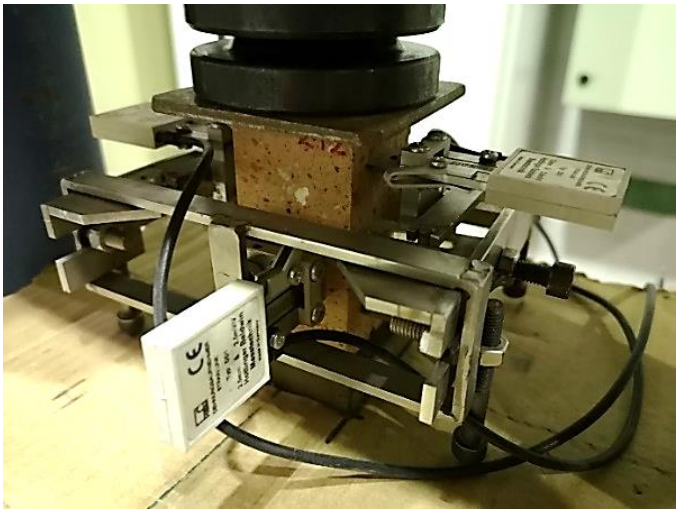

Fig. 54. Cycles of compression in the MSGPlus machine / Apparatus with extensometers where the prism is confined

Table 16. Dimensions of the brick specimens 40×40×80mm

Position of extraction	ID	Thickness [mm]	Dimensions [mm]	
Zone 1	1	79.00	39.90	40.15
	2	78.40	40.35	40.03
	3	80.00	39.78	38.78
	4	77.70	39.80	40.00
	8	79.00	39.68	39.73
	9	78.00	40.03	39.95

Position of extraction	ID	Thickness [mm]	Dimensions [mm]	
Zone 2	1	76.00	40.20	40.40
	2	77.70	40.00	40.03
	3	78.00	40.88	40.08
	5	78.80	38.85	39.58
	6	78.80	39.53	40.03

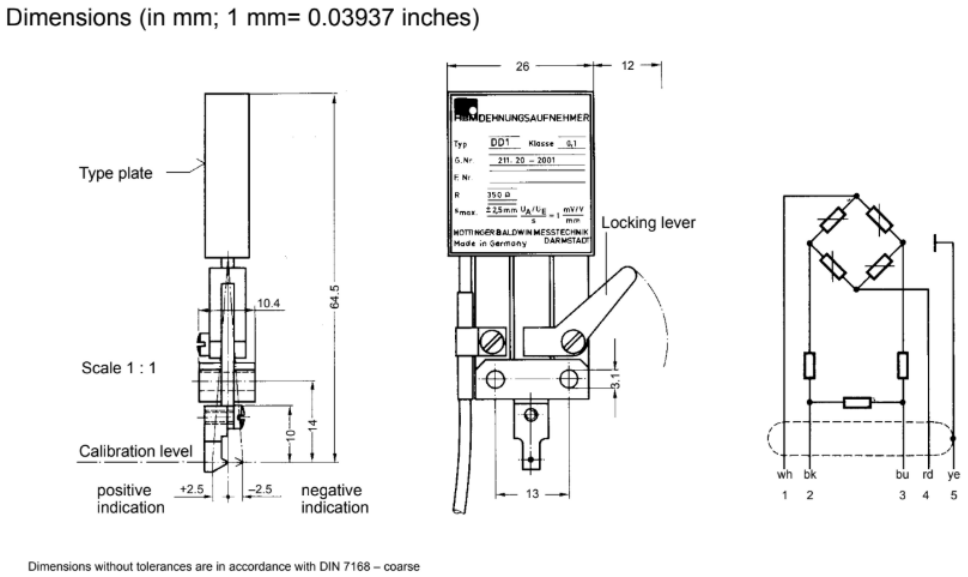

Fig. 55. Details of the extensometer DD1

Type		DD1
Accuracy class		0.1
Nominal displacement	mm	± 2.5
Nominal sensitivity (nominal output signal at nominal displacement)	mV/V	± 2.5
Sensitivity tolerance (deviation of the sensitivity from nominal sensitivity)	%	± 0.1
Temperature effect per 10 K in the nominal temperature range		
of the output signal, related to the actual value	%	< ± 0.03
of the zero signal, related to the nominal sensitivity	%	< ± 0.05
Linearity error including hysteresis, related to the nominal output signal	%	< ± 0.05
Electrical principle of measurement		Strain gauge full bridge
Input resistance at reference temperature	Ω	350 ± 3
Nominal range of supply voltage at reference temperature	V	1...6
Service range of supply voltage	V	1...10
Spring rate (restoring force of the measuring probe tip)	N/mm	approx. 0.23
Reference temperature	°C [°F]	+23 [+73.4]
Nominal temperature range	°C [°F]	–10...+60 [+14 +140]
Service temperature range	°C [°F]	–20...+70 [–4...+158]
Storage temperature range	°C [°F]	–50...+70 [–58...+158]
Cable length	m	1.5
Weight (transducer without cable)	g	20

Fig. 56. Specifications of the extensometer DD1

3.4.2 Tiles

3.4.2.1 Extraction of the tiles

Before the extraction process, the removal of pavement and the crushing of the concrete slab of the upper floor were first carried out as shown in Fig. 57 in order to allow to the tiles to be extracted. Due to the high strength of the slab, it was decided to remove the tiles from the bottom with the removal of the plaster of the arch. The material of the components was the same as that of the vaults as they were built unitarily over the same period, as shown in Fig. 58.

Fig. 57. Process of removing bricks and mortar joints from the vaults

Fig. 58. Extraction of bricks and mortar joint from the inferior part of the vaults

9 tiles were extracted from Zone 5 in the underground floor, with the geometric dimensions given in Table 17.

Table 17. Dimensions of the bricks extracted from the vaults

Position of extraction	ID	Thickness [mm]	Dimensions [mm]	
Zone 5 - Vaults	Tile 1	19.95	300.65	147.95
	Tile 2	19.90	302.75	146.80
	Tile 3	20.40	301.00	147.75
	Tile 4	20.10	295.50	143.50
	Tile 5	21.20	293.55	143.50
	Tile 6	18.68	179.00	146.70
	Tile 7	20.88	186.35	144.50
	Tile 8	20.93	177.20	145.95
	Tile 9	20.35	--	146.00

3.4.2.2. Compressive tests on the tiles

For the characterization of the tile samples of the vaults, the application of EN 772-1 (CEN 2011) is not possible to be implemented due to the reduced height of the samples as observed in Fig. 59. The use of specimens assembled for the compression test aims to allow a reliable and acceptable evaluation of the tiles compressive strength, since their low thickness does not allow the preparation of the tests with the minimum measurements that will provide us with reliable results. The proposed solution as to evaluate the compressive resistance was carried out in the LATEM laboratory and it was used also in previous tests. It consists of assembled tiles with a layer of intermediate cement mortar. The cement mortar layer has the objective only to connect the two tile specimens in order to reduce the slide between them during the test, without significantly affecting the compression resistance of the specimen.

Fig. 59. Initial state of the extracted bricks

Generally, two specimens were obtained from each whole tile, as can be seen in Fig. 60. After the cutting of the pieces, they were dried by air drying for 24 hours at a constant temperature of 105 ± 5 ° C. The final dimensions of these tile specimens are presented in Table 18.

Fig. 60. Tile specimens that created from the position of the vaults

Table 18. Dimensions of the tile specimens

Position of extraction	ID	Thickness [mm]	Dimensions [mm]	
Zone 5 - Vaults	Tile_1.1a	--	--	--
	Tile_1.1b	--	--	--
	Tile_1.2a	19.18	100.80	99.20
	Tile_1.2b	19.93	98.85	99.75
	Tile_1.3a	21.50	100.30	101.40
	Tile_1.3b	20.33	99.20	101.60
	Tile_1.4a	18.50	99.85	100.55
	Tile_1.4b	20.08	99.75	100.10
	Tile_1.5a	21.32	100.35	102.40
	Tile_1.5b	21.18	99.35	102.85
	Tile_1.6	18.25	98.95	102.40
	Tile_1.7	20.40	99.80	102.30
	Tile_1.8	21.00	100.50	101.90
	Tile_1.9	20.23	99.25	102.30

Next, the two tile specimens obtained from the same tile were connected with a 20 mm cement mortar joint with a compressive strength of 30 MPa. The test specimen formed by the tile 1.1 was broken during the assembly process because of the low adherence between the mortar and the tile during the removal of the wooden moulds. Finally, they were dry polished at the sides which would be in contact with the platens of the hydraulic press in order to guarantee plane and parallel surfaces, as shown in Fig. 61.

Fig. 61. Assembled specimens obtained from the bricks

The compression test was carried out with the Ibertest hydraulic press with a load cell of 200 kN capacity (Fig. 62). The tests were performed with displacement control, at an application rate of 0.2 mm/min.

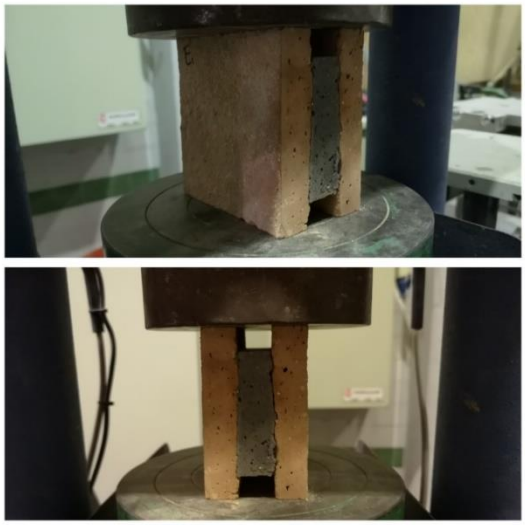

Fig. 62. Tile sample ready to be tested under compression in Ibertest of 200 kN capacity

3.4.3 Stone

3.4.3.1 Extraction of the stone

Three whole stones were extracted, two stones from Zone 4 of the interior wall and one stone from Zone 3ext stone of the facade wall, with the approximate geometric characteristics given in Table 19. The extraction process is executed first with removal of the coating in Zone 4 and the removal of the surrounding mortar joints to access the dismantling of the components, as shown in Fig. 63.

Fig. 63. Stone extraction process of Zone 4

Table 19. Dimensions of the extracted stones

Specimen	Thickness (mm)	Length (mm)	Width (mm)
Stone_3.1	180	430	360
Stone_4.1	260	460	230
Stone_4.2	420	280	270

The extracted stones were tested under compression in accordance with the standard EN 1926. The first step was the preparation of flat and parallel stone surfaces, to ensure a uniform distribution of the load during the compressive test. As it can be seen in Fig. 64, the stones had irregular shapes and from them $50\times50\times50$ mm^3 specimens were obtained by cutting the stones with a table saw as to obtain the dimensions recommended by the standard of EN1926.

Fig. 64. Initial state of the irregular shape stones

Generally, several specimens were obtained for each whole stone, as can be seen in Fig. 65. After the cutting of the specimens was completed, they were dried by air drying for 24 hours at a temperature of 105 ± 5 ° C. The final dimensions of specimens are presented in Table 20.

Fig. 65. Stone specimens of 50×50×50 mm^3 obtained from Zone 3 and Zone 4

Table 20. Final dimensions of the 50×50×50 mm³ stone specimens

	Specimen	Thickness (mm)	Length (mm)	Width (mm)
Zone 3ext	1.A	49.85	51.90	50.00
	1.B	51.90	49.00	49.00
	1.C	48.95	49.25	51.80
	1.D	49.68	51.83	51.60

	Specimen	Thickness (mm)	Length (mm)	Width (mm)
Zone 4	2.A	49.35	50.50	47.40
	2.B	48.18	49.40	50.00
	2.C	48.00	48.75	49.80
	2.D	48.25	49.75	48.80
	2.E	49.85	49.80	48.30
	2.F	50.60	49.20	50.00
	3.A	50.20	49.25	50.50
	3.B	50.00	48.75	47.50
	3.C	50.75	48.75	51.00

3.4.3.2 Compressive tests on the stone specimens

The compression test of the 50×50×50 mm³ stone specimens was performed with the Ibertest hydraulic press with a load capacity of 200 kN as it can be seen in Fig. 66. The tests were performed under force control, at an application velocity of 1 MPa/s. A hinge was also placed above the steel plate and the specimen in order to avoid the eccentricities and to have a uniform distribution of the load.

Fig. 66. Compressive test on the 50×50×50 mm³ stone specimens at the Ibertest hydraulic press with capacity of 200 kN

3.4.4 Mortar

3.4.4.1 Double punch test on the mortar joints (DPT)

The double punch tests were performed on the mortar specimens obtained from each wall zone, on which minor destructive testing were previously performed. Mortar specimens were prepared in the laboratory as to follow the indications from DIN 18555-9, chapter 5.

Indications from DIN 18555-9 in chapter "5. Testing of mortar from masonry", section "5.2 Method III" (Fig. 68).

"Specimens approximately 50 mm square or 50mm in diameter are prepared from samples taken from masonry (e.g. by core drilling or masonry unit/joint assemblies). The specimens are then placed between a pair of loading platens measuring 20mm in diameter and tested for compressive strength."

The objective was to obtain the mechanical characterisation for the mortar from both the minor destructive techniques and the double punch tests. [33]

Procedure:

1. removal of the mortar with chisel and hammer;
2. obtain specimens 50x50 mm approximately;
3. measurement of the specimens;
4. apply gypsum on the centre of each specimen's surface;
5. execution of the test.

The tests were executed at the Ibertest hydraulic press with a load cell capacity of 10 kN. The goal was to achieve the failure between 30 - 90 seconds. The specimens were placed between the platens with a full contact between the specimens and the platens. With the use of gypsum, the load is more uniformly distributed while the failure mechanism observation is easier. There will be a central zone who breaks forming an hourglass and in the surrounding part the cracks propagate (Fig. 67).

In total, 120 mortar specimens were obtained. 64 were obtained from the positions of the brick walls (Zone 1, 2int and 3int brick), 20 were obtained from the position of the stone walls (Zone 3int stone and 4), 18 from the position of the vaults (Zone 5), 12 from the position of the exterior design of facade stone walls and 6 from the position of the foundations while mortar from this position was found in the construction site. The dimensions of them are presented in Table 21.

Fig. 67. Execution of DPT test

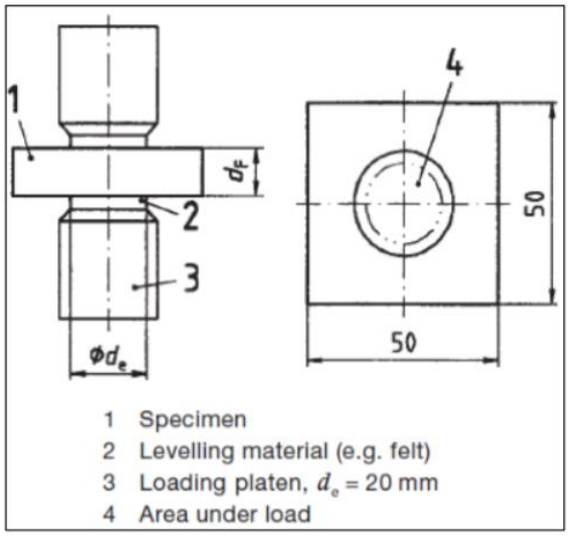

Fig. 68. Test Setup according to DIN 18555-9, Method III

The double punch test was executed for following zones of the Escola Industrial:

- Zone 1 (Fig. 69)
- Zone 2
- Zone 3int brick at the mortars of the interior brick
- Zone 3ext stone at the mortar joints of the exterior stone
- Zone 3 at the mortar of the design of the facade (Fig. 70)
- Zone 4
- Zone 5 from the vaults (Fig. 71)
- Zone F / Foundations (Fig. 72)

Table 21. Dimensions of mortar joint specimens for double punch tests

Position of extraction	ID	Thickness [mm]	Dimensions [mm]	
Zone 1	DPT_1.01	16.0	71.0	55.0
	DPT_1.02	18.0	84.0	70.0
	DPT_1.03	16.0	80.0	88.0
	DPT_1.04	16.0	78.0	84.0
	DPT_1.05	21.0	81.0	93.0
	DPT_1.06	18.0	93.0	66.0
	DPT_1.07	19.0	86.0	68.0
	DPT_1.08	18.0	108.0	55.0
	DPT_1.09	15.0	97.0	78.0
	DPT_1.10	19.0	83.0	74.0
	DPT_1.11	18.0	74.0	71.0
	DPT_1.12	18.0	65.0	48.0
	DPT_1.13	21.0	63.0	47.0
	DPT_1.14	18.0	75.0	49.0
	DPT_1.15	15.0	66.0	46.0
	DPT_1.16	20.0	74.0	59.0
	DPT_1.17	16.0	69.0	54.0
	DPT_1.18	20.0	65.0	54.0
	DPT_1.19	22.0	72.0	69.0
	DPT_1.20	15.0	63.0	50.0
	DPT_1.21	17.0	53.0	44.0
	DPT_1.22	18.0	58.0	44.0
	DPT_1.23	14.0	62.0	44.0
	DPT_1.24	18.0	53.0	50.0
	DPT_1.25	17.0	87.0	82.0
	DPT_1.26	19.0	78.0	75.0

Position of extraction	ID	Thickness [mm]	Dimensions [mm]	
Zone 2int	DPT_2.01	15.5	62.0	60.0
	DPT_2.02	14.0	51.0	95.0
	DPT_2.03	15.5	45.0	70.0
	DPT_2.04	17.0	65.0	47.0
	DPT_2.05	18.0	71.0	45.0
	DPT_2.06	17.0	76.0	46.0
	DPT_2.07	14.0	75.0	63.0
	DPT_2.08	15.0	55.0	49.0
	DPT_2.09	22.0	112.0	66.0
	DPT_2.10	18.0	86.0	62.0
	DPT_2.11	19.0	86.0	45.0
	DPT_2.12	18.0	74.0	49.0
	DPT_2.13	18.5	82.0	61.0
	DPT_2.14	15.0	91.0	66.0
	DPT_2.15	20.0	66.0	59.0
	DPT_2.16	17.5	76.0	53.0
	DPT_2.17	16.0	74.0	46.0
	DPT_2.18	16.0	89.0	51.0
	DPT_2.19	20.5	66.0	48.0
	DPT_2.20	18.0	59.0	50.0
	DPT_2.21	17.5	51.0	40.0
	DPT_2.22	18.5	61.0	56.0
	DPT_2.23	18.5	46.0	44.0
	DPT_2.24	15.5	60.0	60.0
	DPT_2.25	17.5	50.0	48.0

Position of extraction	ID	Thickness [mm]	Dimensions [mm]	
Zone 3int Brick	DPT_3.01	17.0	98.0	60.0
	DPT_3.02	17.0	77.0	60.0
	DPT_3.03	20.0	54.0	41.0
	DPT_3.04	19.0	83.0	48.0
	DPT_3.05	21.0	57.0	50.0
	DPT_3.06	22.0	76.0	51.0
	DPT_3.07	19.0	94.0	72.0
	DPT_3.08	18.0	79.0	78.0
	DPT_3.09	17.0	75.0	53.0
	DPT_3.10	14.0	68.0	67.0
	DPT_3.11	16.5	65.0	43.0
	DPT_3.12	17.0	64.0	57.0
	DPT_3.13	16.0	52.0	49.0

Position of extraction	ID	Thickness [mm]	Dimensions [mm]	
Zone 3ext.ext Design stone facade	DPT_3.01	19.0	110.0	78.0
	DPT_3.02	27.0	127.5	57.0
	DPT_3.03	17.5	153.0	49.0
	DPT_3.04	17.0	83.0	50.5
	DPT_3.05	15.5	94.0	49.5
	DPT_3.06	13.6	126.0	43.0
	DPT_3.07	15.0	110.5	36.5
	DPT_3.08	23.5	53.0	48.5
	DPT_3.09	23.5	57.5	43.5
	DPT_3.10	13.5	89.0	38.0
	DPT_3.11	13.5	49.0	45.0
	DPT_3.12	26.0	84.0	75.0

Position of extraction	ID	Thickness [mm]	Dimensions [mm]	
Zone 3int Stone	DPT_3.01	22.0	66.0	52.0
	DPT_3.02	31.0	63.5	57.0
	DPT_3.03	21.0	65.0	47.0
	DPT_3.04	22.0	64.0	46.0
	DPT_3.05	19.0	64.0	50.0
	DPT_3.06	16.0	64.0	41.0
	DPT_3.07	22.5	60.0	45.0
	DPT_3.08	16.0	54.0	39.0
	DPT_3.09	17.5	93.0	54.0
	DPT_3.10	22.5	108.0	57.0

Position of extraction	ID	Thickness [mm]	Dimensions [mm]	
Zone 4	DPT_4.01	19.9	89.5	60.8
	DPT_4.02	24.0	114.3	60.9
	DPT_4.03	18.8	67.0	46.7
	DPT_4.04	20.2	83.0	52.0
	DPT_4.05	14.0	70.5	49.0
	DPT_4.06	24.0	63.7	42.5
	DPT_4.07	19.3	59.2	57.3
	DPT_4.08	19.1	18.7	47.0
	DPT_4.09	15.0	64.0	38.3
	DPT_4.10	21.8	50.8	39.3

Position of extraction	ID	Thickness [mm]	Dimensions [mm]	
Zone 5	DPT_5.01	10.0	109.0	80.0
	DPT_5.02	9.0	97.0	77.0
	DPT_5.03	13.0	67.0	62.0
	DPT_5.04	12.0	80.0	49.0
	DPT_5.05	12.0	99.0	69.0
	DPT_5.06	9.0	96.0	88.0
	DPT_5.07	12.0	71.0	59.0
	DPT_5.08	11.0	84.0	65.0
	DPT_5.09	9.0	72.0	50.0
	DPT_5.10	8.5	83.0	42.0
	DPT_5.11	12.0	82.0	77.0
	DPT_5.12	8.0	84.0	42.0
	DPT_5.13	11.0	78.0	52.0
	DPT_5.14	9.0	91.0	49.0
	DPT_5.15	11.5	82.0	52.0
	DPT_5.16	14.0	64.0	50.0
	DPT_5.17	9.0	66.0	49.0
	DPT_5.18	13.0	80.0	51.0

Position of extraction	ID	Thickness [mm]	Dimensions [mm]	
Zone F	DPT_F.01	21.0	89.0	82.0
	DPT_F.02	23.0	84.0	71.0
	DPT_F.03	24.0	69.0	59.0
	DPT_F.04	23.0	95.0	53.0
	DPT_F.05	23.0	78.0	66.0
	DPT_F.06	25.0	73.0	65.0

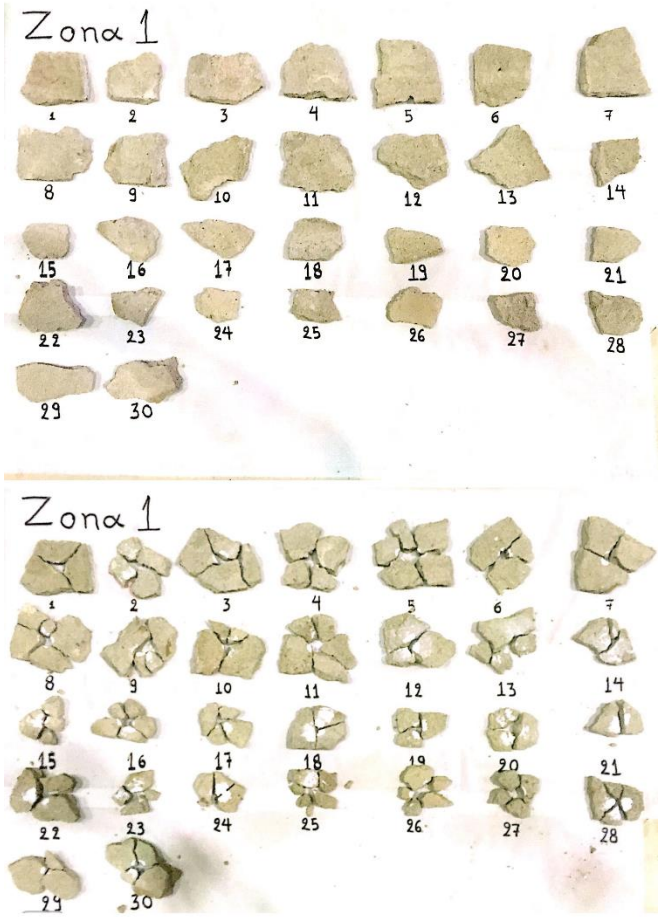

Fig. 69. Double punch test in zone 1 / Specimens ready to test & breaking formations

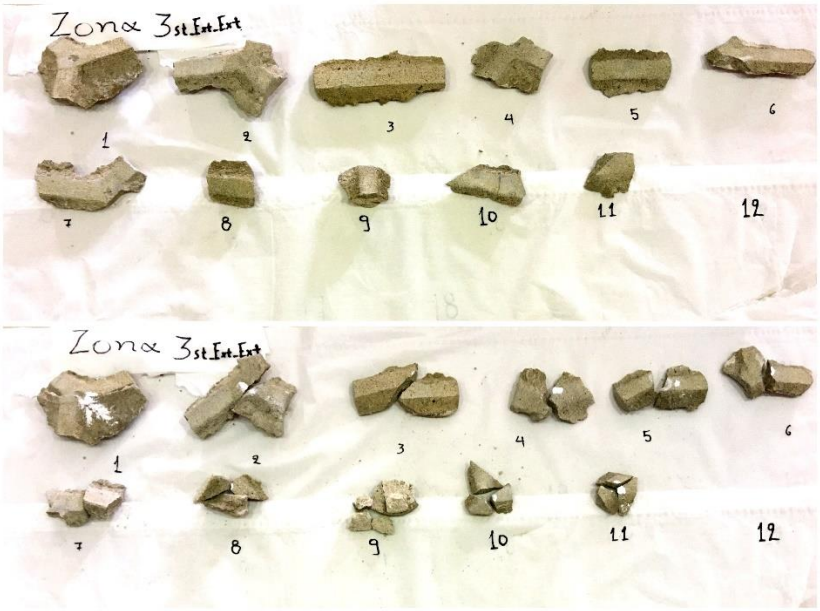

Fig. 70. Double punch test in Zone 3 at the mortar of the facade / Specimens ready to test & breaking formations

Fig. 71. Double punch test in Zone 5 / Specimens ready to test & breaking formations

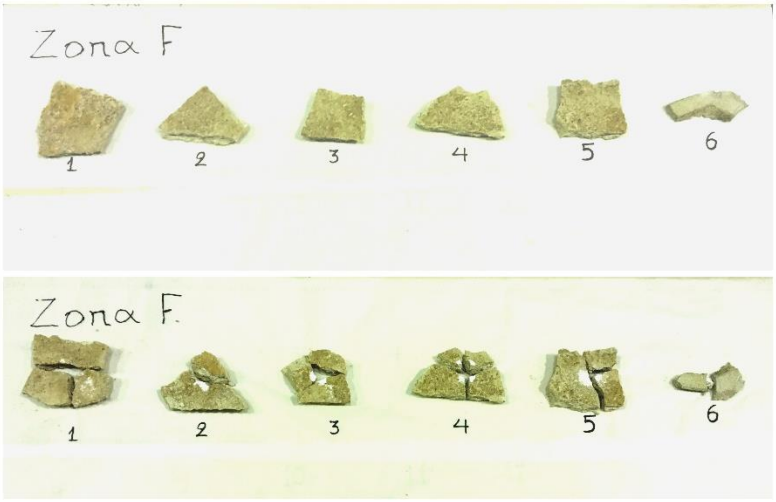

Fig. 72. Double punch test in Zone F / Specimens ready to test & breaking formations

3.4.4.2 Compressive tests on mortar cubic specimens

The compressive strength was evaluated directly by the compression test of the mortar cubes, according to EN 1015-11 which develops the following technique:

"The cubes are placed in a hydraulic press and apply the load without shock and increase it continuously until failure occurs. The standard suggested diferent loading rates depending of the mortar category."

The compressive strength f_m [MPa] is calculated like:

$$f_m = \frac{F}{40^2}$$

Where: F = maximum load [N]; 40^2 = load platens area [mm^2].

Ten cubic specimens were tested. The cubes were prepared in the laboratory by extracting mortar from larger stone pieces and by cutting with a dry hand saw and grinding the surfaces with a polishing rotary machine without water in order to have dimensions of 40×40×40 mm^3 (Fig. 73a & Fig. 73b):

- Zone 1: 1 cube
- Zone 3: 2 cubes
- Zone 4: 7 cubes

Fig. 73. Prism mortar specimens ready to be tested in compression

The tests were performed in the Ibertest hydraulic press with a load cell capacity of 10 KN, under force control. It was tried to keep the load in order to get the rupture in 60 seconds, calibrating according to previous experiments and expected strengths. With the use of gypsum, the load is more uniformly distributed while the failure mechanism observation is easier. There

will be a central zone who breaks forming an hourglass and in the surrounding part the cracks propagate (Fig. 74a). The dimensions of the specimens are shown in Table 22.

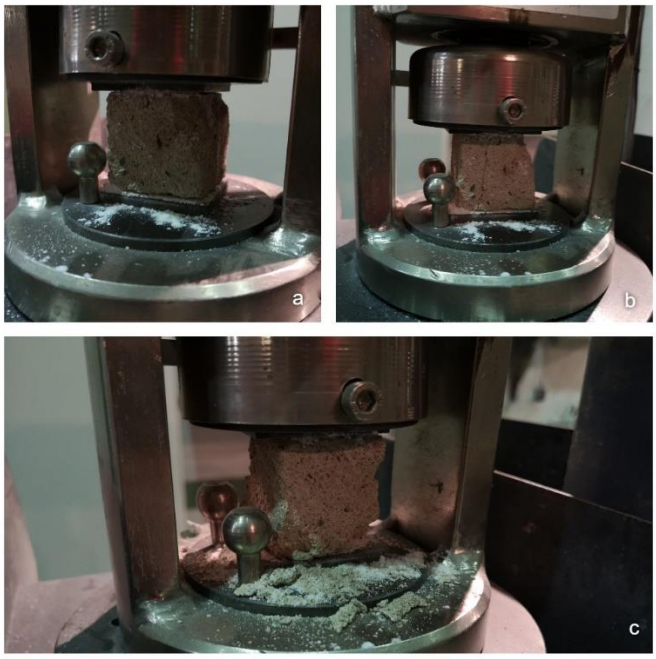

Fig. 74. Compression test of the mortar cubes: a) Gypsum applied and cube set up, b) first breaking formation, c) Hourglass failure mode

Table 22. Dimensions of the mortar cubic specimens of 40×40×40mm.

Position of extraction	ID	Thickness [mm]	Dimensions [mm]	
Zone 1	1	39.6	40.5	39.3

Position of extraction	ID	Thickness [mm]	Dimensions [mm]	
Zone 3	1	41.1	41.1	39.4
	2	37.8	40.4	41.5

Position of extraction	ID	Thickness [mm]	Dimensions [mm]	
Zone 4	1	37.8	40.4	41.5
	2	43.3	42.5	40.6
	3	40.1	37.3	39.5
	4	41.0	36.2	34.2
	5	35.9	31.1	36.7
	6	39.2	31.4	34.1
	7	38.4	35.0	29.1

3.4.5 Masonry

3.4.5.1 Extraction of cylindrical masonry samples

Cylindrical specimens were extracted from 4 different masonry zones. 3 of the zones are from a brick masonry (Zone 1, Zone 2int and Zone 3int brick) and the other (Zone 3ext stone) is a representative facade zone as rubble stone masonry. The specimens required were:

1. 3JC: brick cylinder with three mortar joints and Ø = 152 mm
2. 3JC: stone cylinder with three mortar joints and Ø = 152 mm
3. 1JC: brick cylinder with one mortar joint and Ø = 92 mm
4. 1JC: stone cylinder with one mortar joint and Ø = 92 mm

The extractions in the different zones are shown on Fig. 75.

Fig. 75. Positions of cylinders extractions: a) Zone 1, b) Zone 2int, c) Zone 3int brick, d) Zone 3ext stone

The cylinder extraction using drilling dry procedure is a technique that was developed at UPC [30]. During the drilling dry procedure, the apparatus was connected to a vacuum cleaner as to absorb the dust during the extraction. The extractions were executed in stages in order to avoid overheating and lead to the complete removal of the dust. The specimens were extracted carefully without sudden problems or loss of the mortar joint (Fig. 76, Fig. 77).

Fig. 76. Extraction with dry procedure in zone 1: a) apparatus and drill cylinders, b) holes after the end of the extractions

Fig. 77. Extraction with dry procedure in zone 3int: a) apparatus and drill cylinders, b) holes after the end of the extractions

As it was impossible to use the dry procedure due to the hardness of the stone, the wet procedure that is used from concrete was applied. During the wet procedure which was used in the exterior of Zone 3 (Fig. 78), water was used while drilling to prevent the drill overheating and the gathering of dust inside them. This procedure led to damage of some specimens because the water disaggregated the cylinders as the mortar strength was low.

Fig. 78. Extraction with wet procedure: a) apparatus and drill cylinders, b) hole after extraction, c) end of the extractions

After the extractions finished the following specimens have been obtained:

- 6 brick masonry cylinders / Diameter : 152 mm (3JC)
- 7 brick masonry cylinders / Diameter : 92 mm (1JC)
- 2 stone masonry cylinders / Diameter : 152 mm (3JC)
- 2 stone masonry cylinders / Diameter : 92 mm (1JC)

Most of the brick cylinders were extracted without problems (Fig. 79) while in some of them the cohesion between brick and mortar was low and the masonry was disaggregated. In the wet procedure for the extraction of the stone cylinders there was also some disaggregation due to the mortar joints (Fig. 80 and Fig. 81).

Fig. 79. 1JC & 3JC brick specimens extracted

Fig. 80. 1JC stone specimens extracted

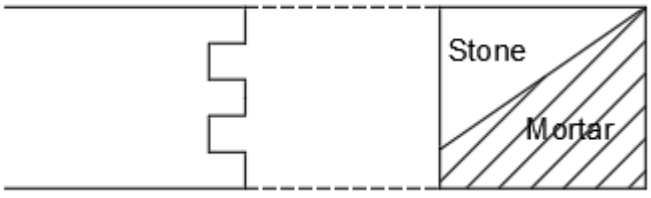

Fig. 81. Cause of disaggregation

3.4.5.2 Regularization of the mortar

High strength cement mortar was used in order to execute the regularization of the mortar caps. The moulds were made specifically for the project and they were composed of wood (Fig. 82).

Fig. 82. Wooden moulds and cylinders ready to be tested

The cylinders were placed into the moulds after they were screwed and the space between them was filled with the produced mortar. The parallelism between the sides of the mould was checked and adjusted before the regularization of each specimen. The purpose of this particular kind of regularization is to ensure an optimum adherence between the specimen and the regularization during the test (Fig. 83).

Fig. 83. Cylinders place in the mould while the space between them is going to be filled with high strength mortar

After the pouring of mortar into the mould, the specimens were kept in laboratory conditions until the mortar reached the adequate strength (Fig. 82). After that, the specimens were extracted from the regularization moulds and were ready to be tested (Fig. 84). On the day of each test, the bases of the cylinders were cleaned from any mortar residue, dirt and other deposits to accommodate the placement of the measurement instruments. Mortar bulging from the joints was similarly treated. The widths of the caps were 110 mm for the 152 mm cores and about 70 mm for the 92 mm cores. These dimensions were chosen to maintain similar width to diameter ratios for the two different types of cylinders [30].

Fig. 84. Brick & Stone cylinders ready for compressive test

3.4.5.3 Compressive test procedure and setup

The cylinders which were extracted from the walls of the Escola Industrial were regularized with cement mortar cap in the laboratory. In order to reduce misleading results, conditionally best specimens were selected and tested. The cylindrical specimens were used to perform a compressive test with the aim of determining the compressive strength of the brick and of the stone masonry. The testing procedure consists of the appliance of a compressive load on the lateral surface of the specimen, in the same way as in the original structure, recording both the vertical displacements with the LVDT extensometers with a range of ± 5mm and a precision of 5 μm. The diameter of the specimens was 152 mm, as recommended by the UIC 778-3E:2011 guidelines. The cylinders with a diameter of 92 mm were tested also, including a single diametric mortar joint and two portions of brick. All the cores had an approximate depth of 145 mm [30].

The cylinders were tested in the Ibertest hydraulic press with a load cell capacity of 3000 kN. The load cell was set in a hinge configuration to facilitate the adjustment of the load plate with the bases for a uniform load distribution and the specimen was centred between two steel plates (Fig. 85). Displacement measurements were taken from 2 LVDTs placed in such a manner as to measure the vertical deformation of the cylinder, as suggested by the references consulted. So, 2 LVDTs were disposed vertically, on the bases of the cylinder, attached on the caps of regularization mortars.

- 2 LVDTs were positioned vertically (LVDT 1 and LVDT 2 with a range of ± 5 mm and a precision of 5 μm)

The LVDT supports were attached using an apparatus which was developed and manufactured in the laboratory in order to achieve good adhesion with minimal disturbance to the surfaces of the units (Fig. 85).

Fig. 85. Apparatus used for attaching the LVDTs

In all the tests, firstly cycles of compression were applied where the load was applied under force in a range of 5% - 30% f_k and then the load was applied under displacement control, until a very low level of residual strength, in order to capture the post peak response of the brick and the stone masonry.

Chapter 4: Results and analysis

4.1 In situ experiments

4.1.1 Results of the PPT in bricks

Penetrometric tests (PPT) of bricks were carried out at three positions (Zone 1, 2int, 3int) of the building. The penetration values read by the micrometre are presented in Table 23. These values have acceptable dispersion and present very similar results. This indicates that the investigated bricks present similar mechanical properties.

Table 23. Penetration depths that obtained from bricks with PPT

PPT	Zona 1 Penetration Depth[mm]	Zona 2int Penetration Depth [mm]	Zona 3int Penetration Depth [mm]
1	5.33	6.45	4.44
2	4.19	6.22	5.71
3	5.21	5.64	5.84
4	5.08	5.08	5.48
5	5.94	10.79	4.85
6	5.56	4.55	4.75
7	5.23	5.08	4.65
8	5.59	4.60	4.47
9	5.28	4.88	5.33
10	4.88	3.86	8.13
11	5.79	4.70	
12	6.32		
Average	**5.37**	**5.62**	**5.37**
Deviation	0.55	1.87	1.10
Coef. Var.	**10.2%**	**33.3%**	**20.4%**

4.1.2 Results of the HPT in bricks

Brick tests with the HPT were performed at the three different construction positions. The pull out force values read by the manometer are presented in Table 24. The pull out force values corresponding to Zone 1, 2int and 3int positions indicate similar mechanical properties.

The compressive strength of the brick f_b is obtained according to the method studied in [34]. By supposing that the tool during the extraction does not produce a significant radial compression state in the brick, the tangential stress τ_H corresponding to the force F pulling out the fastener is derived from the embedment length L and external diameter D_e of the helix:

$$\tau_H = \frac{F}{\pi * D_e * L}$$

where D_e = 6 mm and L = 30 mm. The compressive strength of the bricks f_b can be determined with the method by computing $9\tau_H$. The results are presented in Table 24.

Table 24. Pull out force values of the HPT in bricks

HPT	Zone 1		Zone 2int		Zone 3int	
	Pull out force [N]	Compressive strength fb [MPa]	Pull out force [N]	Compressive strength fb [MPa]	Pull out force [N]	Compressive strength fb [MPa]
1	1250	19.89	1650	26.26	1700	27.06
2	1900	30.24	2550	40.58	1300	20.69
3	1150	18.30	1400	22.28	1600	25.46
4	1350	21.49	1100	17.51	1900	30.24
5	1700	27.06	1400	22.28	1500	23.87
6	1300	20.69	1250	19.89	1750	27.85
7	1000	15.92	2000	31.83	1150	18.30
8	1900	30.24	700	11.14	1400	22.28
9	1100	17.51	1900	30.24	1600	25.46
10	1550	24.67	900	14.32	1700	27.06
Average	**1420**	**23.24**	**1485**	**23.63**	**1560**	**24.83**
Deviation	326		555		226	
Coef. Var.	**22.95%**		**37.39%**		**14.48%**	

4.1.3 Results of the PPT in mortar joints

The penetrometric tests of mortar joints with PPT were carried out in nine positions (Zone 1, 2int, 2ext, 3int brick, 3int stone, 3ext brick, 3ext stone, 4 and 6) of the building. The penetration depth values read by the micrometre are presented in Table 25.

. These values, according to previous studies [16], have an acceptable dispersion apart from Zone 4 results.

The values are very similar for five positions (Zone 1, 2int, 3int brick, 3ext brick, 3int stone), indicating the presence of mechanical properties quite homogeneous to the mortar joints. The depths of penetration are lower in the position of Zone 4. On the other hand, in the positions of Zone 2ext, 3ext and 5, the depth penetration values are inferiors due to the presence of mortar with a high resistance. The positions, Zone 2int and 3ext stone were carefully analysed, and their mortar was verified by means of hydrochloric acid and observations by microscope so as to observe that they contain cement something that could be observed also in situ as shown in Fig. 86.

Fig. 86. Mortar joint of the Zone 3_{ext} stone

Table 25. Penetration depths that obtained from mortar joints with PPT

PPT	Zone 1 [mm]	Zone 2int [mm]	Zone 2ext [mm]	Zone 3int Brick [mm]	Zone 3ext Brick [mm]	Zone 3int Stone [mm]	Zone 3ext Stone [mm]	Zone 4 [mm]	Zone 5 [mm]
1	10.97	13.84	5.41	9.40	9.68	9.78	4.72	8.00	6.86
2	9.83	10.16	5.16	9.17	8.36	10.67	4.17	8.66	5.44
3	7.62	8.64	5.79	9.78	8.43	10.79	4.52	10.87	5.79
4	9.80	7.37	5.77	9.52	10.41	8.64	4.77	7.24	5.97
5	7.75	9.68	5.94	9.91	10.03	8.64	4.60	9.52	5.46
6	8.53	7.04	7.62	8.64	8.97	9.19	4.75	9.14	
7	8.05	9.52	9.65		9.52			6.43	
8	6.98	9.70	7.11		9.02			6.04	
9	8.51	9.83	6.86		9.14			4.44	
10	7.31	7.47	6.48		10.29			6.12	
11	7.62								
Average	**8.45**	**9.32**	**6.58**	**9.40**	**9.38**	**9.61**	**4.59**	**7.65**	**5.90**
Deviation	1.25	1.96	1.33	0.46	0.73	0.96	0.23	1.95	0.58
Coef. Var.	**14.76%**	**21.05%**	**20.25%**	**4.88%**	**7.72%**	**10.00%**	**5.00%**	**25.46%**	**9.82%**

4.1.4 Results of the HPT in mortar joints

Mortar joint tests with the HPT were performed at eight different construction positions. The pull out force values read by the manometer are presented in Table 26. The lower pull out force values correspond to the Zone 2int, 3int brick and 3int stone position, indicating lower mechanical properties and confirming the results obtained with the PPT penetrometer. The highest values of the pull out force derive from Zone 1 and 2 confirming also the results obtained with the PPT penetrometer where the mechanical properties are superior. The highest value corresponds to position of the Zone 5 where the cement mortar joints can be found.

Table 26. Pull out force values of the HPT in mortar joints

HPT	Zone 1 [N]	Zone 2int [N]	Zone 2ext [N]	Zone 3int Brick [N]	Zone 3ext Brick [N]	Zone 3int Stone [N]	Zone 4 [N]	Zone 5 [N]
1	1300	400	1200	350	1300	400	1200	2100
2	800	300	600	250	1400	200	400	2200
3	900	550	1500	200	1000	750	1200	1800
4	500	400	1050	300	1000	350	400	1650
5	1000	350	1300	600	800		1200	1700
6	800	750	1000	350	550		600	
7	1300	500	1600		900		1650	
8	1050	450	550		950		700	
9	600	500	1300		450		900	
10	700	400	1100		600		300	
11	1200							
12	700							
13	1300							
14	1850							
15	1200							
Average	**1013**	**460**	**1120**	**342**	**895**	**425**	**855**	**1890**
Deviation	354	126	343	139	309	233	447	246
Coef. Var.	**34.916%**	**27.50%**	**30.66%**	**40.78%**	**34.48%**	**52.77%**	**52.34%**	**13.01%**

4.1.5 Results of the TPT in mortar joints

Mortar joints were tested with TPT at four different positions. The values of torque read by the dynamometric key and they converted to the compressive strength according to the formula that was calibrated in previous research presented in [18]. The values are presented in Table 27.

The obtained values are very similar, indicating similar mechanical properties. Lower values are obtained in Zone 4, but this is due to operational difficulties in the lime mortar of the rubble stone masonry wall where the irregularities in the stones and the voids inside made it difficult for the nail to touch the mortar as to find representative positions for the implementation of the test.

Table 27. Torque and compressive strength values after conversion by TPT

TPT	Zone 1		Zone 2int		Zone 3int Brick		Zona 4	
	[Mv]	[MPa]	[Mv]	[MPa]	[Mv]	[MPa]	[Mv]	[MPa]
1	7.32	1.87	5.50	1.30	13.79	4.19	7.09	1.80
2	10.52	2.67	8.92	2.41	14.09	4.31	14.68	4.54
3	8.69	2.32	12.71	3.78	10.32	2.89	14.62	4.51
4	13.17	3.95	15.67	4.93	9.63	2.65	6.85	1.72
5	14.10	4.31	13.00	3.89	10.90	3.10	11.88	3.47
6	11.32	3.26	8.78	2.36	7.96	2.08	10.87	3.09
7	17.45	5.66	9.49	2.60	11.64	3.38	5.69	1.36
8	12.49	3.69	8.05	2.11	9.91	2.75	4.26	0.94
9	9.41	2.57	8.60	2.30			9.58	2.64
10	8.29	2.19	6.29	1.54			4.86	1.11
Average		**3.3**		**2.7**		**3.2**		**2.52**
Deviation		1.2		1.1		0.7		1.35
Coef. Var.		**35.21%**		**41.67%**		**24.10%**		**53.47%**

The analytical expression that relates the compressive strength of the mortar to the maximum standardized torque measured during the TPT is the following [18]:

$$f_c = \left[\frac{m_v}{2\sqrt{55 * D_e * (D_e^2 - D_i^2)}}\right]^{1.274}$$

4.1.6 Summary of non-destructive in situ techniques with PPT, HPT and TPT

In the first phase of the experimental campaign, non-destructive in-situ techniques were performed, in order to preliminarily evaluate the variability of the surface properties of the component materials of the walls. Windsor Pin Penetration Test (PPT), Helix Screw Pull-out Test (HPT), and Torque Penetration Test (TPT) were performed where the results obtained with some variability in the joints, indicating some differences in properties on the mortars of different load walls. Zones 2int, 3int brick and stone have similar values, while Zone 1 and 2ext have higher values that indicate higher quality, and Zone 3ext brick and 4 have similar values that indicate intermediate quality as shown in Table 28.

Table 28. Summary of NDT with PPT, HPT, TPT

NDT			Position 1	Position 2int	Position 2ext	Position 3int Brick	Position 3int Stone	Position 3ext Brick	Position 3ext Stone	Position 4	Position 6
Mortar	HPT	Average F (N)	1013	460	1120	342	425	895	--	855	1890
		CV %	34.9%	27.5%	30.6%	40.8%	54.8%	34.5%	--	52.3%	13.0%
	PPT	Average d (mm)	8.45	9.32	6.58	9.40	9.62	9.38	10.26	7.65	5.90
		CV %	14.7%	21.0%	20.2%	4.8%	10.0%	7.7%	5.95%	25.5%	9.82%
	TPT	Average Mv	11.28	10.61	--	11.03	--	--	--	9.04	--
		CV %	27.5%	40.2%	--	18.9%	--	--	--	42.8%	--
Brick	HPT	Average F (N)	1420	1485		1560					
		CV %	22.9%	37.4%		34.5%					
	PPT	Average d (mm)	5.37	5.62		5.37					
		CV %	10.2%	33.3%		20.4%					

Fig. 87 shows a correlation of the compressive strength of the bricks f_b calculated in section 4.1.2 and the HPT results obtained from the in situ experimental research for the bricks. According to Ferguson [35], it is clear from the graph that the results are promising.

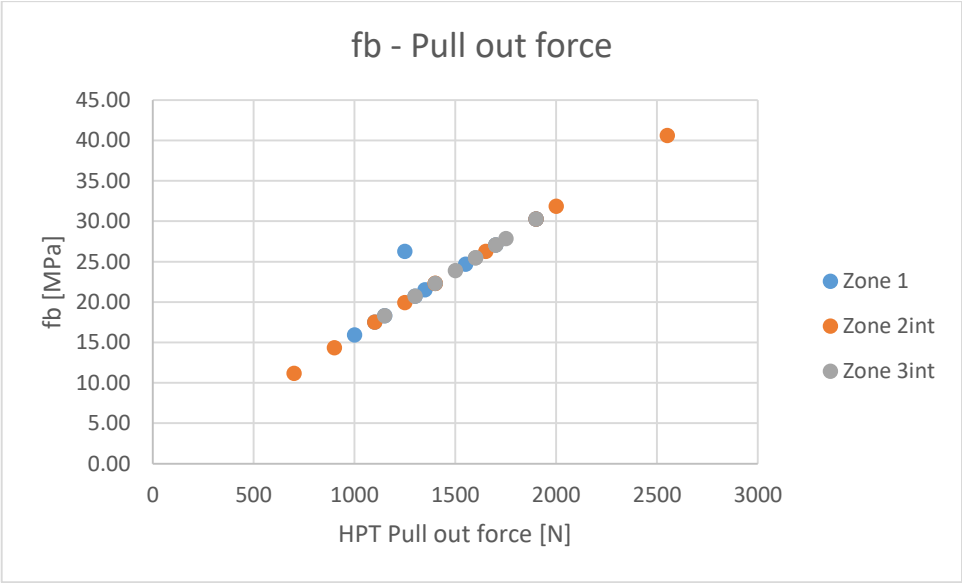

Fig. 87. Compressive strength fb – HPT pull put force : correlation obtained from the in situ experiments in bricks and the formula for the compressive strength

Fig. 88 shows a summary of the HPT and PPT results obtained from the in situ experimental research for mortars. The graph of pull out force values vs. the penetration depth shows the inherent relationship between the two different testing techniques and that their use allows the control of the quality of the in situ experimental results [16]. Fig. 89 presents the exponential trendline and the equation of it which can be used for the evaluation of the mortar characteristics and also for the control of new reporting mortars.

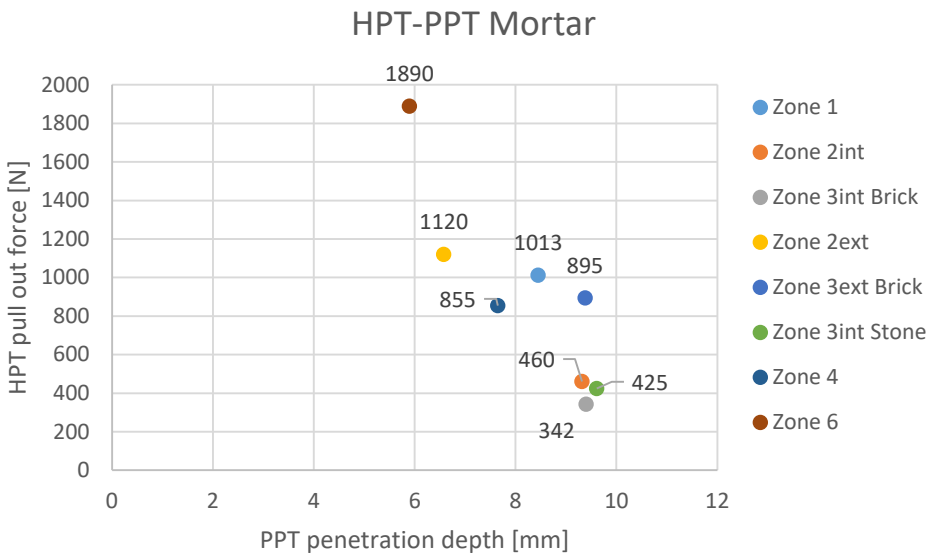

Fig. 88. Helifix pull out force vs Windsor Pin penetration depth: correlation obtained from the in situ experiments in mortar

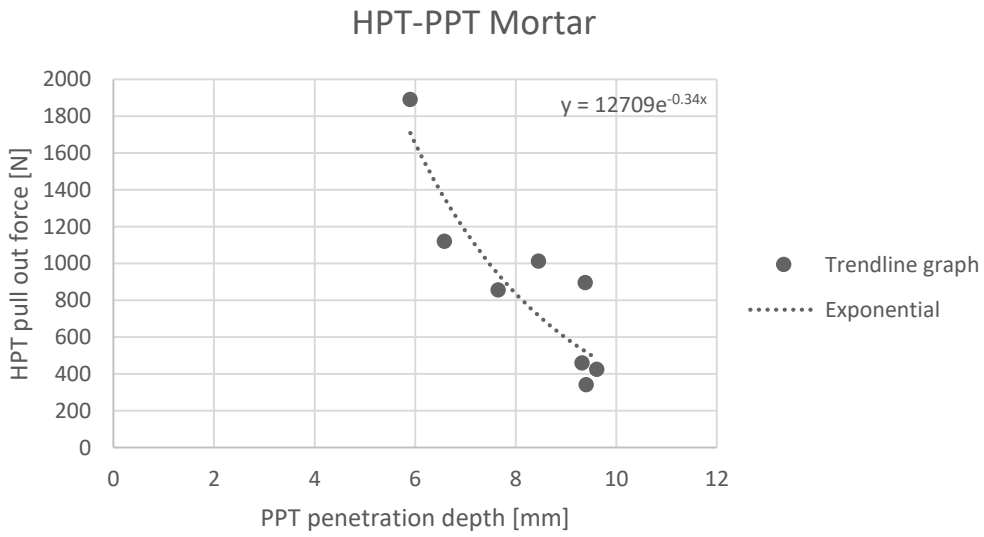

Fig. 89. Exponential trendline between all the zones tested in HPT and PPT for the mortar joints

4.2 Bricks

4.2.1 Brick specimens - Characterization results

The single compression test, according to EN 772-1 (CEN 2011), was performed on the 30 brick specimens obtained from the three positions, 23 specimens of 100×100×40 mm³ and 7 specimens of 50×50×40 mm^3 were tested. Fig. 90 shows the failure of the 100×100×40 mm³ brick specimens and Fig. 91 shows the failure 50×50×40 mm³ brick specimens with the typical hourglass form, which shows the loss of material on the sides.

Fig. 90. Failure of the 100×100×40 mm^3 specimens.

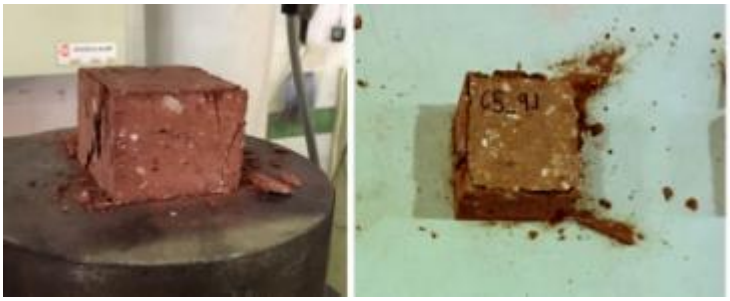

Fig. 91. Failure of the 50×50×40 mm^3 specimens.

The values of the compressive strength f_{b_exp} of each test specimen were shown in Table 29 for the 100×100×40 mm^3 specimens and in Table 30 for the 50×50×40 mm^3 specimens. According to the standard EN 772-1, these resistances must be converted to a standardized scale in order to take into account the shape ratio of the test. The standardized compressive strength f_{b_norm} is obtained by multiplying the resistance obtained with the form factor. The form factor value is 0.7 for the 100×100×40 mm³ specimens and 0.8 for the 50×50×40 mm³, values that were obtained from Table A.1 of Annex A of the standard.

Table 29. Experimental and standardized resistances obtained from brick specimens 100×100×40 mm³

	Specimen	fb_exp [MPa]	Coefficient factor	fb_norm [MPa]
Zone 1	1.A	25.4	0.7	17.8
	1.B	19.4	0.7	13.6
	2.A	19.9	0.7	14.0
	2.B	24.2	0.7	16.9
	3.A	32.4	0.7	22.6
	3.B	33.6	0.7	23.5
	4.A	28.4	0.7	19.9
	5	29.9	0.7	20.9
	6	25.5	0.7	17.8
	7	27.1	0.7	19.0
	Average	**27.1**		**19.0**
	Deviation	4.8		3.4
	Coef. Var.	**17.7%**		**17.7%**

	Specimen	fb_exp [MPa]	Coefficient factor	fb_norm [MPa]
Zone 2int	1.A	32.4	0.7	22.7
	1.B	33.2	0.7	23.2
	2.A	25.3	0.7	17.7
	2.B	26.6	0.7	18.6
	3.A	24.5	0.7	17.2
	3.B	26.8	0.7	18.8
	4.A	30.3	0.7	21.2
	4.B	33.3	0.7	23.3
	5	28.7	0.7	20.1
	6	25.2	0.7	17.6
	Average	**28.6**		**20.0**
	Deviation	3.4		2.4
	Coef. Var.	**12.0%**		**12.0 %**

	Specimen	fb_exp [MPa]	Coefficient factor	fb_norm [MPa]
Zone 3int	4	28.3	0.7	19.8
	5	25.9	0.7	18.2
	6	27.7	0.7	19.4
	Average	**27.3**		**19.1**
	Deviation	1.2		0.9
	Coef. Var.	**4.6%**		**4.6%**

Table 30. Experimental and standardized resistances obtained from brick specimens 50×50×40 mm³

	Specimen	fb_exp [MPa]	Coefficient factor	fb_norm [MPa]
Zone 3int	7	16.9	0.8	13.4
	8	15.9	0.8	12.7
	9.1	19.4	0.8	15.5
	9.2	18.6	0.8	14.9
	10.1	14.1	0.8	11.3
	10.2	14.8	0.8	11.8
	10.3	15.0	0.8	12.0
	Average	**16.4**		**13.1**
	Deviation	2.0		1.6
	Coef. Var.	**12.12%**		**12.1%**

The average compressive strength and the average compressive strength standardized according to EN 772-1 can be seen in Table 31. The observed variability in strength, with a coefficient of variation between 4.6% and 12.0%, which is acceptable, given the heterogeneities inherent in the factory units. In the case of Zone 1, the coefficient of variation of 17.7% indicates the diffuse presence of various qualities of bricks without significantly affecting the final result.

Table 31. Summary of the average of the standardized experimental resistances.

Position	fb_exp [MPa]	fb_norm [MPa]	Coef. Var.
Zone 1 [100×100×40 mm³]	27.1	19.0	17.7 %
Zone 2int [100× 100×40 mm³]	28.6	20.0	12.0 %
Zone 3int [100× 100×40 mm³]	27.3	19.1	4.6 %
Zone 3int [50×50×40 mm³]	16.4	13.1	12.1%

As for the brick specimens of 40×40×40 mm^3, the single compression test was also performed. In total 23 specimens were tested, 6 from Zone 1, 6 from Zone 2 and 11 from Zone 3. The values of the compressive strength f_{b_exp} of each test specimen are shown in Table 32. The standardized compressive strength f_{b_norm} is obtained by multiplying the resistance obtained with the form factor. The form factor value is 1.25 for the 40×40×40 mm³ specimens.

Table 32. Experimental and standardized resistances obtained from brick specimens 40×40×40 mm³

	Specimen	fb_exp [MPa]	Coefficient factor	fb_norm [MPa]
Zone 1	1	15.2	1.25	19.0
	2	11.9	1.25	14.9
	3	20.0	1.25	25.0
	4	21.4	1.25	26.8
	8	18.4	1.25	23
	9	15.1	1.25	18.9
	Average	**17.0**		**21.2**
	Deviation	3.6		4.45
	Coef. Var.	**21.0%**		**21.0%**

	Specimen	fb_exp [MPa]	Coefficient factor	fb_norm* [MPa]
Zone 2	1	15.8	1.25	19.8
	2	8.8	1.25	11.0
	3	14.2	1.25	17.8
	4	17.3	1.25	21.6
	5	16.0	1.25	20.0
	6	14.6	1.25	18.25
	Average	**14.4**		**18.1**
	Deviation	3.0		3.72
	Coef. Var.	**20.7%**		**20.6%**

	Specimen	fb_exp [MPa]	Coefficient factor	fb_norm* [MPa]
Zone 3int	1.1	9.6	1.25	19.0
	2.1	17.8	1.25	14.9
	2.2	18.5	1.25	25.0
	3.1	15.7	1.25	26.8
	3.2	18.1	1.25	23
	3.3	20.0	1.25	18.9
	5.1	17.2	1.25	21.5
	5.2	15.6	1.25	19.5
	6.1	16.5	1.25	20.6
	6.2	15.2	1.25	19.0
	6.3	11.1	1.25	13.9
	Average	**15.9**		**20.2**
	Deviation	3.1		3.86
	Coef. Var.	**19.5%**		**19.1%**

Fig. 92 shows the exponential correlation between the compressive strength and the height to width ratio of the three different type of specimens that were tested.

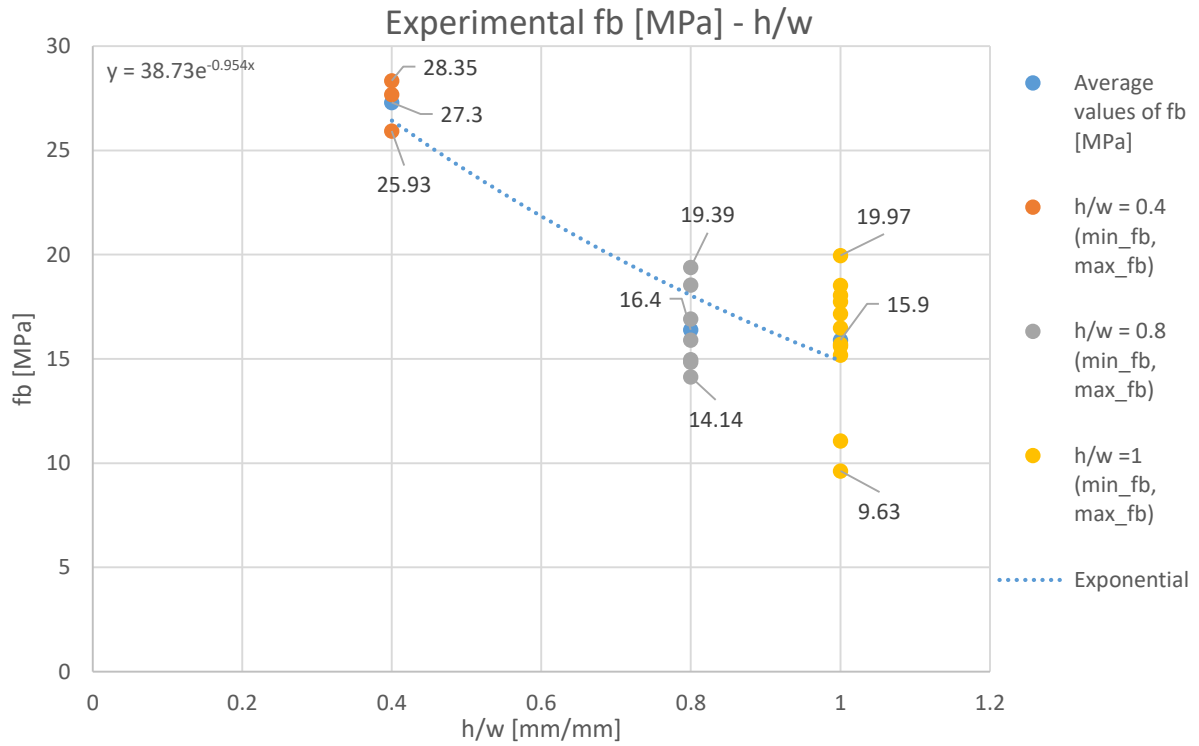

Fig. 92. Exponential correlation between the compressive strength and the height to width ratio of the 50×50×40 mm³ and 100×100×40 mm³ and the 40×40×40 mm³ brick specimens in Zone 3

4.2.2 Brick prisms – Young modulus and Poisson´s ratio

The Young's modulus of the bricks is defined by the brick specimens of 40×40×80 mm^3 as to understand the elastic response of the material. The height to width ratio is maintained at 1:2 and the top and the bottom surfaces of the specimens were polished in order to be completely parallel and have a totally uniform distribution of the compressive load. The load aplication was perpendicular to the width direction of the brick and the horizontal deformation was registered on the bed surface.

In the test for the evaluation of the Young's modulus and the Poisson's ratio, cycles of compression of loading and unloading were applied, remaining in the elastic range, keeping the minimum load value equal to 10% and a maximum load value equal to the one third of the ultimate strength found.

The results of the Young's modulus and the Poisson's ratio after the loading – unloading cycles are presented in Table 33. Comparing the results with the study of [36] where brick prisms with dimensions of 40×40×120 mm^3 were investigated for the evaluation of the Young's modulus between the 30% and 60% of the peak stress it is observed that the evaluation of the 40×40×80 mm^3 bricks gave higher value results. The coefficient of variation for Zone 1 is lower than the one obtained by the brick prisms of 40×40×120 mm^3 while it is similar for Zone 2. The coefficient of variation for the Poisson's ratio is very high for both zones. In Fig. 93 the results for the brick prisms of 40×40×120 mm^3 are presented.

	CB	EB
N. of tests	25	23
f_u[MPa]	14.25	10.52
v	12.93%	20.28%
N. of tests	17	13
$\varepsilon_u 10^{-3}$	9.01	5.66
v	9.32%	10.77%
N. of tests	18	23
$E_{s(30\text{-}60\%)}$[MPa]	2171	2156
v	13.71%	20.15%

Fig. 93. Evaluation of the Young's modulus for brick prisms EB of 40×40×120 mm³ [36]

Table 33. Young modulus and poisson ratio after the compressive test in 40×40×80 mm³ brick specimens in Zone 1 and Zone 2.

	Specimen	Tension [MPa]	Young Modulus [MPa]	Poisson ratio
Zone 1	1	10.4	5993.5	0.21
	2	15.4	9476.8	0.31
	3	16.4	7715.1	0.13
	4	17.9	8572.4	--
	8	21.0	8250.8	0.08
	9	16.8	8335.8	0.14
	Average	**16.3**	**8057.4**	**0.17**
	Deviation	3.5	1163.8	0.09
	Coef. Var.	**21.3%**	**14.44%**	**51.31%**

	Specimen	Tension [MPa]	Young Modulus [MPa]	Poisson ratio
Zone 2	1	23.9	9128.2	0.18
	2	10.4	5098.2	0.05
	3	11.4	6087.9	--
	5	15.6	6266.0	0.08
	6	12.7	7008.8	--
	Average	**14.8**	**6717.8**	**0.11**
	Deviation	5.5	1509.9	0.07
	Coef. Var.	**36.9%**	**22.48%**	**64.41%**

The comparison of the Young's modulus for Zone 1 and Zone 2 is presented in Fig. 94. The order of magnitude of the Young's modulus is in a close range and the results can be considered reliable.

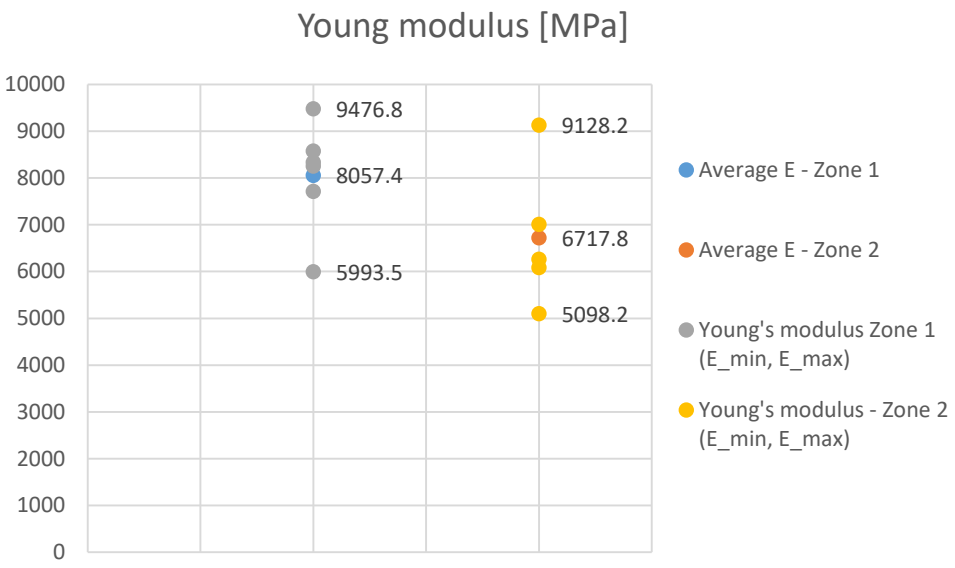

Fig. 94. Comparison of Young's modulus for Zone 1 and Zone 2

The comparison of the Poisson's ratio for Zone 1 and Zone 2 is presented in Fig. 95.

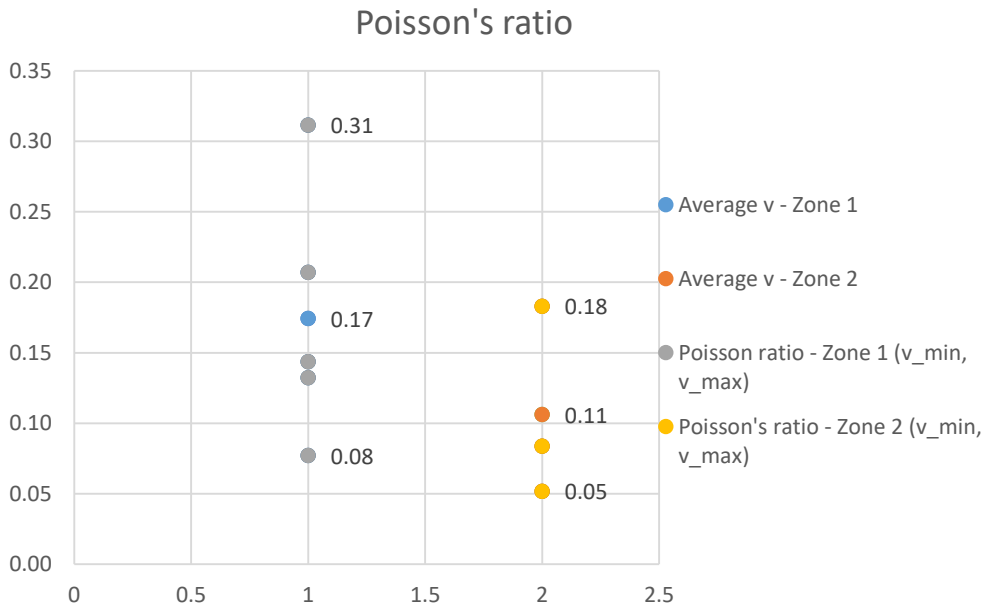

Fig. 95. Comparison of Poisson's ratio for Zone 1 and Zone 2

4.3 Tiles

4.3.1 Characterization results

The compression test of the brick tiles was performed on the 6 assembled specimens obtained from the position of Zone 5 on the vaults of the underground floor. Fig. 96 shows the failure mode of the brick tiles under compression.

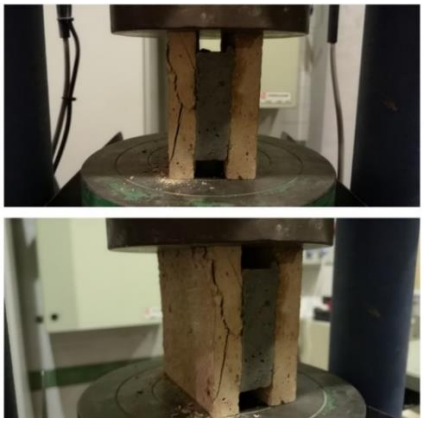

Fig. 96. Cracking failure of the brick tiles

The values of the compressive strength fb_{exp} of each test are presented in Table 34. The specimens from the brick 3 (3a and 3b) are not representative cause the 3b specimen broke due to bending and it could not be used for the study of compression as all the load was concentrated in the specimen 3a. A proportional force is calculated for each tile which is half of the force that is needed for the specimen to reach the failure mode. The compressive strength fb_{exp} is calculated by dividing this proportional force with the area of each tile specimen.

Table 34. Summary of the average of the experimental resistance values.

	Specimen	fb_exp [MPa]
Zone 5 - Vaults	Tile_2a	8.9
	Tile_2b	8.8
	Tile_3a	7.4
	Tile_3b	--
	Tile_4a	21.5
	Tile_4b	19.8
	Tile_5a	21.0
	Tile_5b	21.3
	Tile_6	12.1
	Tile_7	10.7
	Tile_8	13.8
	Tile_9	14.5
	Average	**14.5**
	Deviation	5.5
	Coef. Var.	**37.7 %**

4.4 Stone

4.4.1 Characterization results of the stone specimens

The compression tests of the 13 specimens obtained from the 3 stones extracted from the Zone 3ext and Zone 4 was completed according to the EN 1926 standard. Fig. 97 shows the rupture of the 50×50×50 mm³ stone specimens with the typical hourglass shape, where you can see the loss of material on the sides.

Fig. 97. Failure of the 50×50×50 mm³ stone specimens

During the tests, the values of the *R_exp* compressive strength of each test specimen were obtained as it can be seen in Table 35. According to Annex C of the EN 1926 standard, the average is calculated based on the values obtained for each of the specimens. 4 specimens of the stone '1' of Zone 3ext, 6 specimens of the stone '2' and 3 specimens of the stone '3' of Zone 4 were tested.

Table 35. Experimentally obtained compressive strengths of the 50×50×50 mm³ stone specimens

Specimen	R_exp [MPa]
1.A	56.3
1.B	46.8
1.C	64.3
1.D	52.8
Average	**55.0**
Deviation	7.3
Coef. Var.	**13.3%**

Specimen	R_exp [MPa]
2.A	29.7
2.B	35.1
2.C	30.9
2.D	34.6
2.E	36.2
2.F	37.3
Average	**34.0**
Deviation	3.0
Coef. Var.	**8.8%**

Specimen	R_exp [MPa]
3.A	47.4
3.B	64.4
3.C	61.3
Average	**57.7**
Deviation	9.1
Coef. Var.	**15.7%**

From the compressive tests of the stone specimens for the load-bearing walls, the standardized mean strength values *fb_norm* according to EN 1926 are given in Table 36. Table 36 gives the averages for the standardized strengths of the specimens corresponding to each of the extracted stones.

Table 36. Summary of the compressive tests on the stone specimens

Position	fb_exp [MPa]	CV
Zona 3ext	**55.0**	13.3%
Zona 4	**34.0**	8.9%
	57.7	15.7%

From the study of Siegesmund and Snethlage in [37] in Fig 3.53 pg. 172, it can be observed that stone '1' of Zone 3ext with an average compressive strength of 55 MPa, stone '2' of Zone 4 with an average compressive strength of 34 MPa and stone '3' of Zone 4 with an average compressive strength of 58 MPa have a value of compressive strength that belongs in the range of the sandstone of porosity class III, the carbonate rock of oolithic limestone, the carbonate rock of limestone < 2.60 g/cm^3 and the carbonate rock of travertine.

4.5 Mortar

4.5.1 DPT on the mortar joints

The double punch test was performed on 120 mortars specimens in total, 84 specimens from the positions of the walls (Zone 1, 2int, 3int brick, 3ext stone and 4) and 18 specimens from the position of the vaults (Zone 5), 12 from the position of the exterior design of facade stone walls (Zone 3ext_ext stone) and 6 from the position of the foundations (Zone F). Table 37 shows the results of the resistance obtained by dividing the maximum force by the area of the load plate, which in this case is 314 mm^2.

Table 37. Compressive resistances after DPT in the mortar joints

Extraction position	ID	fm [MPa]	Extraction position	ID	fm [MPa]	Extraction position	ID	fm [MPa]
Zone 1	DPT_1.01	3.0	Zone 2int	DPT_2.01	2.8	Zone 3int	DPT_3.01	3.6
	DPT_1.02	5.3		DPT_2.02	2.0		DPT_3.02	1.8
	DPT_1.03	4.5		DPT_2.03	2.6		DPT_3.03	1.8
	DPT_1.04	2.6		DPT_2.04	1.6		DPT_3.04	1.8
	DPT_1.05	3.3		DPT_2.05	1.7		DPT_3.05	1.7
	DPT_1.06	5.1		DPT_2.06	2.4		DPT_3.06	1.3
	DPT_1.07	3.9		DPT_2.07	2.8		DPT_3.07	1.3
	DPT_1.08	4.3		DPT_2.08	2.6		DPT_3.08	1.3
	DPT_1.09	3.0		DPT_2.09	2.0		DPT_3.09	1.6
	DPT_1.10	2.6		DPT_2.10	1.2		DPT_3.10	1.2
	DPT_1.11	3.3		DPT_2.11	1.3		DPT_3.11	1.0
	DPT_1.12	4.8		DPT_2.12	2.7		DPT_3.12	2.4
	DPT_1.13	2.3		DPT_2.13	1.4		DPT_3.13	2.3
	DPT_1.14	5.3		DPT_2.14	3.0			
	DPT_1.15	1.6		DPT_2.15	2.4			
	DPT_1.16	4.1		DPT_2.16	1.0			
	DPT_1.17	2.9		DPT_2.17	1.9			
	DPT_1.18	2.3		DPT_2.18	3.7			
	DPT_1.19	2.7		DPT_2.19	1.4			
	DPT_1.20	2.3		DPT_2.20	2.7			
	DPT_1.21	1.2		DPT_2.21	1.2			
	DPT_1.22	4.6		DPT_2.22	2.1			
	DPT_1.23	1.6		DPT_2.23	2.4			
	DPT_1.24	5.3		DPT_2.24	1.2			
	DPT_1.25	3.2		DPT_2.25	1.3			
	DPT_1.26	5.1						
	Average	**3.5**		**Average**	**2.1**		**Average**	**1.8**
	Deviation	1.3		Deviation	0.7		Deviation	0.7
	Coef. Var.	**36.6%**		**Coef. Var.**	**34.3%**		**Coef. Var.**	**38.7%**

Extraction position	ID	fm [MPa]	Extraction position	ID	fm [MPa]
Zone 3ext Stone	DPT_3.01	3.5	Zone 4	DPT_4.01	5.2
	DPT_3.02	4.4		DPT_4.02	4.3
	DPT_3.03	2.4		DPT_4.03	4.1
	DPT_3.04	3.9		DPT_4.04	4.1
	DPT_3.05	1.5		DPT_4.05	2.9
	DPT_3.06	2.6		DPT_4.06	3.3
	DPT_3.07	2.9		DPT_4.07	2.7
	DPT_3.08	3.2		DPT_4.08	3.4
	DPT_3.09	2.9		DPT_4.09	4.3
	DPT_3.10	3.5		DPT_4.10	3.9
	Average	**3.1**		**Average**	**3.8**
	Deviation	0.8		Deviation	0.8
	Coef. Var.	**26.2%**		**Coef. Var.**	**20.0%**

Extraction position	ID	fm [MPa]
Zone 5	DPT_5.01	11.2
	DPT_5.02	9.1
	DPT_5.03	10.2
	DPT_5.04	7.2
	DPT_5.05	7.2
	DPT_5.06	10.5
	DPT_5.07	5.8
	DPT_5.08	8.3
	DPT_5.09	7.3
	DPT_5.10	6.3
	DPT_5.11	7.3
	DPT_5.12	10.6
	DPT_5.13	7.0
	DPT_5.14	7.2
	DPT_5.15	6.3
	DPT_5.16	5.1
	DPT_5.17	7.2
	DPT_5.18	6.5
	Average	**7.8**
	Deviation	1.8
	Coef. Var.	**22.8%**

Extraction position	ID	fm [MPa]	Extraction position	ID	fm [MPa]
	DPT_3.01	5.67		DPT_F.01	16.56
	DPT_3.02	6.56		DPT_F.02	9.05
	DPT_3.03	--		DPT_F.03	12.56
	DPT_3.04	12.56		DPT_F.04	13.68
Zone 3ext_ext	DPT_3.05	8.76		DPT_F.05	9.66
Stone	DPT_3.06	17.42	Zone F	DPT_F.06	18.37
	DPT_3.07	20.82			
	DPT_3.08	--			
	DPT_3.09	6.77			
	DPT_3.10	21.10			
	DPT_3.11	15.09			
	DPT_3.12	18.37			
	Average	**13.3**		**Average**	**13.3**
	Deviation	6.1		Deviation	3.7
	Coef. Var.	**45.54%**		**Coef. Var.**	**27.79%**

Table 38 presents the summary of the results obtained in the different areas. According to the UIC regulations (UIC 1995), the experimental compressive strengths obtained from the DPT must be corrected to take into account the reduced shape of the specimen, in order to evaluate the uniaxial compressive strength of the material. The standardized compressive strength fm_{norm} is obtained by multiplying the strength obtained by a coefficient factor of 0.7 recommended by the standards. The lower strength values for the walls were obtained in the 2int and 3int brick Zones, while the rest of the values of Zone 1, 3ext stone and 4 show similar strength values. These values confirm the results obtained from in situ tests with PPT, HPT and TPT except for the 3int brick and stone positions which have shown certain inconsistencies. Mortar of the Zone 5 of the vaults, mortar of the exterior stone facade 3ext_ext and mortar from zone F of the foundations have shown much higher compressive strength.

Table 38. Summary table with the average of the experimental and the standardized strength

Position	fm_{exp} [MPa]	fm_{norm} [MPa]	Coef. Variation
Zone 1	3.5	2.4	36.6%
Zone 2int	2.1	1.4	34.3%
Zone 3int brick	1.8	1.2	38.7%
Zone 3ext stone	3.1	2.2	26.2%
Zone 4	3.8	2.7	20.0%
Zone 5	7.8	5.5	22.8%
Zone 3ext_ext stone	13.3	9.3	45.5%
Zone F	13.3	9.3	27.8%

Fig. 98 presents the relationship between the DPT strength results obtained in the laboratory and the HPT results obtained from the in situ experimental technique. The diagram shows very

good agreement for the two different testing techniques as while the pull out force increases, the compressive strength increases simultaneously. Fig. 99 presents the exponential curve that shows the capability of the HPT technique to represent the monotonically increase of the DPT mortar strengths [16].

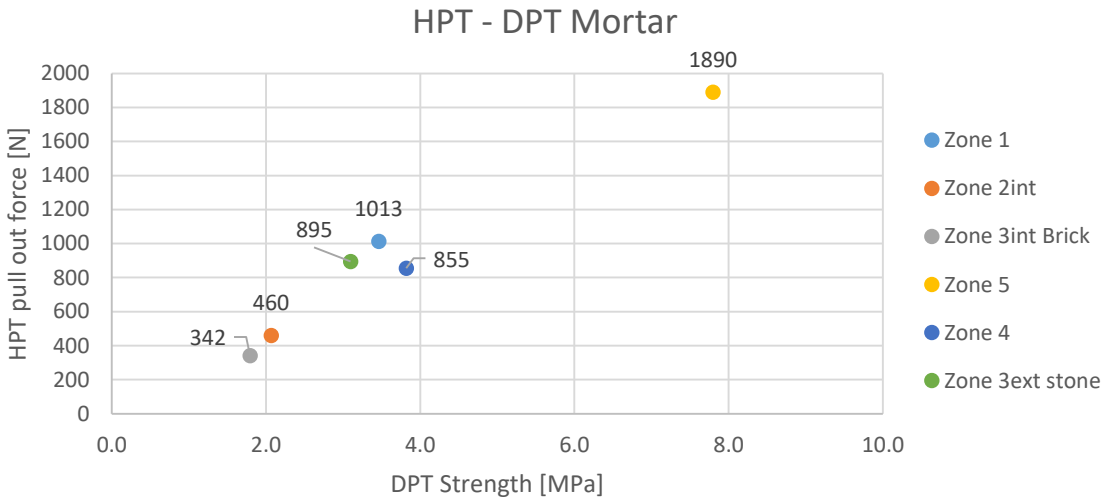

Fig. 98. Empirical relationship between double punch tests strengths and helifix pull out forces

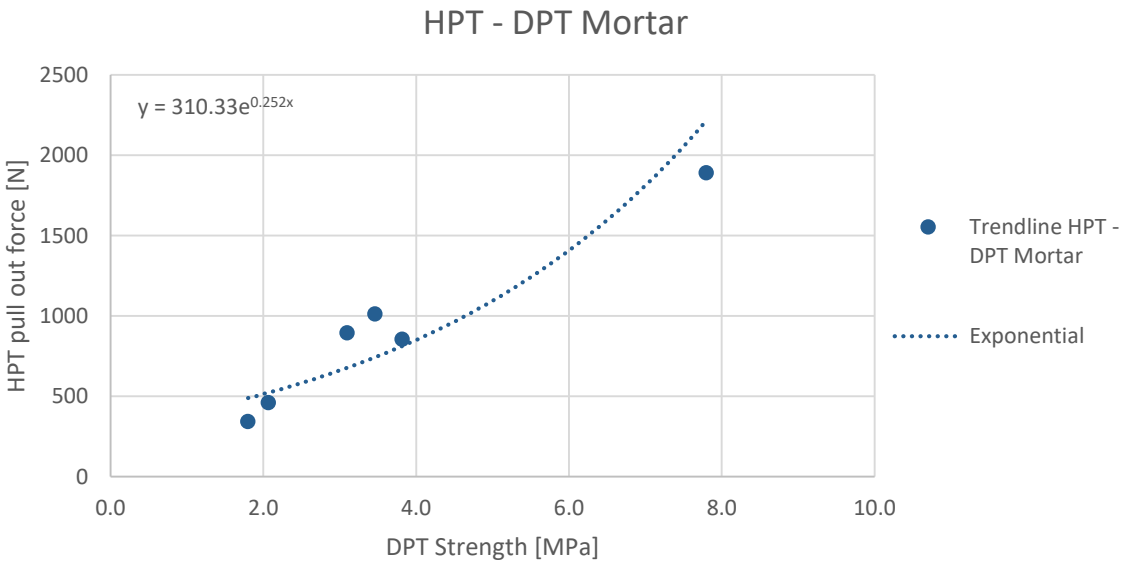

Fig. 99. Exponential trendline between all the common zones tested in HPT and DPT for the mortar joints

Fig. 100 presents the relationship between the PPT readings from the in situ experimental technique and the DPT strengths of the mortar carried out in the laboratory. The depth of the penetration decreases as the mortar hardens and its strength increases. Fig. 101 presents the exponential curve that shows the capability of the PPT technique to represent the monotonically decrease of the DPT mortar strengths [16].

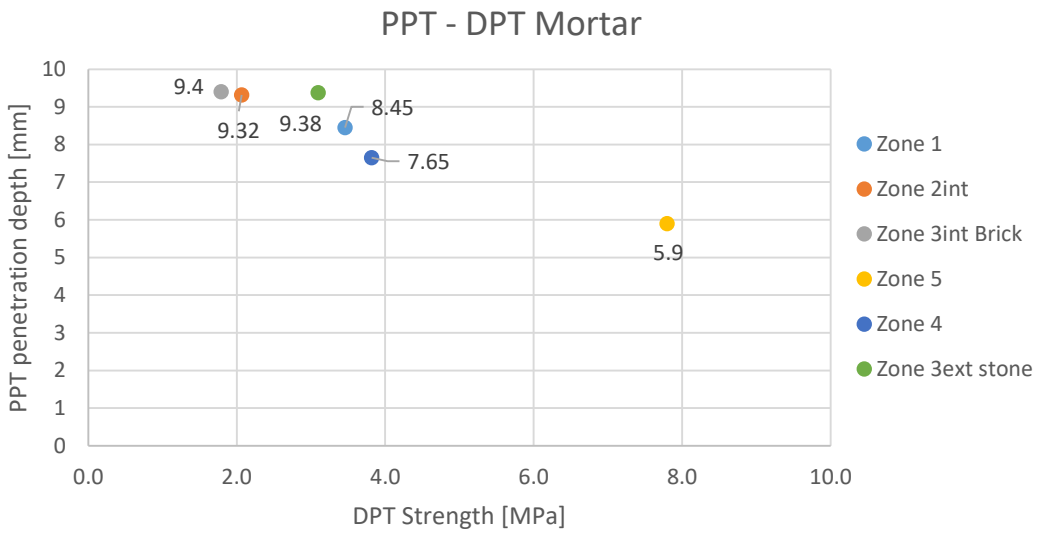

Fig. 100. Empirical relationship between double punch tests strengths and pin penetration depths

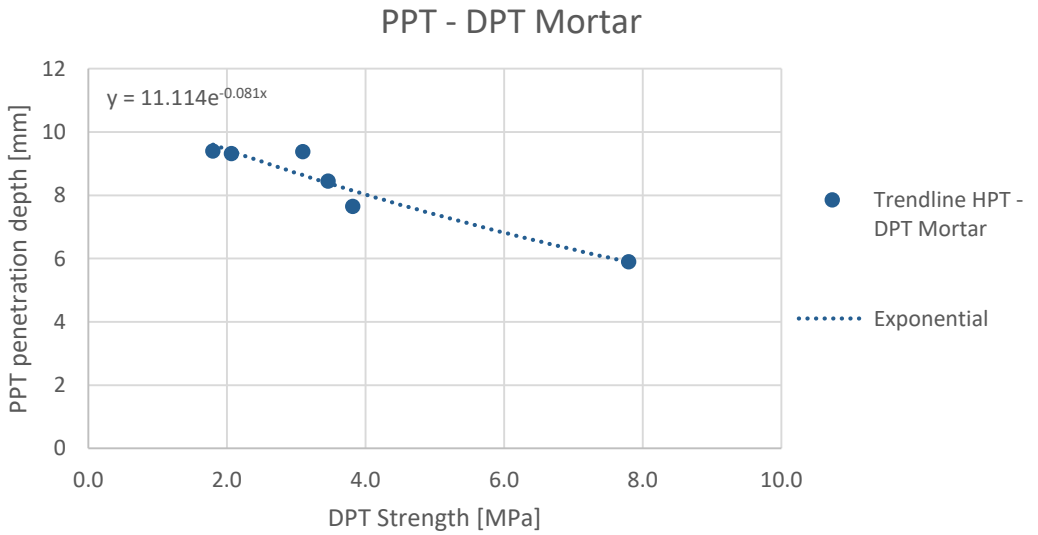

Fig. 101. Exponential trendline between all the common zones tested in PPT and DPT for the mortar joints

4.5.2 Compressive tests on the mortar cubes

The strength of the mortar cubes is calculated according to the EN 1015-11 as the maximum load carried by the specimen divided by its cross-sectional area. The results obtained are shown in Table 39.

Table 39. Compressive strengths of the 40×40×40 mm³ mortar cubes

	Specimen	Tension [MPa]	Deformation [mm]
Z.1	1	2.0	0.0521

	Specimen	Tension [MPa]	Deformation [mm]
Z. 3	1	1.8	0.0315
	2	1.5	0.0388
	Average	**1.7**	**0.0351**
	Deviation	0.2	0.0052
	Coef. Var.	**10.1%**	**14.66%**

	Specimen	Tension [MPa]	Deformation [mm]
Zone 4	1	2.9	0.0279
	2	2.8	0.0336
	3	4.0	0.0314
	4	3.5	0.0199
	5	2.2	0.0309
	6	4.2	0.0389
	7	3.5	0.0486
	Average	**3.3**	**0.0330**
	Deviation	0.7	0.0090
	Coef. Var.	**21.12%**	**27.20%**

4.6 Estimation of compressive strength from component resistances

The Basic Document "SE-F Seguridad estructural: Fábrica" (Código Técnico de la Edificación 2009), allows to deduce indirectly the characteristic resistance of the wall (f_k_SE-F), using the following formula, indicated in Annex C of the regulations:

$$f_{k\_SE-F} = K\, f_b^{0.65} f_m^{0.25}$$

Where f_b represents the standardized average compressive strength of the brick, f_m represents the average compressive strength of the mortar and K is a factor corresponding to the value 0.6 for solid brick pieces.

Zone 1 - $f_{k_{SE-F}} = 0.6 \cdot\ 19.0^{0.65} \cdot 2.4^{0.25} = 5.06\ MPa$

Zone 2int - $f_{k_{SE-F}} = 0.6 \cdot\ 20.0^{0.65} \cdot 1.4^{0.25} = 4.57\ MPa$

Zone 3int - $f_{k_{SE-F}} = 0.6 \cdot\ 19.1^{0.65} \cdot 1.2^{0.25} = 4.27\ MPa$

The same formula is used for the zone 5 of the vaults:

Zone 5 - $f_{k_{SE-F}} = 0.6 \cdot\ 14.5^{0.65} \cdot 5.5^{0.25} = 5.22\ MPa$

Regarding the stone, there is not specific formula which can be used in order to evaluate the compressive strength.

The formula of the Eurocode 6 differs from the Spanish standards where the exponent of f_b is 0.7, the exponent of f_m is 0.3 and the factor K is equal to 0.55.

Zone 1 - $f_{k_{SE-F}} = 0.55 \cdot\ 19.0^{0.70} \cdot 2.4^{0.30} = 5.62\ MPa$

Zone 2int - $f_{k_{SE-F}} = 0.55 \cdot\ 20.0^{0.70} \cdot 1.4^{0.30} = 4.95\ MPa$

Zone 3int - $f_{k_{SE-F}} = 0.55 \cdot\ 19.1^{0.70} \cdot 1.2^{0.30} = 4.58\ MPa$

The same formula is used for the Zone 5 of the vaults:

Zone 5 - $f_{k_{SE-F}} = 0.55 \cdot\ 14.5^{0.70} \cdot 5.5^{0.30} = 5.96\ MPa$

Table 40 shows that the characteristic values of the compressive strength of the experimentally obtained value f_k_exp are lower than the estimated values using the analytical expression of the Basic Document SE-F of the Technical Building Code f_k_DE-F and the Eurocode EC6 1996-1-1 f_k_EC6 the Zone 1, 2int and 3int positions.

Table 40. Comparison between the typical values of compressive strength estimated with DB SE-F and EC6 1996-1-1 based on the components, and those obtained experimentally.

Position	DB SE-F fκ [MPa]	EC 6 1996-1-1 fk [MPa]	experimental fk [MPa]
Zone 1	5.06	5.62	4.96
Zone 2int	4.57	4.95	4.29
Zone 3int	4.27	4.58	3.94*

For the Zone 5, vault zone, due to the inability to extract entire samples and to perform test specimens including tiles and mortar joints, the characteristic compressive strength has been calculated by means of the analytical expression of the Basic Document SE-F of the Technical Building Code f_k_DE-F and Eurocode EC6 1996-1-1 based on the experimental average resistances of the component materials. The values obtained by Zone 5 are shown in Table 41.

Table 41. Characteristic values of compressive strength of the bricks of the vaults estimated with the DB SE-F regulations from the components.

Position	DB SE-F fk [MPa]	EC 6 1996-1-1 fk [MPa]
Zone 5	5.22	5.96

4.7 Masonry

4.7.1 Compressive tests on the brick cylinders

The results for the brick cylinder specimens that were drilled from the masonry are explained in section 4.7.1. Compressive strengths are calculated and stress – strain curves are presented. Also, the failure modes are shown and the Young's modulus of elasticity is presented.

Compressive tests on the brick cylinders that were extracted from the masonry were performed with a goal to evaluate the compressive strength and the Young's modulus of elasticity. Specifically, 6 specimens of 152 mm diameter with three joints and 7 specimens of diameter of 92 mm with one joint where analysed. In both types of cylinders, the load was applied under displacement control until a very low level of residual strength, in order to capture the post peak response of the brick masonry. Two LVDTs were attached on the two caps of regularization mortar, in vertical position, to measure the vertical displacements necessary for the calculation of the Young's modulus. Cycles of compression were applied from 5% to 30% of the maximum load expected.

The strength was directly obtained from as the maximum experimental strength divided by the cross section of the cylinder (diameter by length), as suggested by the UIC regulations (UIC 1995) and recent works performed on the Polytechnic University of Catalonia [31][29][30].

Experimental evidence shows that the specimen's crack occurs in correspondence with the lateral ends of the high-strength mortar caps, leading to the detachment of the less confined lateral parts. Fig. 102 shows the failure modes after the test, and clearly the correspondence of the cracks, with the limits of the high-strength mortar caps on which the load is applied, is observed.

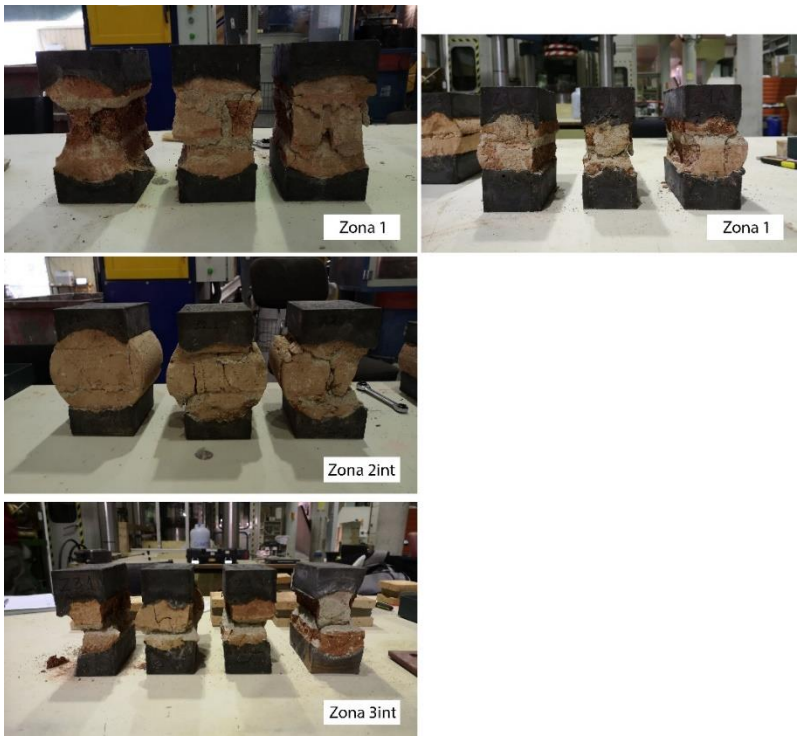

Fig. 102. Crack mechanisms of the cylinders where the typical failure in the hourglass mode is observed

4.7.2 Stress – deformation curves

The compressive stress – vertical deformation curves of the specimens with three joints and one joint are shown respectively in Fig. 103. At the upper part are presented the 6 cylinders of 152 mm diameter, while at the lower part are presented the 7 cylinders of the 90 mm diameter.

It can be observed the presence of a peak in the loading branch, corresponding to the appearance of the first crack. After the peak, the cylinder follows to resist to higher loads, until reaching the maximum level of compression and the beginning of the unloading branch, where the deformation increases gradually with the diminution of the stress. The part of the curve after the first peak has an uneven trend, probably due to the failure for propagation of cracks across the specimen.

Table 42 presents the compressive strength values obtained for each cylinder according to the maximum load obtained in each experiment.

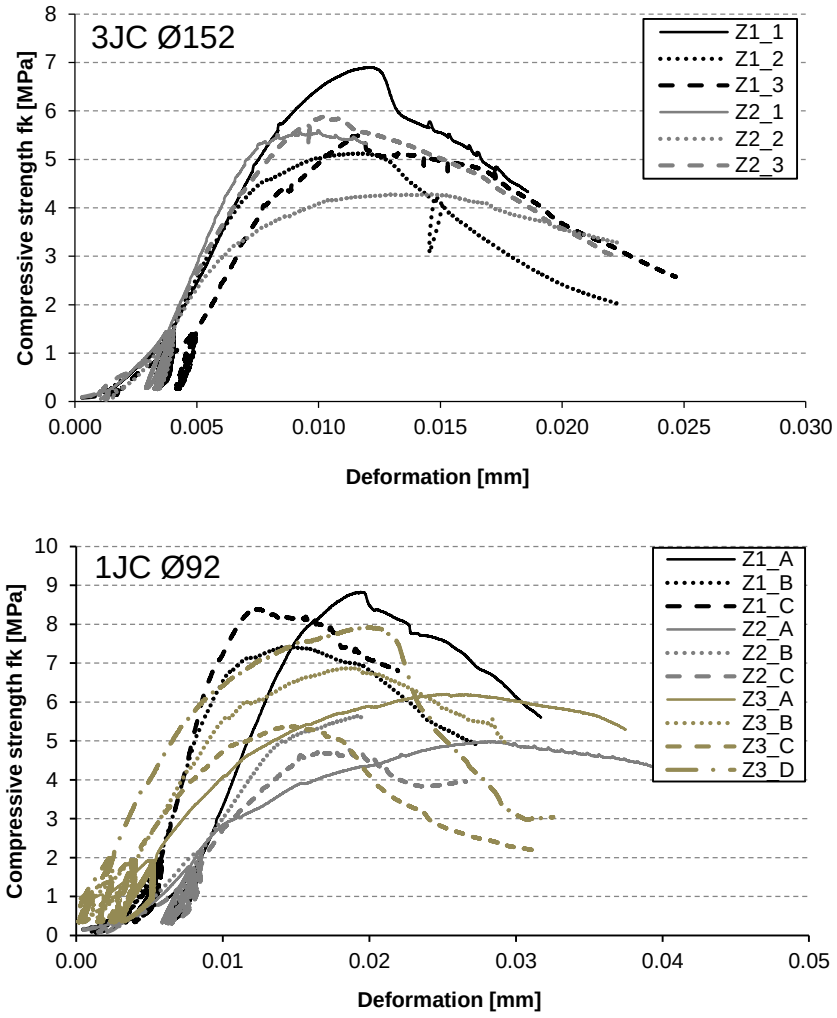

Fig. 103. Compressive stress vs. Vertical deformation derived from compression tests of cylindrical specimens. Up: cylinders of 152mm diameter, Down: 92mm cylinders

Table 42. Compressive strength of cylindrical specimens

Position of extraction	Specimen Ø152	f max [kN]	fc [MPa]	Specimen Ø92	f max [kN]	fc [MPa]
Zone 1	Z1_1	116.59	5.45	Z1_A	114.45	8.63
	Z1_2	148.46	6.90	Z1_B	94.81	7.28
	Z1_3	124.96	5.50	Z1_C	104.30	8.20
		Average	**5.95**		**Average**	**8.04**
		Deviation	0.82		Deviation	0.69
		Coef. Var.	**13.9%**		**Coef. Var.**	**8.61%**
Zone 2int	Z2_1	122.18	5.59			
	Z2_2	92.73	4.29			
	Z2_3	132.05	5.89			
		Average	**5.26**			
		Deviation	0.85			
		Coef. Var.	**16.16%**			
Zone 3int				Z3_A	76.40	6.07
				Z3_B	87.75	6.73
				Z3_C	65.66	5.26
				Z3_D	95.27	7.75
					Average	**6.45**
					Deviation	1.05
					Coef. Var.	**16.32%**

Based on the experimental average value obtained for each extraction zone, it is possible to calculate the characteristic value according to the criteria indicated in EN 1052-1 (CEN 1999) in section 10.2.a for Zones 1, 2int and 3int. Table 43 shows the results obtained for each zone.

Table 43. Compressive characteristic strength of the 152 mm and 92 mm diameter cylindrical specimens

Position	fk_exp [MPa] Ø152	fk_exp [MPa] Ø92
Zone 1	4.96	6.70
Zone 2int	4.29	--
Zone 3int	--	5.26

In Zone 3int the factor of 0.75 between the strengths of the 152 mm cylinders and the 92 mm cylinder is assumed, as it was obtained either experimentally from Zone 1 in the Escola Industrial campaign or from the similar experimental campaign that were carried out previously at the Polytechnic University of Catalonia and published in the international journal ‘’Construction and Building Materials’’ [30]. This relationship and the results obtained are shown in Table 44.

Table 44. Relationship between cylinders of 92 mm and 152 mm

Position	fk_exp [MPa] Ø152
Zone 1	4.96
Zone 2	4.29
Zone 3int	3.94*

* Estimated ratio based on the factor of 0.75 for the cylinders with a diameter of 92 mm.

4.7.3 Compressive tests on the stone cylinders

A total of 2 cylindrical samples of 152 mm diameter and 2 cylindrical samples of 92 mm diameter were tested in compression. The strength was directly obtained as the maximum experimental strength divided by the cross section of the cylinder (diameter by length), as suggested by the UIC regulation (UIC 1995).

Due to the irregularity of the stone masonry, the fracture occurs irregularly, although a tendency to fractures can be observed in correspondence with the lateral ends of the high-strength mortar, leading to a detachment of the side parts that are less confined. Fig. 104 shows the cylinder specimens after the compression test.

Fig. 104. Fracture mechanisms in the cylindrical samples where typical hourglass failure is observed

Fig. 105 shows the compression - vertical displacement curves obtained from the experimental tests, on the left the tests were performed on the 2 cylindrical samples of 152 mm diameter and on the right the tests were performed on the 2 cylindrical samples of 92 mm diameter. Table 45 presents the compressive strength values obtained for each cylinder according to the maximum load obtained in each experiment.

4.7.4 Stress – deformation curves

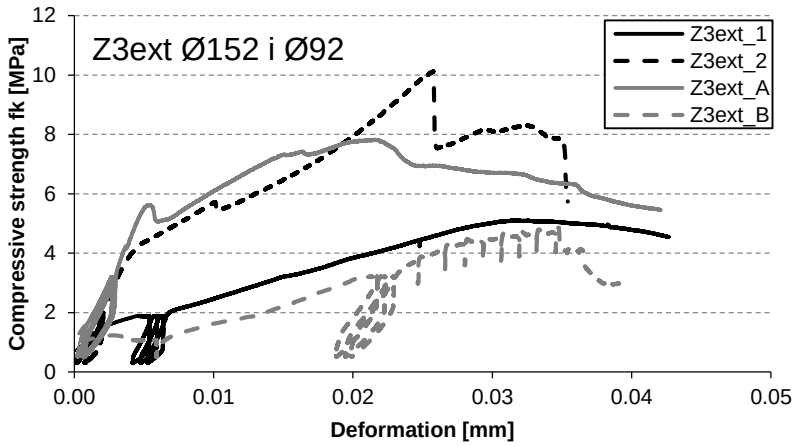

Fig. 105. Compression - vertical displacement curves of the stone cylindrical specimens

Table 45. Compressive strength of the cylindrical specimens (92 mm and 152 mm)

Extraction position	Specimens Ø152	f max [kN]	fc [MPa]	Specimens Ø92	f max [kN]	fc [MPa]
Zone 3ext	Z3_1	81.73	5.10	Z3_A	73.42	7.82
	Z3_2	160.49	10.14	Z3_B	45.58	4.84
		Average	**7.62**		**Average**	**6.33**
		Deviation	3.56		Deviation	2.11
		Coef. Var.	**46.7%**		**Coef. Var.**	**33.3%**

The large dispersion obtained in the experimental results, with very high coefficients of variation (even equal to 46.7% in the 152 mm diameter cylinder specimens), is due to the significant irregularities observed in the test specimens taken from the existing masonry, in the presence of significant thicknesses or defects in mortar joints, as well as the very irregular shapes of the units.

All these aspects demonstrate that it is impossible to clearly define a single representative value and a characteristic strength value of this type of masonry because there is a limited number of specimens. In fact, it should be mentioned that due to the heritage value of the researched construction, only 4 extractions from the outer leaf of the stone masonry facade wall were authorized, and therefore no further testing was possible.

The great complexity and irregularity of the stone masonry that composes the outer facade wall complicates the procedure of the assessment of the compressive strength of the facade wall. Eurocode 6 (EC6 1996-1-1) and the Basic Document SE-F of the Technical Building Code do not provide formulas for obtaining the compressive strength of the wall.

However, the experimental results obtained can be compared with the following recommendations of specific international regulations on existing stone masonry:

- The Italian regulation NTC2018 Circolare 21 of 2019, specifically in table C8.5.I, gives maximum values of compressive strength of 2.0 MPa and minimums of 1.0 MPa for masonry of the type “Disordered Stone Masonry (Gravel, discontinuous and irregular stone)”.
- The UIC (UIC 1995), specifically in the "Crushed Stone" table in section A3.3.1, gives values based on the strength of the components. For mortar resistances of 2.5 MPa and stone resistances of 60 MPa and 40 MPa, it indicates maximum values of compressive strength of 1.8 MPa and minimum values of 1.6 MPa.

Table 46 shows the ranges of the compressive strengths for an irregular stone wall according to the two regulations. It is worth mentioning that the values obtained in this campaign by means of cylindrical specimens are far higher than the ones from the ranges indicated in the Table 46 and in any case they can only refer to the outer part of the facade wall.

Table 46. Comparison between the compressive strength values of irregular stone masonry estimated with NTC2018 Circolare 21 of 2019 and UIC (1995) based on the experimental strengths of the components.

Position	NTC2018 C8A fm min. fm max [MPa]	UIC (1995) fck min. fck max [MPa]
Zone 3	1.00 2.00	1.80 1.60

4.8 Discussion of the results

- In the first phase of the experimental campaign, non-destructive in-situ procedures were carried out with a view to preliminary evaluation of the quality of the surface properties of the wall components. Windsor Pin Penetration Test (PPT), Helix Screw Pull-out Test (HPT) and Torque Penetration Test (TPT) were performed where the findings were obtained with some joint variability, suggesting some variations in mortar properties of different load walls. Zones 2int, 3int brick and stone have similar values, while Zones 1 and 2ext indicated inferior quality and Zone 3ext brick and 4 showed medium quality.

- In the characterization of the compressive strength of the bricks for the 100×100×40 mm³ specimens the tests showed an average experimental compressive strength of 27.1 MPa for Zone 1, 28.6 MPa for Zone 2int and 27.3 MPa for Zone 3int. Specimens of 50×50×40 mm^3 were also tested for Zone 3int with an average experimental compressive strength of 16.4 MPa, while specimens of 40×40×40 mm^3 which were tested under compression for Zone 1, 2int and 3int showed an average experimental compressive strength of 17.0 MPa, 14.4 MPa and 15.9 MPa respectively. The observed variability in strength, with a coefficient of variation between 4.6% and 12.0% regarding Zone 3int for the 100×100×40 mm³ and the 50×50×40 mm^3 specimens respectively is acceptable due to the heterogeneities inherent in the units. In the case of Zone 1, the coefficient of variation of 17.7% for the 100×100×40 mm³ and 21.0% for the 40×40×40 mm³ regarding Zone 1 indicates the diffuse presence of various qualities of bricks without significantly affecting the final result.

- From the Young's modulus evaluation it is observed that the bricks from Zone 1 have shown to be way stiffer than the bricks from Zone 2, presenting a Young's modulus of 8057 MPa and 6718 MPa respectively.

- From the tiles characterization it is observed that the compressive strengths are higher closer to the slender column that the vaults conclude ranging from 9 to 21 MPa.

- As for the characterization of the stone specimens obtained from three different type of stones, the compressive strength is ranging from 34 to 58 MPa, values corresponding to the compressive strength range of the sandstone of porosity class III, the carbonate rock of oolithic limestone, the carbonate rock of limestone < 2.60 g/cm^3 and the carbonate rock of travertine.

- After the double punch test implementation on the mortar joints it is observed that the lower strength values for the walls are presented in the Zone 2int and 3int brick, while the rest of the values of Zone 1, 3ext stone and 4 show similar strength values. These values confirm the results obtained from in situ tests with PPT, HPT and TPT except for the 3int brick and stone positions which have shown certain inconsistencies. Mortar of the zone 5 of the vaults, mortar of the exterior stone facade 3ext_ext and mortar from zone F of the foundations have shown much higher compressive strength. Furthermore, through the DPT the importance of the thickness and the confinement in the compressive behaviour is underlined.

- Compression test on cylindrical masonry and estimation of the compressive strength through the components are used to obtain the compressive strength of the masonry. The results come to an agreement calculating a compressive strength with the two methods which ranges from 4 to 5.5 MPa for the different zones tested.

Chapter 5: Numerical simulation of the double punch tests on mortar specimens

5.1 Introduction

The DPT is a very useful minor destructive technique for the evaluation of the compressive strength of masonry's mortar. The experimental results have been obtained after the implementation of the test in 120 specimens. The experimental results presented in the section 4.5.1 show that the specimen's dimensions affect the response of the mortar under compression. The objective of this chapter is to examine numerically the mortar's behaviour during the DPT, evaluate the relationship between uniaxial compressive and maximum experimental strength, identify the influence of the various numerical and mechanical properties on the compressive strength and evaluate the effect of the specimen's geometry (thickness and area). To achieve this objective, a reference model is calibrated considering the experimental results for the mortar specimen 1,3 and 8 of zone 2 with dimensions of $62\times60\times15.5$ mm^3, $45\times70\times15.5$ mm^3 and $55\times49\times15$ mm^3 , which have a thickness approximately 15 mm. The compressive strength obtained experimentally for these specimens is equal to 2.78 MPa, 2.60 MPa and 2.60 MPa respectively.

The chapter is organised in the following way. Firstly, the reference model is presented with dimensions considered according to the DIN standards of $50\times50\times15$ mm^3, followed by the numerical results of this case. Then, a parametric analysis of the mechanical and the numerical properties is carried out and finally the last step is the sensitivity analysis as to evaluate the effect of the specimen's geometry by increasing its thickness to 17.5 and 20 mm and by modifying the area to 40×40 mm and 60×60 mm.

5.2 Numerical model

A three dimensional numerical model of the mortar specimen for different geometries of $50\times50\times15$ mm^3, $50\times50\times17.5$ mm^3, $50\times50\times20$ mm^3, $40\times40\times15$ mm^3 and $60\times60\times15$ mm^3 was modelled in the FEM software COMET, developed at the International Centre for Numerical Methods in Engineering (CIMNE, Barcelona). Pre and post processing is carried out with GiD that is also developed at CIMNE.

The mortar sample is simulated by using a continuum finite element approach. The mechanical behaviour of the mortar is simulated using a continuum damage mechanics formulation and is presented in section 5.2.1.

Fig. 106 presents the meshes created for the numerical simulations of the mortar specimen for the mortar specimen of $50\times50\times15$ mm^3, $50\times50\times17.5$ mm^3, $50\times50\times20$ mm^3 composed of 48427 isoparametric solid tetrahedral elements (9464 nodes), 56007 isoparametric solid tetrahedral elements (10805 nodes) and 63299 isoparametric solid tetrahedral elements (12112 nodes) respectively.

The experiment is modelled by restraining the horizontal movement at the upper side of the mortar and by applying a vertical displacement on the circular area of the compressive

hydraulic press. At the lower side of the mortar, all displacements are restrained at the area corresponding to the compressive hydraulic press. The area of the press is equal to 314.16 mm.

The system of nonlinear equilibrium equations is solved at each analysis step through the use of a secant method along with a line-search procedure. Convergence is attained when the ratio between the norm of the iterative residual forces and the norm of the total external forces is lower than 10^{-2} (1%).

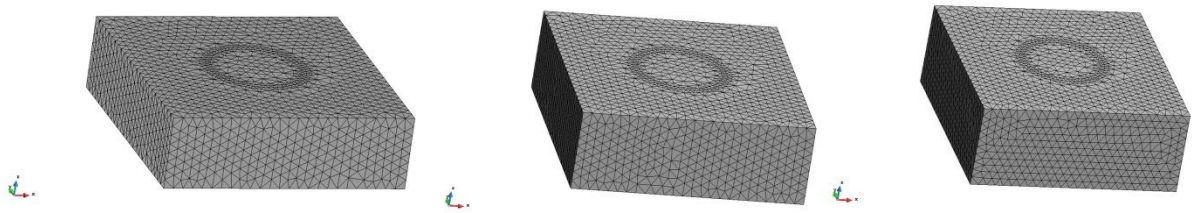

Fig. 106. Finite element meshes used in the numerical simulations for the mortar specimens of 50x50mm with a thickness of: a) 15mm, b) 17.5mm, c) 20mm

5.2.1 Constitutive model

The numerical analysis simulates the cracking and crushing of the mortar by using a continuum damage mechanics model with damage induced orthotropic behaviour along the principal axes. The model uses two distinct damage indices to distinguish between tensile and compressive damage [28].

The 2-parameter d^+ / d^- damage model defines the stress tensor as [38]:

$$\boldsymbol{\sigma} = (1 - d^+)\overline{\boldsymbol{\sigma}}^+ + (1 - d^-)\overline{\boldsymbol{\sigma}}^-$$

where $\overline{\boldsymbol{\sigma}}$ is the effective (elastic) stress tensor

$$\overline{\boldsymbol{\sigma}} = \mathbf{C} : \boldsymbol{\varepsilon}$$

while $\overline{\boldsymbol{\sigma}}^+$ and $\overline{\boldsymbol{\sigma}}^-$ are, respectively, the positive and negative components, computed as :

$$\overline{\boldsymbol{\sigma}}^+ = \sum_{i=1}^{3} \langle \bar{\sigma}_i \rangle \boldsymbol{p_i} \otimes \boldsymbol{p_i}$$

$$\overline{\boldsymbol{\sigma}}^- = \overline{\boldsymbol{\sigma}} - \overline{\boldsymbol{\sigma}}^+$$

d^+ and d^- are tensile and compressive damage indexes, affecting respectively the positive $\overline{\boldsymbol{\sigma}}^+$ and negative $\overline{\boldsymbol{\sigma}}^-$ components of the effective stress $\overline{\boldsymbol{\sigma}}$. These damage indexes are scalar variables ranging from 0 (intact material) to 1 (completely damaged material). In the above equations C stands for the isotropic linear-elastic constitutive tensor and (:) the tensor product contracted on two indices. $\boldsymbol{p_i}$ is the unit vector of the respective principal direction i. Symbol $\langle \quad \rangle$ denotes the Macaulay brackets ($\langle x \rangle = x$, if $x \geq, \langle x \rangle = x$, if $x < 0$). For more details on the continuum damage see [39]

Tensile damage

The tensile damage was defined using the evolution law for d^+ presented in [38].

The resulting stress strain relationship is made of a linear part [(0, 0) - (ε_0, σ_t)] and a softening part [(ε_0, σ_t) - (+∞, 0)], as shown in Fig. 107.

The stress-strain relationship is regularised according to the crackbandwidth approach [40] considering the fracture energy per unit area in tension G_f and the crackbandwidth $l_{dis} = \sqrt[3]{V}$ of a 3D tetrahedral element with volume V.

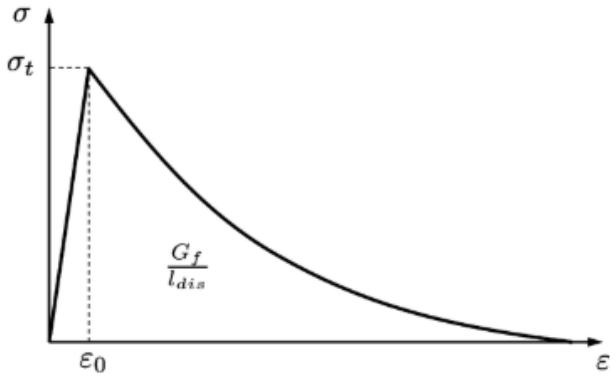

Fig. 107. Tensile uniaxial law [38]

Compressive damage

The compressive damage is also defined using the evolution law for d^- presented in [38]. The evolution of the compressive damage d^- is governed by an ad hoc uniaxial law as shown in Fig. 108.

The curve is made of a linear part [(0, 0) - (ε_0, σ_0)], a hardening part [(ε_0, σ_0) - (ε_p, σ_p)] and two softening parts [(ε_p, σ_p) - (ε_k, σ_k)] [(ε_k, σ_k) - (ε_u, σ_u)], followed by a final residual plateau [(ε_u, σ_u) - (+∞, σ_u)].

The hardening and softening portions are three quadratic Bezier curves. Each one of them has three control points that define their shape, the end-positions, and the tangents to the curve to the curve at the end positions [38].

As for the tensile damage, stress-strain relationship is regularised according to the crackbandwidth approach [40] considering the fracture energy per unit area in compression G_c and the crackbandwidth l_{dis} of each finite element.

For more information on the definition of the compressive law, the interested reader is referred to [38].

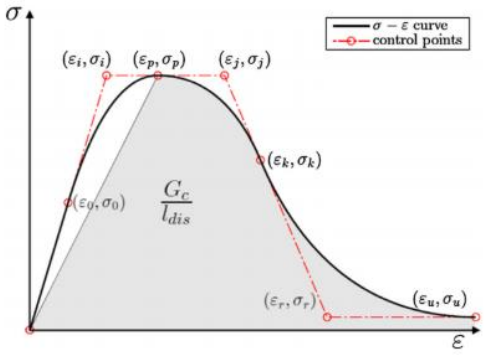

Fig. 108. Compressive uniaxial law [38]

5.2.2 Mechanical parameters

Table 47 presents the mechanical properties of the mortar used for the numerical simulations. The parameters have been selected on the basis of a parametric analysis presented in section 5.4 and using values from the literature. Due to the lack of experimental evidence, a Young's modulus equal to 100MPa was used in the reference model, with its effect analysed in Section 5.4.1. The tensile strength f_t was defined using the experimental results and the expressions proposed by CEB-FIB [41]. The uniaxial compressive strength was defined through a sensitivity analysis in order to reach the compressive strength of the experiments in the range of 2.60 to 2.90 MPa. The tensile fracture energy G_t was defined with the use of the formula suggested by the standard [41], while the compressive fracture energy was estimated as $G_c=1.6f_c$, according to [42]. The values of the elastic limit of the compressive strength f_{c0} was selected as $f_{c0} = f_c/2$ and the reference value for the strain ε_{pc} was selected as $\varepsilon_{pc} =1.075f_c/E$ in the absence of sufficient evidence and was further investigated and presented in section 5.4.2. The ratio between biaxial and uniaxial compressive strength f_{bc}/f_c is defined equal to 1.50 [28]. Parameter ρ defines the shape of the compressive failure surface under triaxial compression and is considered equal to 0.8 Typical values range from 0.64 and 0.66 to about 0.8 [43], which are investigated in Section 5.4.4. Parameter k_1 controls the influence that the compressive criterion has on the dilatant behaviour of the model and ranges from 0 to 1 [38]. A value of 0 leads to the Drucker-Prager criterion, while a value of 1 leads to the criterion presented in [43] as shown in Fig. 109. As shown in Section 5.4.3, this parameter has little influence on the current experiment and for the reference model a value of $k_1 = 1$ is used.

Table 47. Mechanical properties of the mortar used for the numerical simulations

Properties	Mortar
E [MPa]	100
v	0.25
f_t [MPa]	0.24
f_c [MPa]	1.30
G_t [J/m^2]	80
G_c [J/m^2]	2080
f_{c0} [MPa]	0.65
ε_{pc}	0.014
f_{bc}/f_c	1.50
ρ	0.8
κ_1	1

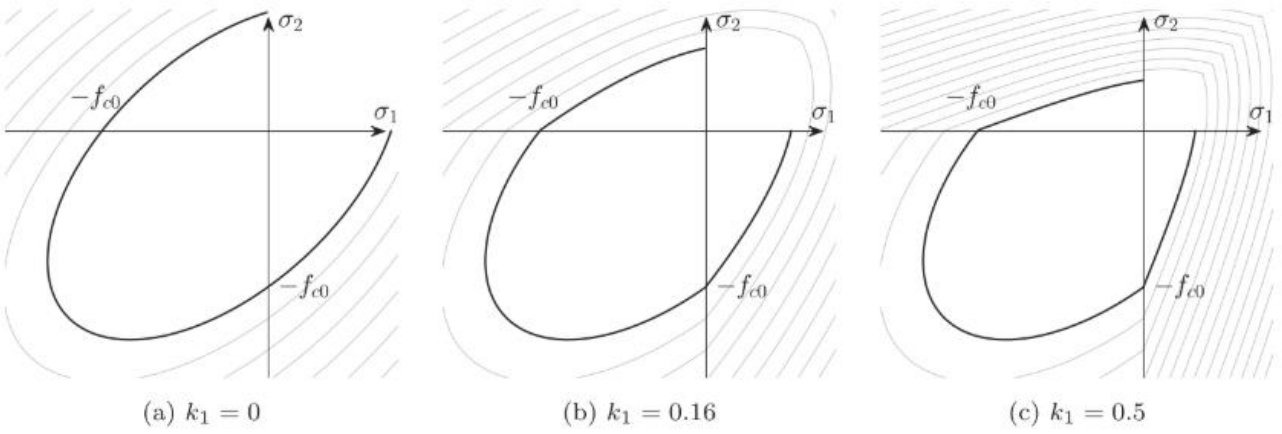

Fig. 109. Proposed compressive failure surface for the continuum model. Influence of the parameter k.

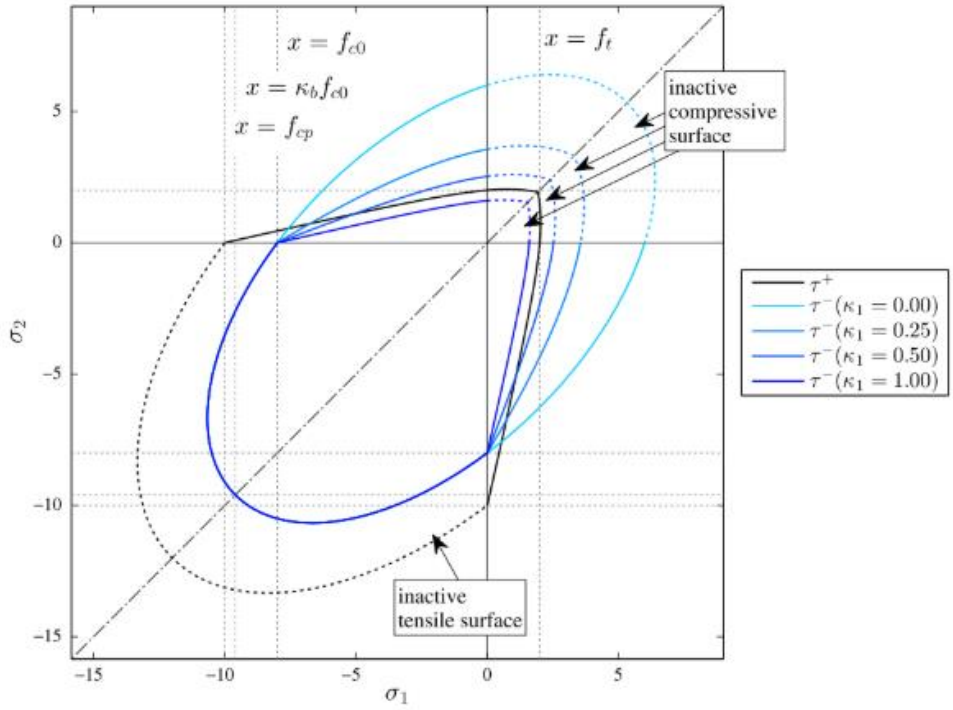

Fig. 110. Initial damage surfaces for the plane-stress case.

Fig. 110 shows the two initial damage surfaces for d^+ and d^-, for the plane-stress case, superimposed in the principal stress space. The negative surface τ^- is represented for various values of the constant k_1 [38].

The values for f_{bc}/f_c, ρ and k_1 are selected based on values used in the literature due to the difficulty of their derivation from standard experimental procedures. Their influence is investigated in the parametric analysis of Section 5.4.

5.3 Numerical results: Reference model

Fig. 111 presents the graph of the experimental vertical stress of the three reference specimens represented as a horizontal line and the numerical vertical stress against the applied vertical displacement at the upper side of the mortar.

The DPT experiment was force controlled and the output was the force and the stroke of the hydraulic press. As the stroke includes different components and not only the one of the test, the experimental stress – displacement graph has not been used for comparative reasons as it is not representative of the mortar's deformation.

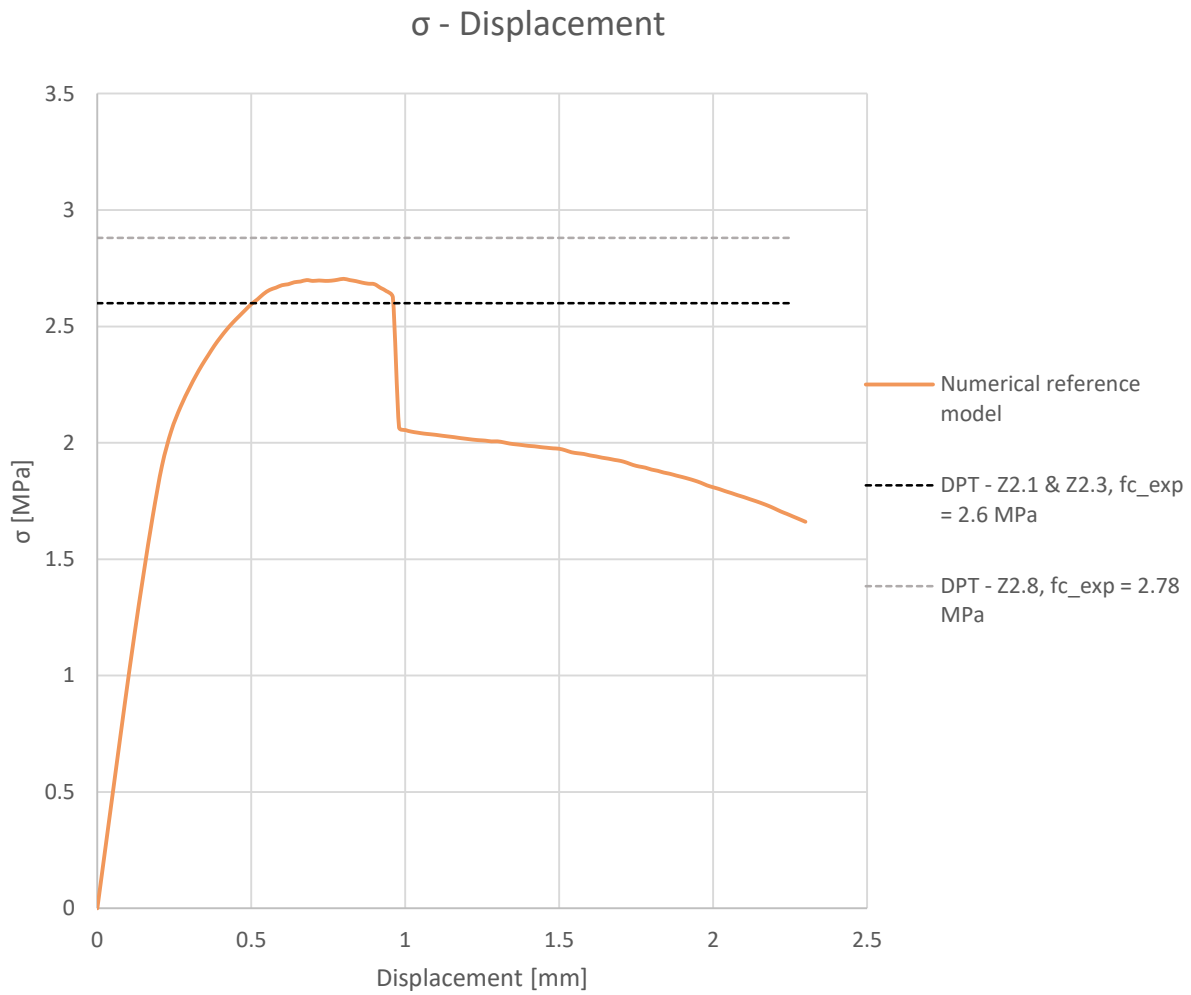

Fig. 111. Stress – Vertical displacement versus vertical stress graph for the numerical DPT and comparison with maximum stress obtained from the experiments on Z2.1, Z2.3 and Z2.8 specimens

As Fig. 111 shows, the numerical reference model was calibrated to match the experimentally obtained compressive capacity.

The numerical simulation predicts a peak stress of 2.69 MPa at a vertical displacement of *uz = 0.68 mm*, which falls within the range given by the experimental results with a peak stress of approximately 2.60 MPa for Z2.1 and Z2.3 specimen and of 2.78 MPa for the Z2.8 specimen.

The simulation shows that the first cracks in the mortar specimen appear to the external part of the circular area of the hydraulic press while the tensile damage starts spreading at the lateral side of the mortar specimen as shown in the first column of Fig. 112. At this stage of the analysis with a vertical displacement of *uz = 0.48 mm*, most compressive damage exists at the same point, around the loaded circular area of the mortar specimen.

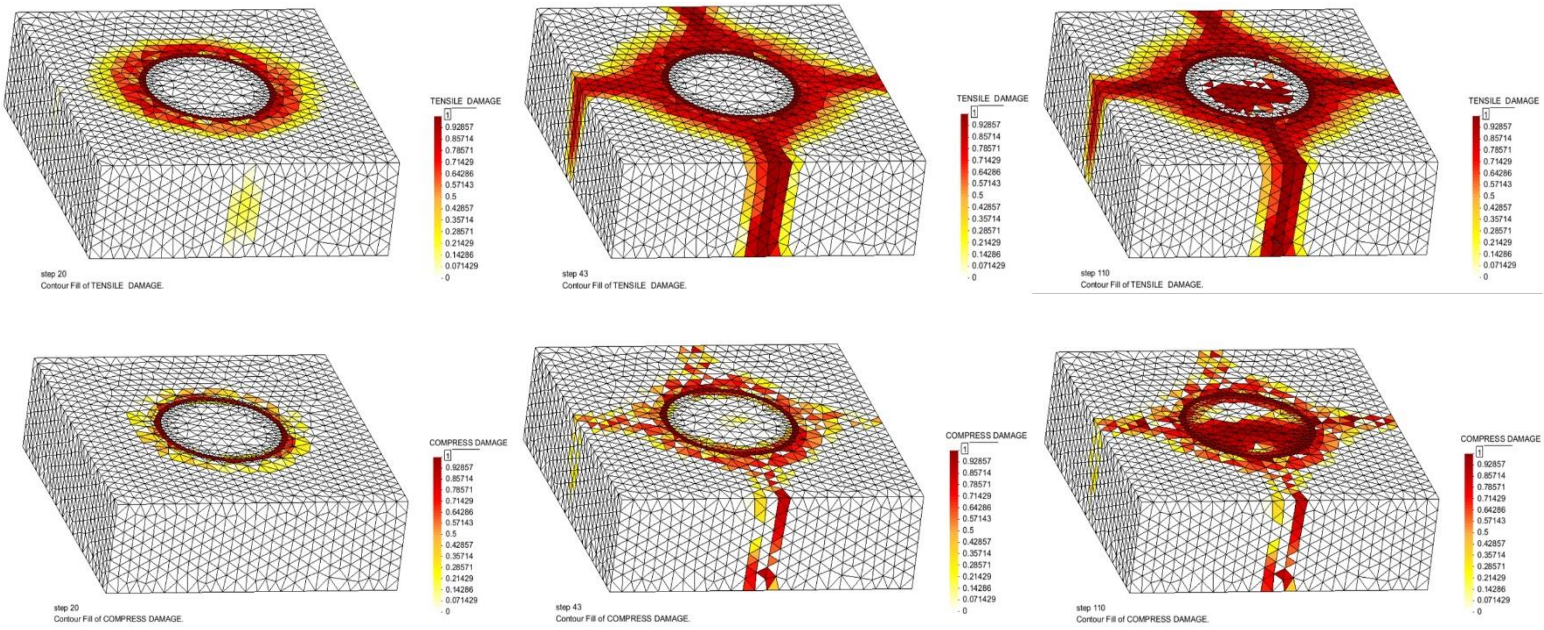

Fig. 112. Numerical simulation of the DPT on the reference's model mortar specimen: Tensile damage & Compressive damage

As it can be seen in the second column of Fig. 112 which refers to a point after the peak stress with a vertical displacement 0.94 mm, the cracks extend from the center to the outer parts of the specimen creating the pattern of the four cracks similar to the ones observed in the experimental results while a steep drop of the stress can be observed in the capacity curve. At this point, compressive damage starts evolving in the loaded area of the mortar specimen. This damage is increasing as the analysis continues until the end of the simulation (third column in Fig. 112) as it leads to the degradation of the mortar at the already damaged locations.

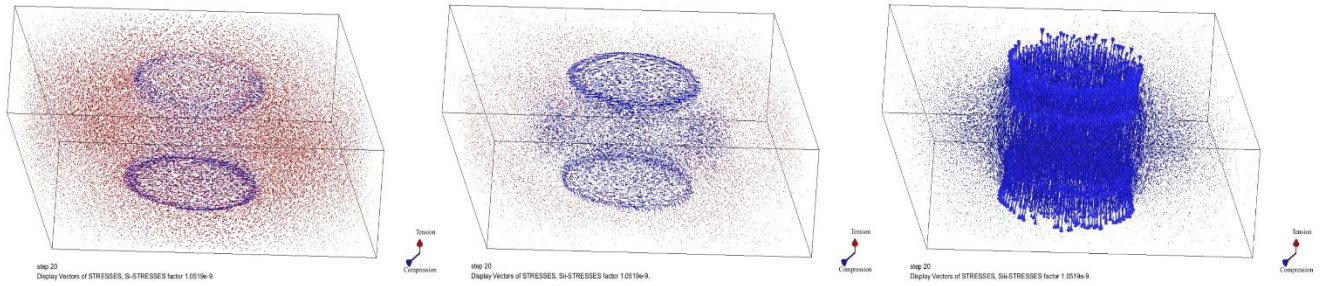

Fig. 113. Numerical simulation of the DPT on the mortar specimen: vectors on the principal σz stresses before the peak stress for a vertical displacement of uz=0.48 mm

Fig. 113 presents the distribution of the vectors of the principal stresses. The not loaded part is under tension – compression stress state, which explains the presence of the four tensile cracks during the experiment. The internal loaded part is under triaxial compression until the peak stress (Fig. 113). As soon as the tensile cracks open, there is a separation between the internal and the external part and the stress distribution changes to biaxial compression. For this reason there is the tensile damage at the end of the analysis (third column in Fig. 112).

Fig. 114 presents the crack surface in the mortar specimen at the end of the numerical simulation as the isosurface of the tensile damage. The numerical simulation predicts correctly the typical failure mode of the mortar as this was observed from the experimental results for the reference specimens (Fig. 115).

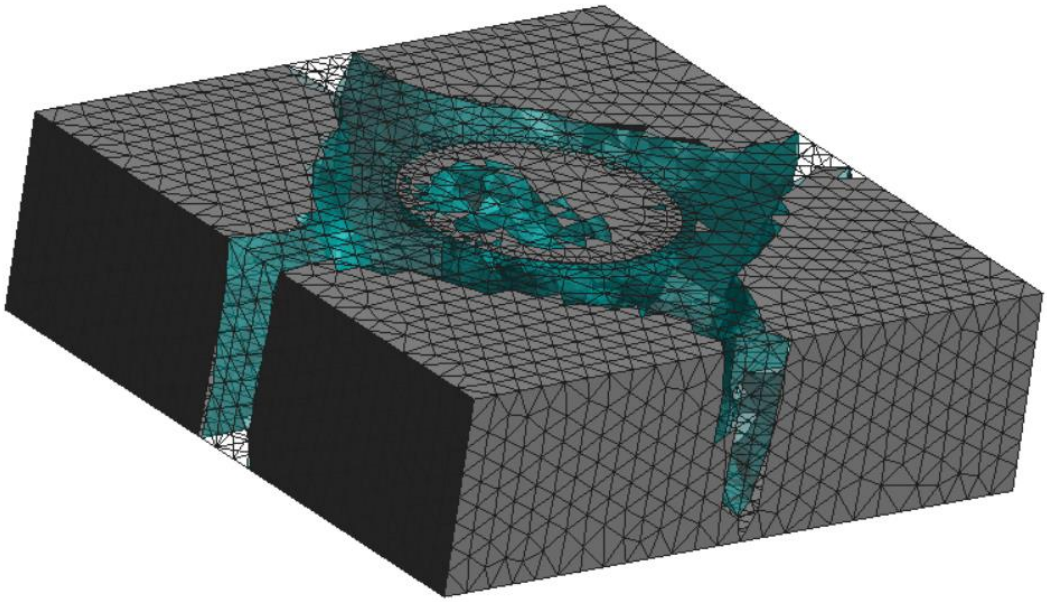

Fig. 114. Numerical simulation of the DPT on the mortar specimen: final failure pattern shown as the isosurface of the tensile damage

Fig. 115. Experimental failure mode of the mortar specimens after the DPT / Zone 2.

5.4 Sensitivity analysis: Numerical and mechanical properties

This section investigates the effect of the different mechanical properties in the capacity of the mortar given by the DPT. The following parameters are investigated: $f_{bc}/f_{c,}\rho$, k, ε_{pc} and E. Apart from the reference value shown in Table 47 and presented on the following graphs with a yellow colour, two more values are examined for each parameter.

The values for $f_{bc}/f_{c,}\rho$, k, ε_{pc} and the modulus of elasticity E of the reference model are selected based on a sensitivity analysis due to the difficulty of their derivation from standard experimental procedures as forementioned in the previous subchapter.

5.4.1 Modulus of elasticity E

In order to identify the effect of the modulus of elasticity *E*, a sensitivity analysis was carried out with the selection of the value at 100 MPa (≈75f_c), 200 MPa (≈150f_c) and 500 MPa (≈375f_c). Fig. 116 presents the stress – displacement graph of this sensitivity analysis for the different values of the modulus of elasticity *E*.

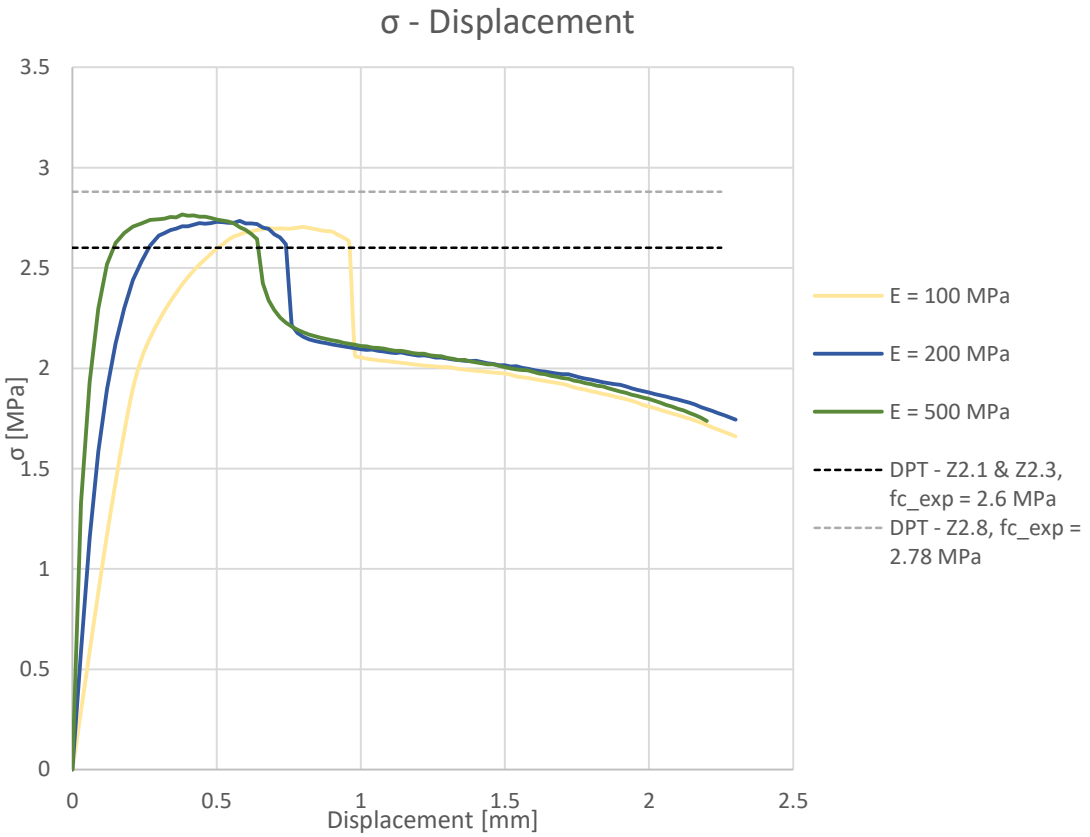

Fig. 116. Sensitivity analysis for the modulus of elasticity E / Stress – Vertical displacement graph

Table 48. Ratio of the uniaxial compressive strength to the experimentally obtained compressive strength for the limit values of E

Limit values of Young's modulus E	Ratio of the uniaxial compressive strength to the experimentally obtained compressive strength
100 MPa	1.3 / 2.69 = 0.483
200 MPa	1.3 / 2.73 = 0.476
500 MPa	1.3 / 2.77 = 0.469

The ratio of the uniaxial compressive strength of the mortar inserted in the simulation to the compressive strength that is obtained from the model is studied and presented in Table 48 in order to understand the influence of the Young's modulus *E*.

The difference obtained between the reference model with a modulus of elasticity of 100 MPa and the one of 200 MPa is 1.45%, while the one obtained between the reference model and the one of 500 MPa is 2.90 %.

As it can be observed, the compressive capacity is not affected significantly by the value of the Young's modulus. The collapse mechanism is also not affected by the Young's modulus as it is the same for all the three cases, and thus it is not presented.

5.4.2 Strain ε_{pc}

In order to identify the effect of the peak strain ε_{pc}, a sensitivity analysis was carried out with the selection of the value at $1.075f_c/E$, $5.0f_c/E$ and $10.0f_c/E$.

Fig. 117 presents the stress – displacement curves for the different values of ε_{pc}, while the experimental results are shown as a horizontal line representing the maximum experimental compressive strength.

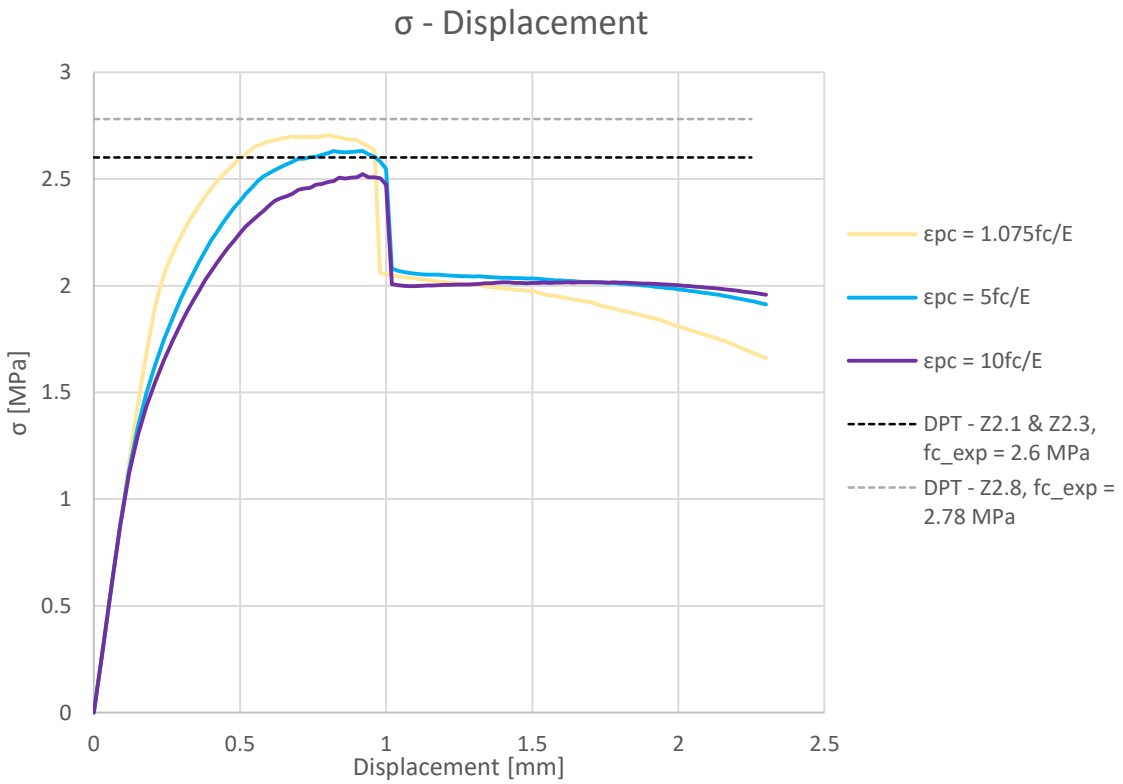

Fig. 117. Sensitivity analysis for the strain εpc / Stress – Vertical displacement graph

Table 49. Ratio of the uniaxial compressive strength to the experimentally obtained compressive strength for the limit values of εpc

Limit values of strain ε_{pc}	Ratio of the uniaxial compressive strength to the experimentally obtained compressive strength
1.075fc/E = 0.014	1.3 / 2.69 = 0.48
5.0fc/E = 0.065	1.3 / 2.63 = 0.494
10.0fc/E = 0.13	1.3 / 2.52 = 0.52

The ratio of the uniaxial compressive strength of the mortar inserted in the simulation to the compressive strength that is obtained from the model is studied and presented in Table 49 in order to understand the influence of the strain ε_{pc}.

The difference obtained between the reference model with a ε_{pc} = 0.014 and the one with an ε_{pc} = 0.065 is 2.92 %, while the one obtained between the reference model and the one with an ε_{pc} = 0.13 is 8.33 %.

The compressive capacity is not affected significantly by the value of the strain ε_{pc}. The collapse mechanism is slightly affected by the ε_{pc} and presented in Fig. 118 and Fig. 119. The reference model with ε_{pc} = *0.014* is damaged differently compared to the models with ε_{pc} = *0.065 and* ε_{pc} =*0.13,* presenting a more brittle response which results in a crack at the one semicircle of the loaded area of the mortar.

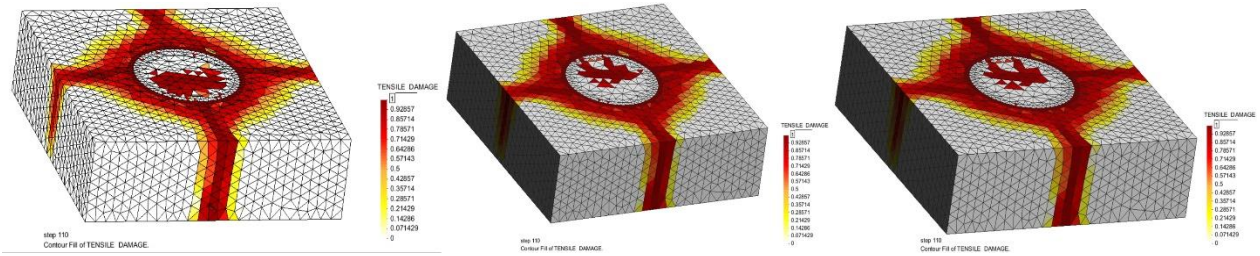

Fig. 118. Tensile of the mortar specimen with a value of strain epc of: a) reference model 0.014, b) 0.065, c) 0.13

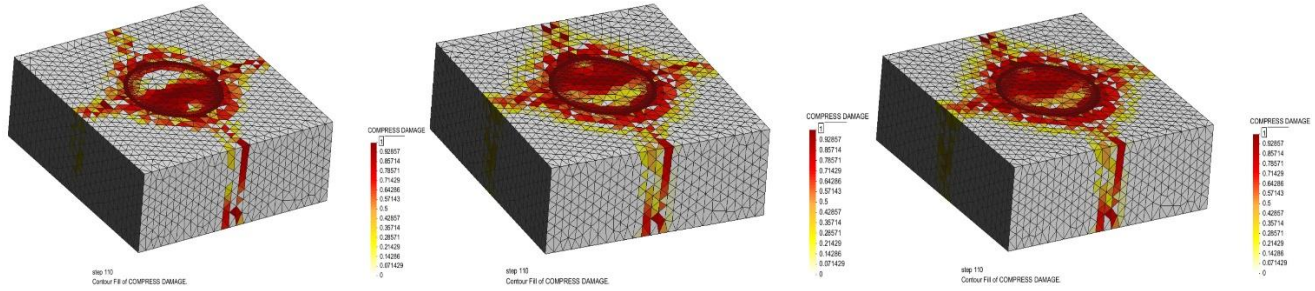

Fig. 119. Compressive damage of the mortar specimen with a value of strain epc of: a) reference model 0.014, b) 0.065, c) 0.13

5.4.3 Parameter k_1

In order to identify the effect of the constant *k* which controls the influence that the compressive failure criterion has on the dilatant behaviour of the model, a sensitivity analysis was carried out with the selection of the value at k_1 = 0, 0.5, 1.0.

Fig. 120 presents the stress – displacement curves for the different values of *k*, while the experimental results are shown as a horizontal line representing the maximum experimental compressive strength for each of the three cases. The ratio of the uniaxial compressive strength of the mortar inserted in the simulation to the compressive strength that is obtained from the model is studied and presented in Table 50 in order to understand the influence of the parameter κ_1. The difference obtained between the reference model with a κ_1 = 1 and the one with a κ_1 = 0 is 1.04 %, while the one obtained between the reference model and the one of 500 MPa is 0.62 %.

As it can be observed from Fig. 120 the influence of the parameter κ_1 on the compressive strength of the DPT for the mortar specimen is very limited. The compressive capacity is not affected significantly by the value of the parameter κ_1. The collapse mechanism is also not affected by the κ_1 as it is the same for all the three cases and thus not presented here. For this, the value of the parameter κ_1 was defined equal to 1.

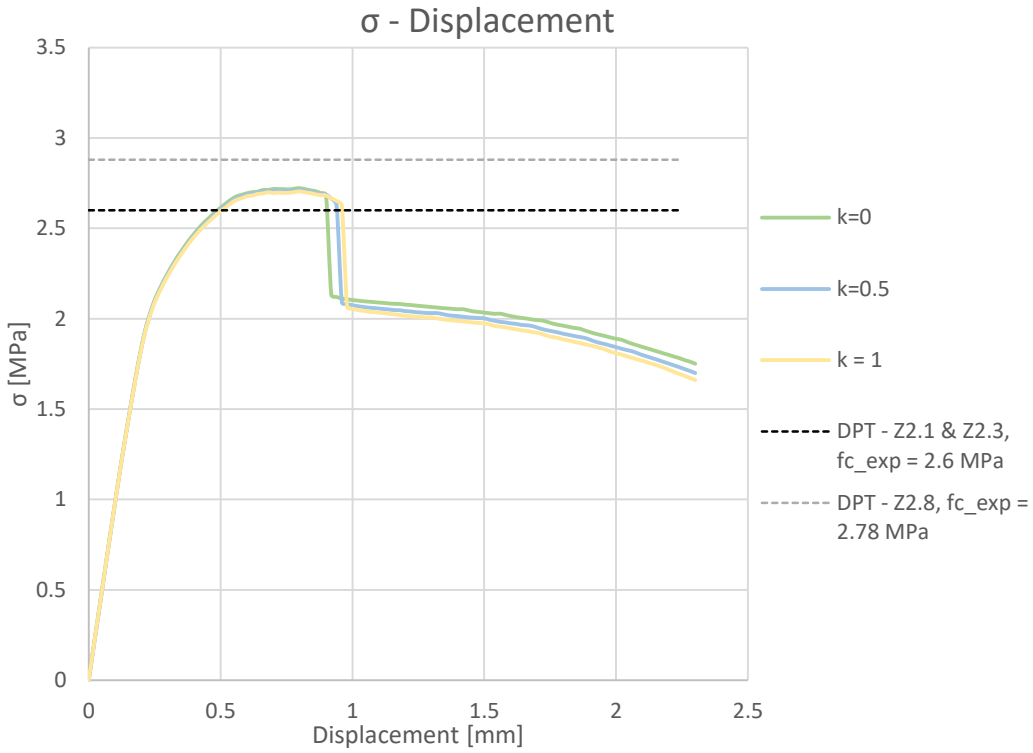

Fig. 120. Sensitivity analysis for the parameter k / Stress – Vertical displacement graph

Table 50. Ratio of the uniaxial compressive strength to the experimentally obtained compressive strength for the limit values of the parameter k

Limit values of parameter k	Ratio of the uniaxial compressive strength to the experimentally obtained compressive strength
0	1.3 / 2.72 = 0.478
0.5	1.3 / 2.71 = 0.480
1	1.3 / 2.69 = 0.483

5.4.4 Parameter ρ

In order to identify the effect of the parameter ρ which defines the shape of the compressive failure surface under triaxial compression, a sensitivity analysis was carried out with the selection of the value at 0.6, 0.7, 0.8, which are values found in the literature.

Fig. 121 presents the stress – displacement curves for the different values of ρ, while the experimental results are shown as a horizontal line representing the maximum experimental compressive strength for each of the three cases.

The ratio of the uniaxial compressive strength of the mortar inserted in the simulation to the compressive strength that is obtained from the model is studied and presented in Table 51 in order to understand the influence of the parameter ρ.

The difference obtained between the reference model with a ρ = 0.8 and the one with a ρ = 0.6 is 33.33 %, while the one obtained between the reference model and the one of ρ = 0.7 is 14.58 %.

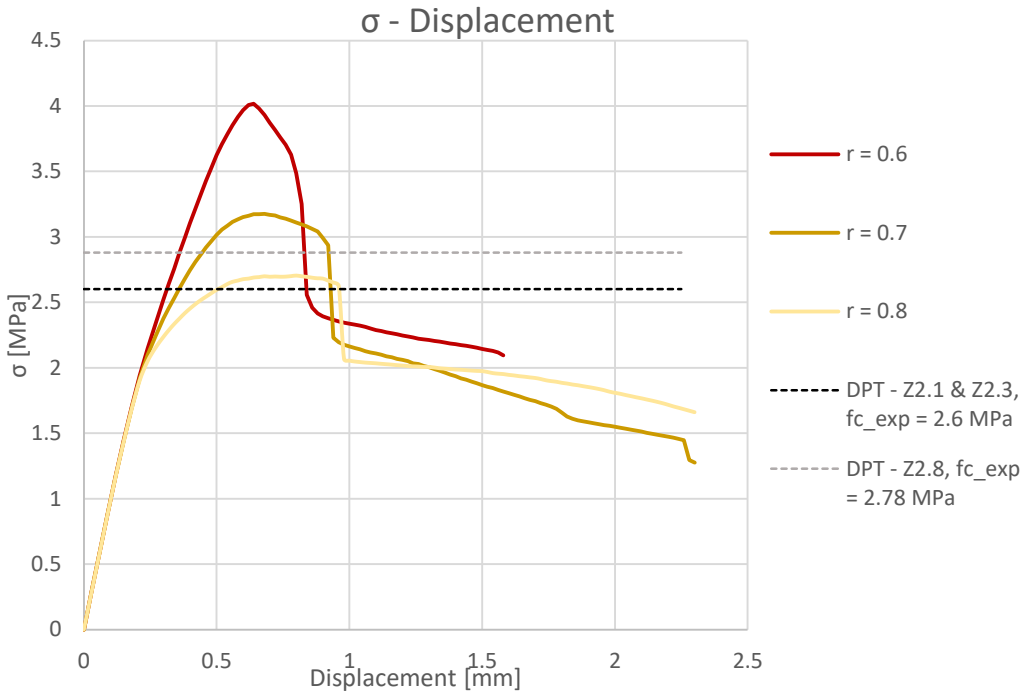

Fig. 121. Sensitivity analysis for the parameter ρ / Stress – Vertical displacement graph

Table 51. Ratio of the uniaxial compressive strength to the experimentally obtained compressive strength for the limit values of ρ

Limit values of parameter ρ	Ratio of the uniaxial compressive strength to the experimentally obtained compressive strength
0.6	1.3 / 4.01 = 0.32
0.7	1.3 / 3.17 = 0.41
0.8	1.3 / 2.69 = 0.48

As it can be observed from Fig. 121, the influence of the parameter ρ on the compressive strength of the DPT for the mortar specimen is very important.

The collapse mechanism is also affected by the ρ and presented in Fig. 122 and Fig. 123. The reference model with $\rho = 0.8$ is damaged differently compared to the models with $\rho = 0.6$ and $\rho = 0.7$, presenting a crack at the one semicircle of the loaded area of the mortar, while the one of ρ = 0.6, 0.7 are presenting a splitting crack at the middle of the loaded area of the mortar.

The value of the parameter ρ was defined equal to 0.8 as it is similar to the value calibrated for lime mortar presented in [28].

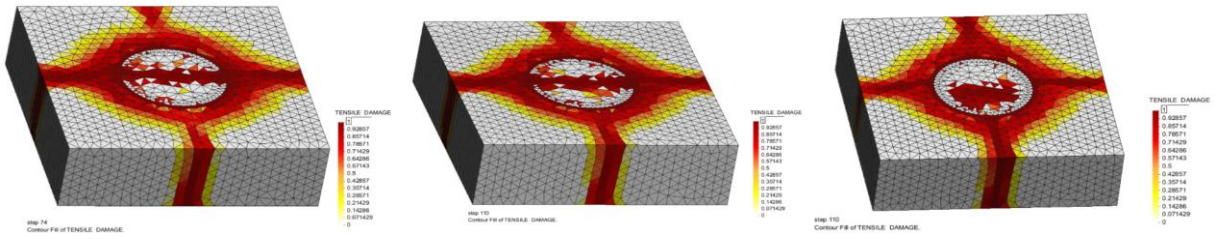

Fig. 122. Tensile damage of the mortar specimen with a value of the parameter ρ of: a) 0.6, b) 0.7, c) reference model 0.8

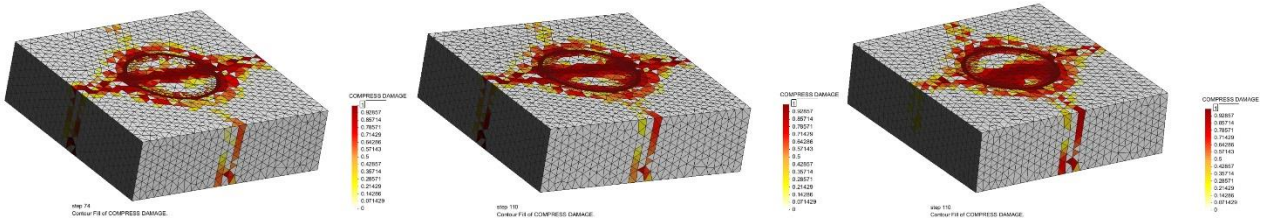

Fig. 123 Compressive damage of the mortar specimen with a value of the parameter ρ of: a) 0.6, b) 0.7, c) reference model 0.8

5.4.5 Parameter f_{bc}/f_c

In order to identify the effect of the parameter f_{bc}/f_c which defines the ratio between biaxial and uniaxial compressive strength, a sensitivity analysis was carried out with the selection of the value at 1.0, 1.25, 1.50.

Fig. 124 presents the stress – displacement curves for the different values of f_{bc}/f_c, while the experimental results are shown as a horizontal line representing the maximum experimental compressive strength for the three cases.

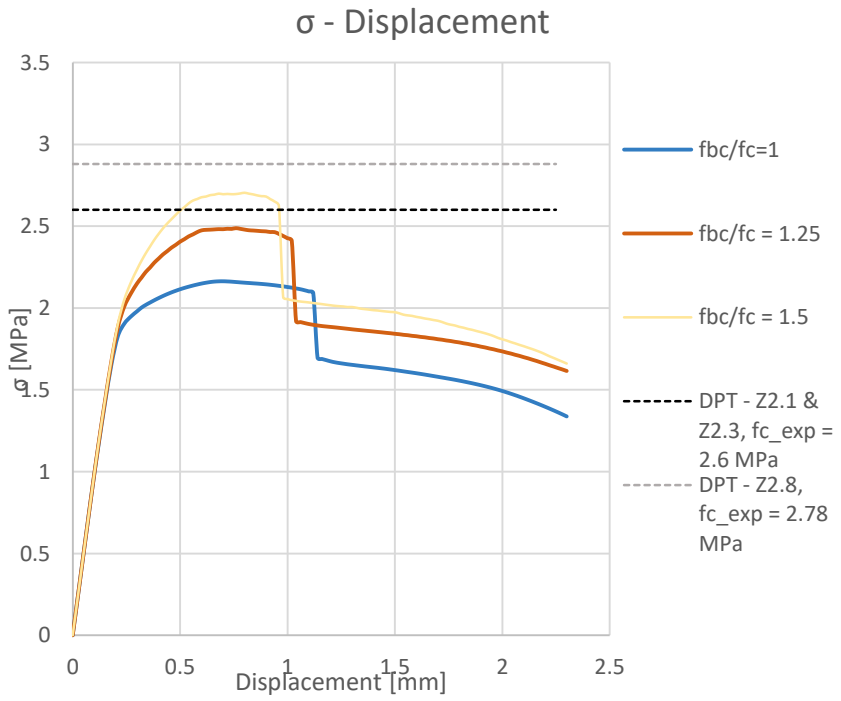

Fig. 124. Sensitivity analysis for the parameter f_{bc}/f_c / Stress – Vertical displacement graph

Table 52. Ratio of the uniaxial compressive strength to the experimentally obtained compressive strength for the limit values of f_{bc} / f_c

Limit values of parameter f_{bc}/f_c	Ratio of the uniaxial compressive strength to the experimentally obtained compressive strength
1.0	1.3 / 2.16 = 0.60
1.25	1.3 / 2.49 = 0.52
1.50	1.3 / 2.69 = 0.48

The ratio of the uniaxial compressive strength of the mortar inserted in the simulation to the compressive strength that is obtained from the model is studied and presented in Table 52.

The difference obtained between the reference model with f_{bc}/f_c = 1.5 and the one with f_{bc}/f_c = 1.0 is 25 %, while the one obtained between the reference model and the one of f_{bc}/f_c = 1.25 is 8.33 %.

As it can be observed from Fig. 124, the influence of the parameter f_{bc}/f_c, on the compressive strength of the DPT for the mortar specimen is important. As expected, the increase in the biaxial strength has an important influence in the final capacity of the mortar. Neverteless, the collapse mechanism very similar for all the cases, with some minor differences in the final cracking in the central zone as showin in Fig. 125 and Fig. 126. The reference model with f_{bc}/f_c = 1.50 is damaged differently in the circular loaded area compared to the models with f_{bc}/f_c = 1.0 and f_{bc}/f_c = *1.25*. The value of the parameter f_{bc}/f_c was defined equal to 1.50, which is equal to the calibrated value for lime mortar presented in [28]

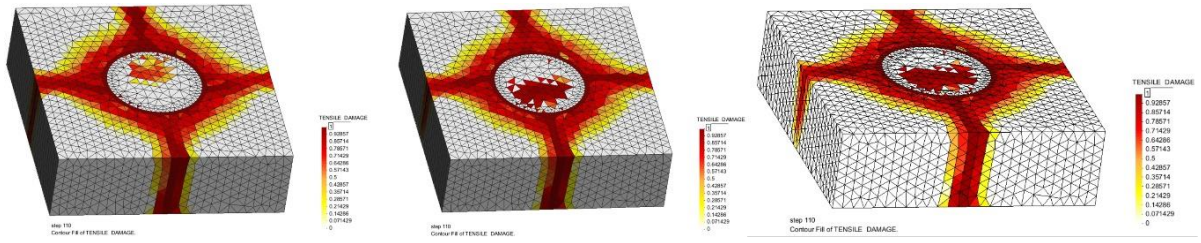

Fig. 125. Tensile damage of the mortar specimen with a value of the parameter fbc/fc of: a) 1.0, b) 1.25, c) reference model 1.5

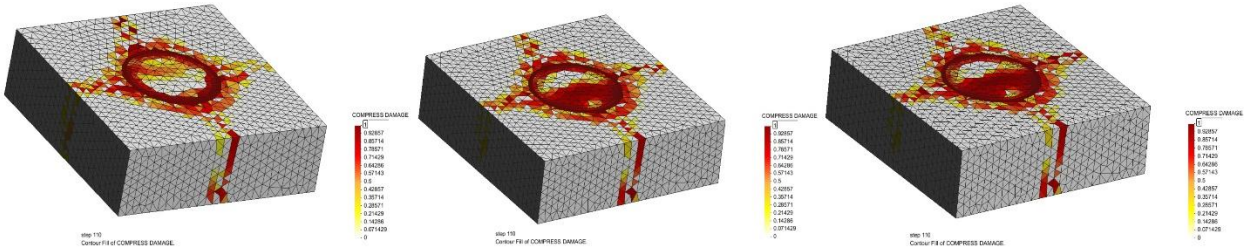

Fig. 126 Compressive damage of the mortar specimen with a value of the parameter fbc/fc of: a) 1.0, b) 1.25, c) reference model 1.5

5.4.6 Discussion on the results of the sensitivity analysis of the material properties

After the sensitivity analysis for E, ε_{pc}, f_{bc}/f_c, ρ and k was carried out, the influence of the parameters in terms of capacity and collapse mechanism was determined. Table 53 presents the variation of the ratio between the uniaxial compressive strength and the capacity given by each analysis for each of the studied parameters.

The Young's modulus and the k_1 parameter present the lower influence on both the capacity and the failure mechanism.

ε_{pc} has also a minor influence in the capacity, but affects slightly the final damage at the central part of the specimen.

On the other hand, the properties associated with the compressive behaviour ρ, f_{bc}/f_c show a very important influence on the numerical results as they highly affect the compressive capacity and slightly affect the failure mechanism presenting some minor differences in the final damage of the central zone.

Table 53. Range of the ratio of the uniaxial compressive strength to the experimentally obtained compressive strength for the limit values of the parameters studied in the sensitivity analysis

Limit values of the parameters	Range of the ratio of the uniaxial compressive strength to the experimentally obtained compressive strength
E = 100 – 500 MPa	0.483 – 0.469
ε_{pc} = 0.014 – 0.13	0.48 – 0.52
k = 0 - 1	0.478 – 0.483
ρ = 0.6 – 0.8	0.32 – 0.48
f_{bc}/f_c = 1 – 1.50	0.60 – 0.48

The parameteric analyses show that the ratio between uniaxial compressive strength and strength capacity given by the experiment varies between 0.32 and 0.60. The analysis shows that among the studied parameters the most influential are the ρ and the f_{bc}/f_c. These parameters should be further calibrated by simulation of more experiments of existing masonry elements in order to estimate the respresentative values for historical mortars.

5.5 Sensitivity analysis: Geometrical properties

5.5.1 Thickness

This sensitivity analysis is implemented to mortar specimens of 50×50 mm^2 in order to evaluate the effect of the specimen's thickness by considering three values of 15, 17.5 and 20 mm. Fig. 127 presents the stress – displacement curves for the different thickness models, while the experimental result are shown as horizontals line representing the maximum experimental compressive strength.

The tensile and the compressive damage of the mortar specimens are shown in Fig. 128 and in Fig. 129 at same stages of the analysis which were shown for the reference model in Fig. 112.

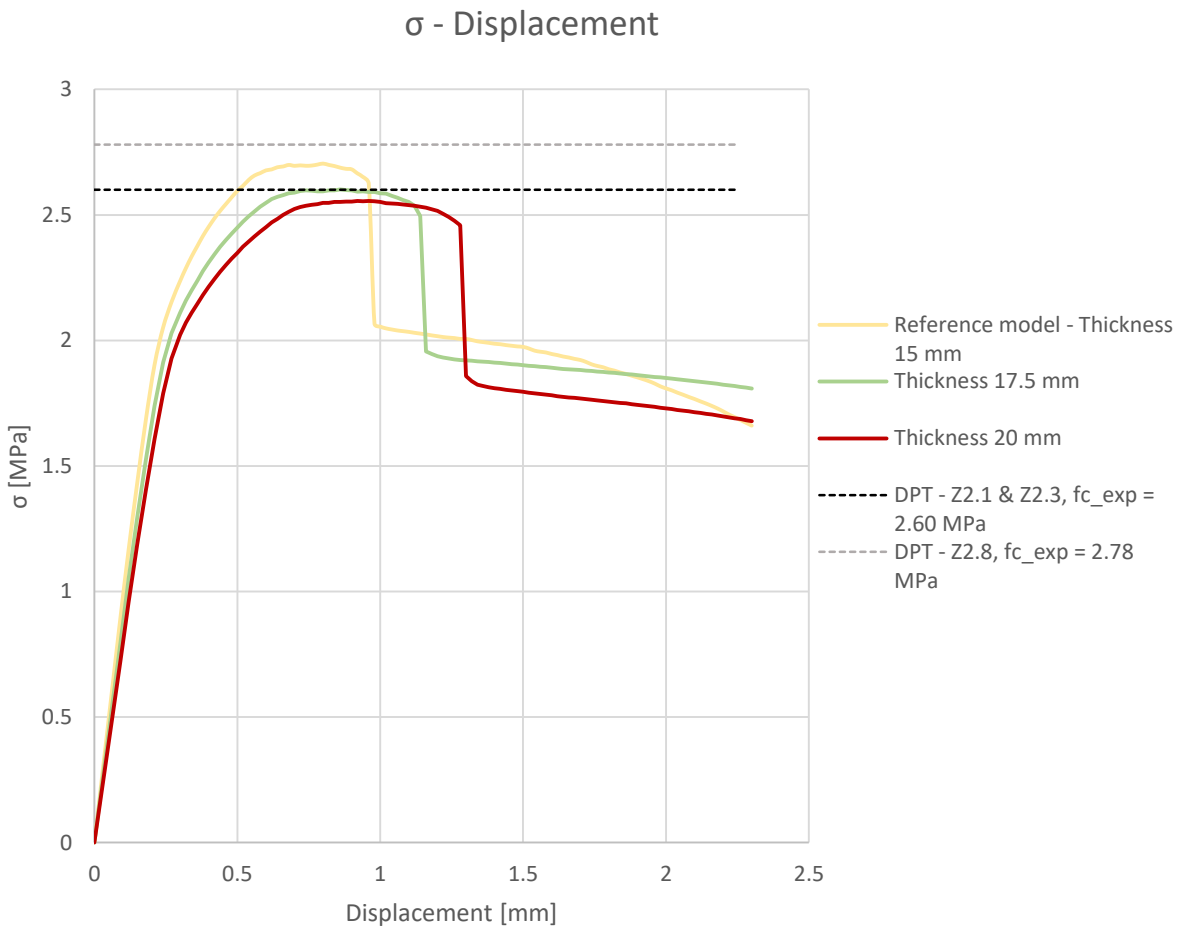

Fig. 127. Sensitivity analysis for the thickness of the mortar specimen / Stress – Vertical displacement graph

The numerical simulations predict a peak stress of *2.69 MPa* with a vertical displacement of *uz=0.68 mm* for the reference model with a thickness of 15 mm, *2.60 MPa* with a vertical displacement of *uz=0.80 mm* for the model with a thickness of 17.5 mm and *2.56 MPa* with a vertical displacement of *uz=0.96 mm* for the model with a thickness of 20 mm.

These simulations show that the mortar specimens with a thickness of 17.5 and 20 mm have the same initial behaviour with the reference model as the first cracks appear to the external part of the circular area of the hydraulic press while the tensile damage starts spreading at the lateral side of the mortar specimen as shown in the first column of Fig. 128 and Fig. 129. At this stage of the analysis with a vertical displacement of *uz=0.48 mm*, most compressive damage exists at the same point, around the loaded circular area of the mortar specimen for both specimens, while for the thinner one is slightly increased.

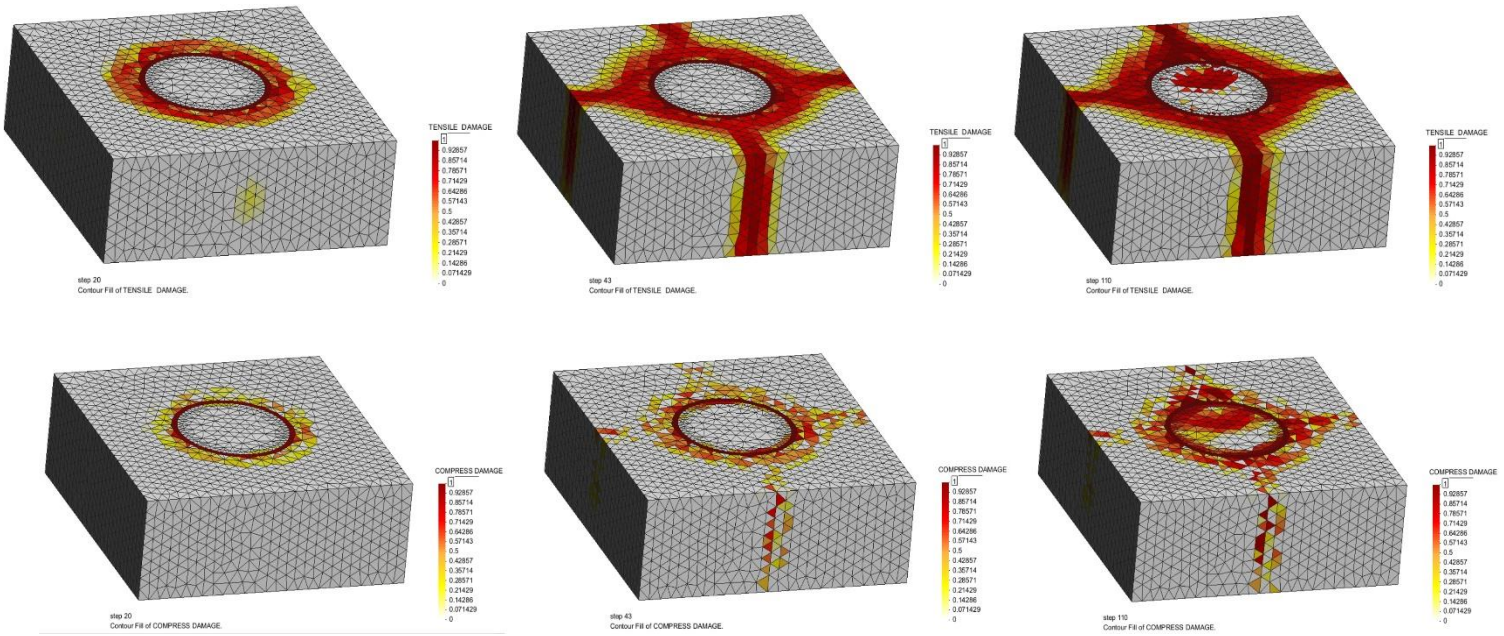

Fig. 128. Numerical simulation of the DPT on the mortar specimen with a thickness of 17.5 mm: Tensile damage & Compressive damage

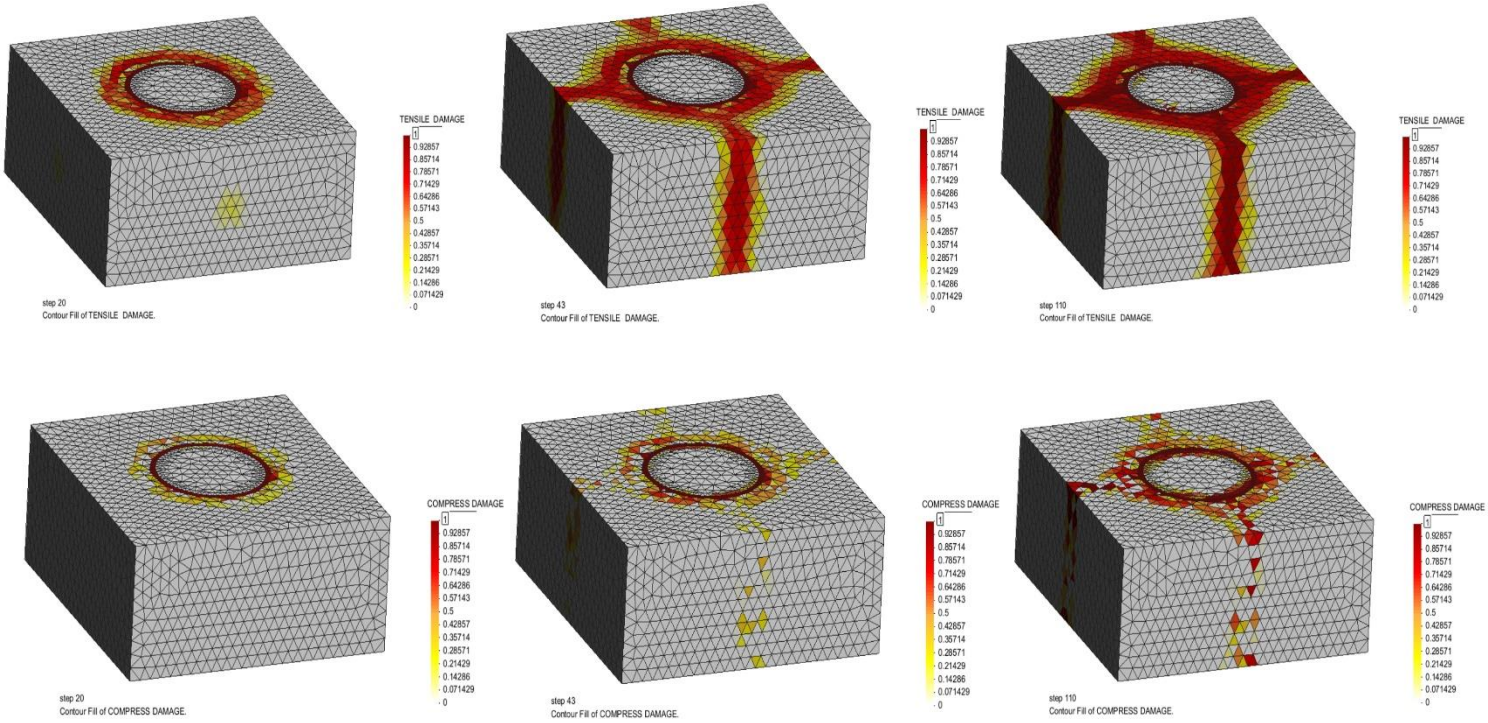

Fig. 129 Numerical simulation of the DPT on the mortar specimen with a thickness of 20 mm: Tensile damage & Compressive damage

As it can be seen in the second column of Fig. 128 and Fig. 129 which refers to a point after the peak stress with a vertical displacement *uz=0.94 mm*, the cracks extend from the center to the outer parts of the specimen creating the pattern of the four cracks similar to the ones observed in the experimental results while the softening part is reached for both specimens in the capacity curve. At this point, a compressive damage starts evolving in the loaded area of the mortar specimen with a the thickness of 17.5 mm. The mortar specimen with the thickness of 20 mm is not damaged in the loaded area. This damage is increasing as the analysis continues

until the end of the simulation (third column in Fig. 128 and Fig. 129) as it leads to the degradation of the mortar at the already damaged locations for the 17.5 mm thickness specimen while for the 20 mm one, the central loaded area remains undamaged until the end of the simulation.

Table 54. Ratio of the uniaxial compressive strength to the experimentally obtained compressive strength for the limit values of the thickness

Limit values of the thickness	Ratio of the uniaxial compressive strength to the experimentally obtained compressive strength
15 mm	1.3 / 2.69 = 0.48
17.5 mm	1.3 / 2.60 = 0.50
20 mm	1.3 / 2.56 = 0.51

The ratio of the uniaxial compressive strength of the mortar inserted in the simulation to the compressive strength that is obtained from the model is studied and presented in Table 54.

The difference obtained between the reference model with thickness of 15 mm and the one with thickness of 17.5 mm is 4.17 %, while the one obtained between the reference model and the one with thickness of 20 mm is 6.25 %.

The compressive capacity is not affected significantly by the change of the thickness, while the collapse mechanism is slightly affected by the change of the thickness as described above and presented in Fig. 128 and Fig. 129.

5.5.2 Length & Width

This sensitivity analysis is implemented to mortar specimens with a thickness of 15 mm in order to evaluate the effect of the length and width by considering three specimens of $40\times40\times15$ mm^3, $50\times50\times15$ mm^3 and $60\times60\times15$ mm^3.

The area is a factor which affects the DPT and the compressive strength of the mortar as it can be seen in Fig. 130.

The numerical simulations predict a peak stress of *2.69 MPa* with a vertical displacement of *uz=0.68 mm* for the reference model with dimensions of $50\times50\times15$ mm^3, *2.34 MPa* with a vertical displacement of *uz=0.64 mm* for the model with dimensions of $40\times40\times15$ mm^3 and *3.07 MPa* with a vertical displacement of *uz=1.08 mm* for the model with dimensions of $60\times60\times15$ mm^3.

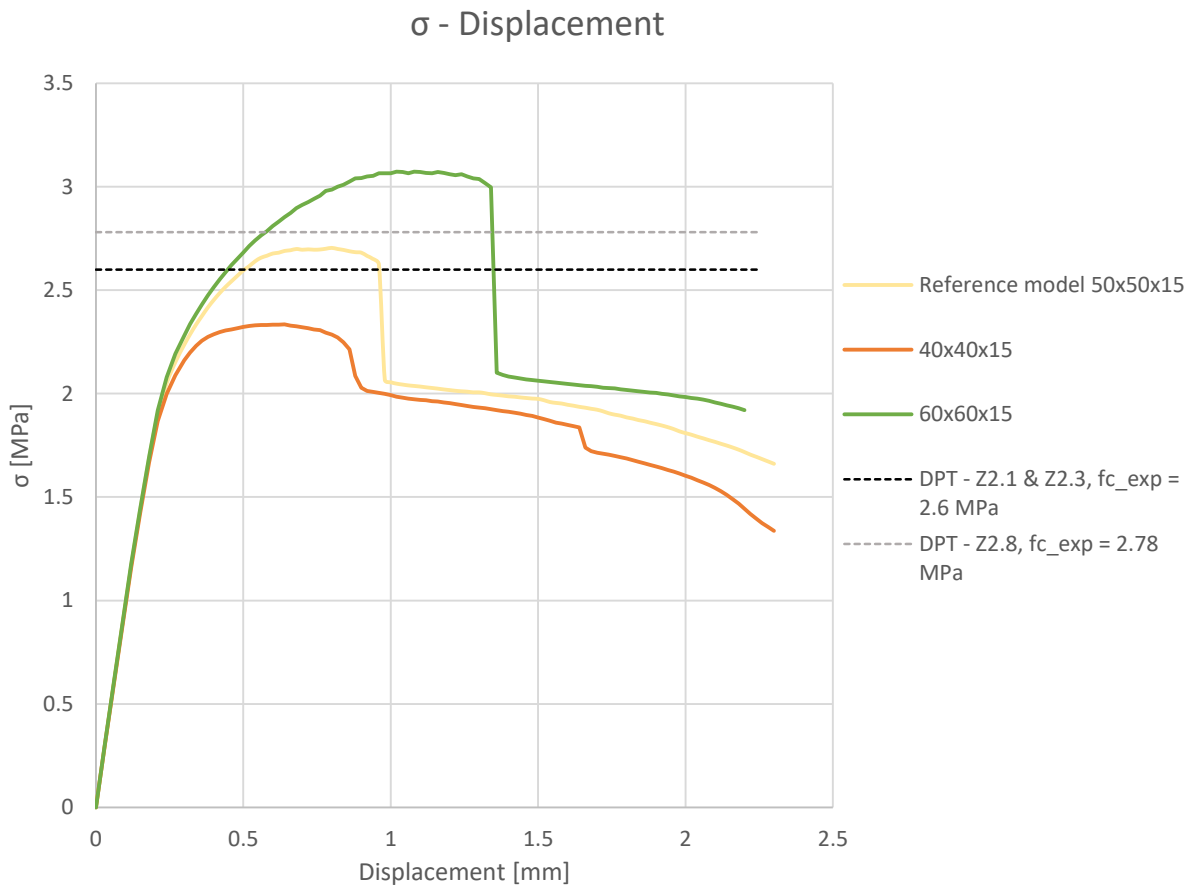

Fig. 130. Sensitivity analysis for the area of the mortar specimen / Stress – Vertical displacement graph

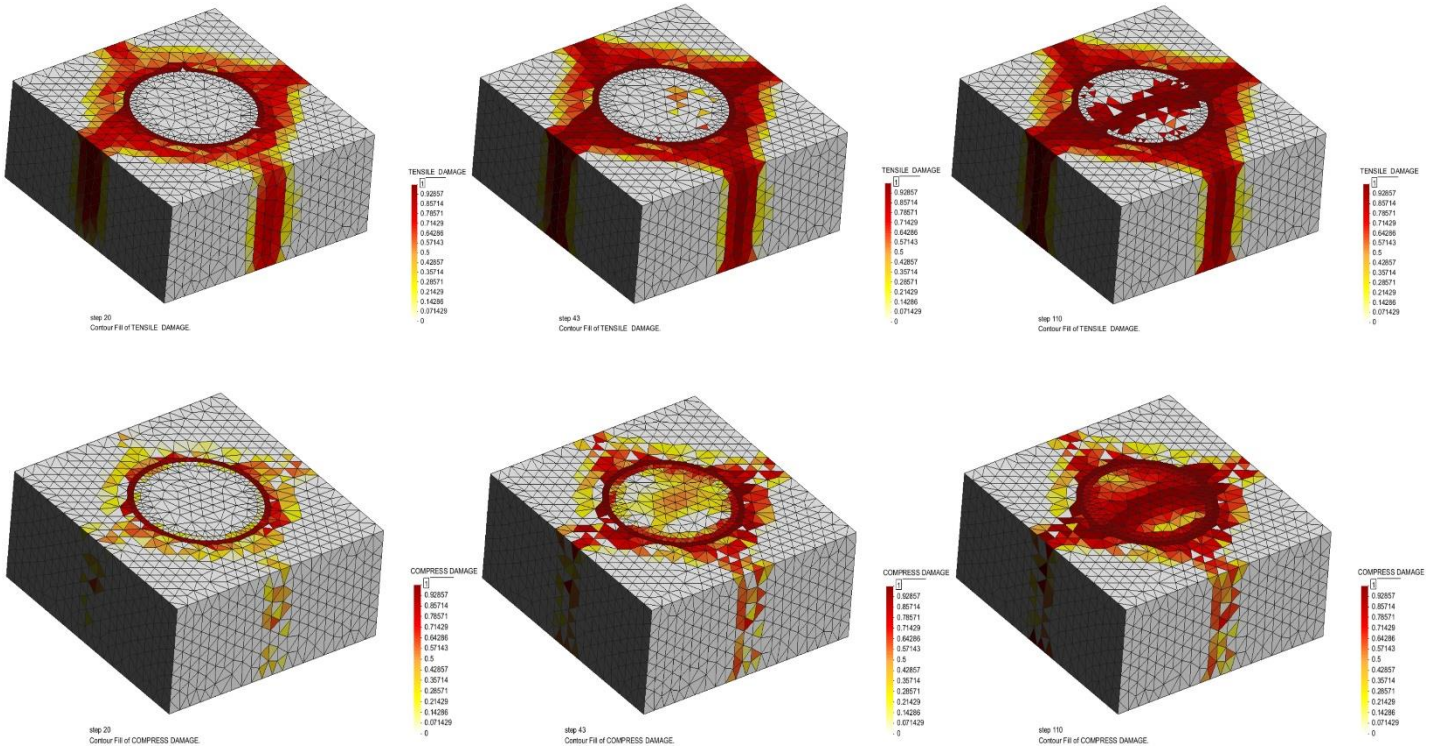

Fig. 131. Numerical simulation of the DPT on the mortar specimen with dimensions of 40x40x15 mm^3: Tensile damage & Compressive damage

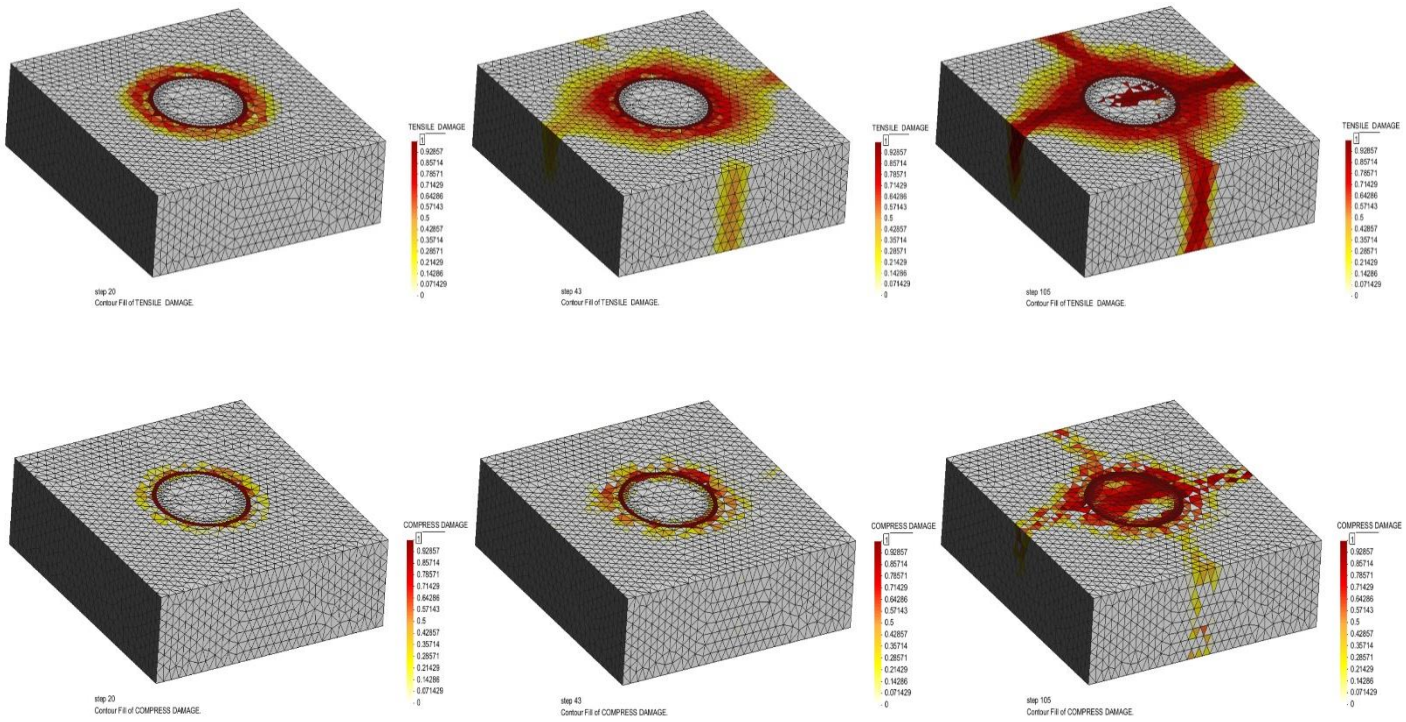

Fig. 132. Numerical simulation of the DPT on the mortar specimen with dimensions of 60x60x15 mm^3: Tensile damage & Compressive damage

The tensile and the compressive damage of the mortar specimens are shown in Fig. 131 and in Fig. 132 at same stages of the analysis which were shown for the reference model. The simulation of the mortar specimen with dimensions of 40×40×15 mm^3 shows that at the stage of the analysis with a vertical displacement of *uz = 0.48 mm* (first column of Fig. 131) the cracks have already been extended from the center to the outer parts of the specimen creating the pattern of the four cracks similar to the ones observed in the experimental results, while the mortar specimen has not reached yet the peak stress. Most compressive damage exists around the circular loaded area and it is also already spread to the outer parts. At the stage of the analysis with a vertical displacement of *uz = 0.94 mm* (second column of Fig. 131), the cracks extend to the circular central loaded area of the specimen while a steep drop of the stress can be observed in the capacity curve. At this point, most compressive damage is observed at the outer parts while the mortar specimen is starting being damaged also in the circular loaded area. This damage is increasing as the analysis continues until the end of the simulation (third column in Fig. 131) as it leads to the degradation of the mortar at the already damaged locations.

The simulation of the mortar specimen with dimensions of 60×60×15 mm^3 shows that the first cracks in the mortar specimen appear to the external part of the circular area of the hydraulic press similar to reference model but the tensile damage have not started spreading at the lateral side of the mortar specimen yet (first column of Fig. 132). At this stage of the analysis with a vertical displacement of *uz = 0.48 mm*, most compressive damage exists at the same point, around the loaded circular area of the mortar specimen.

At the point of the analysis with a vertical displacement of *uz = 0.94 mm* (second column of Fig. 132) which refers to a point slightly before the peak stress, the cracks extend from the center to the lateral sides of the specimen while the pattern of the four cracks similar to the

ones observed in the experimental results is not yet observed. At this point most compressive damage exists around the circular loaded area of the mortar specimen. This damage is increasing as the analysis continues until the end of the simulation (third column in Fig. 132) as it leads to the degradation of the mortar at the already damaged locations. At this point of the analysis, the pattern with the four cracks similar to the one observed experimentally can be also observed.

Table 55. Ratio of the uniaxial compressive strength to the experimentally obtained compressive strength for the limit values of the area

Limit values of the area	Ratio of the uniaxial compressive strength to the experimentally obtained compressive strength
$40\times40\times15$ mm^3	1.3 / 2.34 = 0.56
$50\times50\times15$ mm^3	1.3 / 2.69 = 0.48
$60\times60\times15$ mm^3	1.3 / 3.07 = 0.42

The ratio of the uniaxial compressive strength of the mortar inserted in the simulation to the compressive strength that is obtained from the model is studied and presented in Table 55.

The difference obtained between the reference model with dimensions of $50\times50\times15$ mm^3 and the one with dimensions of $40\times40\times15$ mm^3 is 16.67 %, while the one obtained between the reference model and the one with dimensions of $60\times60\times15$ mm^3 is 12.50 %.

The compressive capacity is affected significantly by the change of the area as bigger surface seems to provide better confinement of the mortar which leads to the increase of the compressive capacity, while the collapse mechanism is slightly affected as described above and presented in Fig. 131 and Fig. 132 where all the specimens present four radial tensile cracks and compressive damage at the middle area. The main difference is the splitting crack at the middle of the loaded area of the mortar affecting the $40\times40\times15$ mm^3 specimen.

Chapter 6: Conclusions and suggestions for future work

6.1 Summary

The present research aims to evaluate the compressive behaviour of the brick and stone masonry by the implementation and the assessment of minor destructive techniques in situ to preliminarly determine the parameters and the strength of masonry and destructive laboratory tests such as compressive tests on brick specimens along with the evaluation of the Young's modulus and Poisson ratio, compressive tests on tile specimens, compressive tests on stone specimens, compressive tests on mortar specimens and compressive tests on the extracted masonry brick and stone cylinders.

These destructive tests are calibrated in the in the Laboratory of Structural Technology of the Technical University of Catalonia (UPC – BarcelonaTech).

The compression test on extracted masonry cylinders is carried out according to the guidelines of UIC 778-3R formed by International Union Railways and the results of the test are compared with the standard equations using the mechanical values obtained with the characterisation of the components.

The double punch tests on the mortar is verified and analysed numerically for the first time in order to constitute a novel contribution to the field. The objective is to examine numerically the mortar's behaviour during the DPT, evaluate the relationship between uniaxial compressive and maximum experimental strength, identify the influence of the various numerical and mechanical properties on the compressive strength and evaluate the effect of the specimen's geometry.

Finally, in the last sections the final conclusion of this research will be discussed and suggestion for future work will be suggested.

6.2 Conclusions

After the results obtained and the observations made, the following conclusions can be drawn:

- From the preliminarily evaluation of the variability of the surface properties of the component materials of the walls, the in situ exprerimental techniques, Zone 1 and 2ext have shown to have higher values that indicate higher quality of the components while Zone 3ext brick and 4 indicate intermediate quality;

- By the Young modulus evaluation we observed that the bricks from Zone 1 have shown to be way stiffer than the bricks from Zone 2, presenting a Young's modulus of 8057 MPa which is in good agreement with the expected one;

- The characterization of the tiles has shown that their compressive strength ranges from 9 to 21 MPa where the higher values representing the tiles closer to the column where the stresses under compression are higher;

- For the three different type of stones tested in Zone 3ext and 4, two have shown shown an average compressive strength of 56 MPa, while the other shown an average of 34 MPa;

- The lower strength values for the walls after the DPT were obtained in the 2int and 3int brick zone, while the rest of the values of zone 1, 3ext stone and 4 show similar strength values. These values confirm the results obtained from in situ tests with PPT, HPT and TPT except for the 3int brick and stone positions which have shown certain inconsistencies. Mortar of the zone 5 of the vaults, mortar of the exterior stone facade 3ext_ext and mortar from zone F of the foundations have shown much higher compressive strength;

- The dry extraction performed in the experimental program has shown to be more suitable for historical masonry than the water-cooled drilling, since weak mortars are often present and the water may spoil the specimens.

- The compressive strength of the masonry can be obtained either by the compression test on cylindrical masonry presented in section 4.7 or by the estimation from the component resistances presented in section 4.6. The results of both come to an agreement calculating a compressive strength which ranges from 4 to 5.5 MPa for the different zones tested;

- The double punch tests on the mortar highlight the importance of the thickness and the confinement in the compressive behaviour, an observation made both by the experimental and the numerical results;

- The collapse mechanism was calibrated accurately in the numerical simulation as the four crack pattern failure given by the experiment is observed;

- From the numerical assessment of the double punch test on the mortar it is observed that the Young's modulus E and the k_1 parameter present the lower influence on both the capacity and the failure mechanism, ε_{pc} has a minor influence in the capacity, but affects slightly the final damage at the central part of the specimen, while the properties associated with the compressive behaviour ρ, f_{bc}/f_c show a very important influence on the numerical results as they highly affect the compressive capacity and slightly affect the failure mechanism presenting some minor differences in the final damage of the central zone;

- From the numerical assessment it is observed that the ratio between uniaxial compressive strength and strength capacity given by the experiment varies between 0.32 and 0.60.

6.3 Suggestions for future works

Based on the results of the experimental and the numerical campaign, the following suggestions can be carried out to deepen the research topic:

- Try to obtain more regular specimens with regular mortar joints in order to decrease the experimental scattering and help the post processing of the experimental results;

- Increase the database of the in situ experimental techniques in order to propose possible improvements to the evaluations of the results;

- Explore more combinations of material components in the laboratory, in order to enlarge the experimental database for a better calibration of the MDT techniques;

- Continuing the evaluation of the double punch tests of the mortar since it seems accurate to get a more realistic characterization, considering the actual size of the mortar specimens and the confinement;

- Continuing to investigate the compressive tests on the masonry cylinders to improve the implementation because of their promising and minimally invasive potential;

- Simulating of the degradation processes of the cylinders in the laboratory, for instance through freeze-thaw cycles, mechanical actions, chemical attack, etc;

- Enhance the evaluation of the Young's modulus and the Poisson ratio of the bricks, since a reliable prediction is very important, by using more precise instrumentation and experimental evidence with objective to contribute in the current regulations both at national and European level;

- Looking for a better matching to the first elastic branch of the response of the mortar specimen throughout the DPT, in order to obtain the same displacement at the maximum force for both the experimental and numerical analysis of the test;

- The parameters ρ and the f_{bc}/f_c. should be further calibrated by numerical simulation of more experiments of existing masonry elements in order to estimate the respresentative values for historical mortars.

References

[1] P. B. Lourenço, “Experimental and numerical issues in the modelling of the mechanical behaviour of masonry,” *Struct. Anal. Hist. Constr. II*, no. April, pp. 57–91, 1998.

[2] Arnold W. Hendry, *Structural Masonry*, 2nd ed. London: Red Globe Press.

[3] K. Elert, G. Cultrone, C. Rodriguez Navarro, and E. Sebastián Pardo, “Durability of bricks used in the conservation of historic buildings - Influence of composition and microstructure,” *J. Cult. Herit.*, vol. 4, no. 2, pp. 91–99, 2003.

[4] P. B. Lourenço, F. M. Fernandes, and F. Castro, “Handmade clay bricks: Chemical, physical and mechanical properties,” *Int. J. Archit. Herit.*, vol. 4, no. 1, pp. 38–58, 2010.

[5] J. A. Martín-Caro Álamo, “Análisis estructural de puentes arco de fábrica. Criterios de Comprobación,” 2001.

[6] S. Siegesmund and R. Snethlage, *Stone in Architecture*, 4th editio. Springer-Verlag Berlin Heidelberg, 2011.

[7] D. V. Oliveira, P. B. Lourenço, and P. Roca, “Cyclic behaviour of stone and brick masonry under uniaxial compressive loading,” *Mater. Struct. Constr.*, vol. 39, no. 2, pp. 247–257, 2006.

[8] M. Como, *Statics of Historic Masonry Constructions*. Springer-Verlag Berlin Heidelberg, 2013.

[9] Deutsches Institut für Normung (DIN), “DIN 18555-9: Testing of mortar containing mineral binders - Part 9: Determining the compressive strength of hardened mortar,” no. 0107, pp. 1–8, 1999.

[10] M. Bošnjak-Klečina and S. Lozančić, “Testing of physical and mechanical properties of bricks and mortar in historic structures,” *Teh. Vjesn.*, vol. 17, no. 2, pp. 209–215, 2010.

[11] J. Valek and R. Veiga, “Characterisation of mechanical properties of historic mortars - Testing of irregular samples,” *WIT Trans. Built Environ.*, vol. 83, pp. 365–374, 2005.

[12] F. Sandrolini and E. Franzoni, “Characterization procedure for ancient mortars’ restoration: The plasters of the Cavallerizza courtyard in the Ducal Palace in Mantua (Italy),” *Mater. Charact.*, vol. 61, no. 1, pp. 97–104, 2010.

[13] M. Drdácký, “Non-standard testing of mechanical characteristics of historic mortars,” *Int. J. Archit. Herit.*, vol. 5, no. 4–5, pp. 383–394, 2011.

[14] J. Henzel and S. Karl, “Determination of Strength of Mortar in the Joints of Masonry by Compression Tests on Small Specimens,” *Darmstadt Concrete*, vol. 2. pp. 123–136, 1987.

[15] A. Benedetti and L. Pelà, “Experimental Characterization of Mortar By Testing on Small Specimens,” *15th Int. Brick Block Mason. Conf.*, p. CD, 2012.

[16] L. Pelà, P. Roca, and A. Aprile, “Combined In-Situ and Laboratory Minor Destructive Testing of Historical Mortars,” *Int. J. Archit. Herit.*, vol. 12, no. 3, pp. 334–349, 2018.

[17] P. D. V. Christiansen, “In Situ Determination of the Compressive Strength of Mortar Joints Using an X-Drill,” *Mason. Int.*, vol. 24, no. 2, pp. 31–38, 2011.

[18] D. Marastoni, A. Benedetti, L. Pelà, and G. Pignagnoli, “Torque Penetrometric Test for the in-situ characterisation of historical mortars: fracture mechanics interpretation and experimental validation,” *Constr. Build. Mater.*, vol. 157, pp. 509–520, 2017.

[19] W. S. Mcnary, D.P. Abrams, “Mechanincs of masonry in compression”, vol. I, no. 4, pp. 857–870, 1985.

[20] F. M. Fernandes, P. B. Lourenço, and F. Castro, “Materials, Technologies and Practice in Historic Heritage Structures,” *Mater. Technol. Pract. Hist. Herit. Struct.*, 2010.

[21] a. T. Vermeltfoort, *Brick-mortar interaction in masonry under compression*, no. 2005. 2005.

[22] H. K. Hilsdorf, “Investigation into the Failure Mechanism of Brick Masonry Loaded in Axial Compression,” *Des. Eng. Constr. with Mason. Prod.*, pp. 34–41, 1969.

[23] A. Drougkas, P. Roca, and C. Molins, “Compressive strength and elasticity of pure lime mortar masonry,” *Mater. Struct. Constr.*, vol. 49, no. 3, pp. 983–999, 2016.

[24] J. Segura, L. Pelà, and P. Roca, “Monotonic and cyclic testing of clay brick and lime mortar masonry in compression,” *Constr. Build. Mater.*, vol. 193, pp. 453–466, 2018.

[25] Y. Boffill, H. Blanco, I. Lombillo, and L. Villegas, “Assessment of historic brickwork under compression and comparison with available equations,” *Constr. Build. Mater.*, vol. 207, pp. 258–272, 2019.

[26] A. W. Page, “Biaxial Compressive Strength of Brick Masonry.,” *Proc. Inst. Civ. Eng. (London). Part 1 - Des. Constr.*, vol. 71, no. pt 2, pp. 893–906, 1981.

[27] A. Brencich and E. Sterpi, “Compressive Strength of Solid Clay Brick Masonry : Calibration of Experimental Tests and Theoretical Issues,” *Struct. Anal. Hist. Constr.*, no. 1995, pp. 757–766, 2006.

[28] L. Pelà, S. Saloustros, and P. Roca, “Cylindrical samples of brick masonry with aerial lime mortar under compression: Experimental and numerical study,” *Constr. Build. Mater.*, vol. 227, pp. 11–13, 2019.

[29] L. Pelà, P. Roca, and A. Benedetti, “Mechanical Characterization of Historical Masonry by Core Drilling and Testing of Cylindrical Samples,” *Int. J. Archit. Herit.*, vol. 10, no. 2–3, pp. 360–374, 2016.

[30] J. Segura, L. Pelà, P. Roca, and A. Cabané, “Experimental analysis of the size effect on the compressive behaviour of cylindrical samples core-drilled from existing brick masonry,” *Constr. Build. Mater.*, vol. 228, p. 116759, 2019.

[31] L. Pelà, E. Canella, A. Aprile, and P. Roca, “Compression test of masonry core samples extracted from existing brickwork,” *Constr. Build. Mater.*, vol. 119, pp. 230–240, 2016.

[32] J. Milosevic, A. S. Gago, M. Lopes, and R. Bento, “Experimental assessment of shear strength parameters on rubble stone masonry specimens,” *Constr. Build. Mater.*, vol. 47, pp. 1372–1380, 2013.

[33] L. Binda, “2.4 Mechanical tests on mortars and assemblages,” no. March, pp. 57–76, 2005.

[34] A. Benedetti and M. Tarozzi, “Interpretation formulas for in situ characterization of mortar strength,” *Constr. Build. Mater.*, vol. 242, p. 118093, 2020.

[35] W.A. Ferguson and J. Skandamoorthy " The screw pull out test for the in situ measurement of the strength of masonry materials" 10th IB2MaC, Calgary, Canada, July 5-7, 1994.

[36] L. Binda, G. Mirabella Roberti, C. Tiraboschi, and S. Abbaneo, “Measuring Masonry Material Properties,” *U.S.-Italy Work. Guidel. Seism. Eval. Rehabil. Unreinforced Mason. Build.*, pp. 326–347, 1994.

[37] M. Steiger, A. E. Charola, and K. Sterflinger, *Weathering and deterioration*. 2011.

[38] M. Petracca, L. Pelà, R. Rossi, S. Zaghi, G. Camata, and E. Spacone, “Micro-scale continuous and discrete numerical models for nonlinear analysis of masonry shear walls,” *Constr. Build. Mater.*, vol. 149, pp. 296–314, 2017.

[39] R. Faria, J. Oliver, and M. Cervera, “A strain-based plastic viscous-damage model for massive concrete structures,” *Int. J. Solids Struct.*, vol. 35, no. 14, pp. 1533–1558, 1998.

[40] B. H. Bazant, Z.P & Oh, “Crack band theory for fracture of concrete,” *Matériaux Constr.*, vol. 16, no. 3, pp. 155–177, 1983.

[41] J. C. Walraven and A. Bigaj-Van Vliet, “The 2010 fib Model Code for Structural Concrete: A new approach to structural engineering,” *Struct. Concr.*, vol. 12, no. 3, pp. 139–147, 2011.

[42] P. B. Lourenço, “Recent Advances in Masonry Modelling :,” *Multiscale Model. Solid Mech.*, 2009.

[43] J. Lubliner, “A PLASTIC-DAMAGE MODEL FOR CONCRETE,” vol. 25, no. 3, pp. 299–326, 1989.